UNESP – Universidade Estadual Paulista "Júlio de Mesquita Filho"

Instituto de Química de Araraquara

Beatriz Lucas Garrote

Label-Free Electrochemical Capacitive Biological Sensors for Molecular Diagnostics

Thesis submitted to post-graduation program from São Paulo State University (UNESP, Brazil) in part fulfilment of the requirement for the PhD in Chemistry.

Supervisor: Prof. Paulo Roberto Bueno

Araraquara
2022

Garrote, Beatriz Lucas
G243L Label-Free electrochemical capacitive biological sensors for molecular diagnostics/ Beatriz Lucas Garrote – Araraquara: [s.n.], 2022
90 p.: il.

Thesis (doctor) – Universidade Estadual Paulista, Instituto de Química
Advisor: Paulo Roberto Bueno

1. Biosensor. 2. Electrochemical analysis. 3. Impedance spectroscopy. 4. Molecular diagnostics. 5. Transducers. I. Title.

Sistema de geração automática de fichas catalográficas da Unesp. Biblioteca do Instituto de Química, Araraquara. Dados fornecidos pelo autor(a).

Essa ficha não pode ser modificada

UNESP – Universidade Estadual Paulista "Júlio de Mesquita Filho"

Instituto de Química de Araraquara

Beatriz Lucas Garrote

Sensores biológicos de capacitância eletroquímica sem marcagem para o diagnóstico molecular

Tese apresentada ao Instituto de Química, Universidade Estadual Paulista (UNESP) como parte dos requisitos para obtenção do título de doutora em Química.

Orientador: Prof. Paulo Roberto Bueno

Araraquara
2022

UNIVERSIDADE ESTADUAL PAULISTA

Câmpus de Araraquara

CERTIFICADO DE APROVAÇÃO

TÍTULO DA TESE:

"Label-Free Electrochemical Capacitive Biological Sensors for Molecular Diagnostics"

AUTORA: BEATRIZ LUCAS GARROTE
ORIENTADOR: PAULO ROBERTO BUENO

Aprovada como parte das exigências para obtenção do Título de Doutora em Química, pela Comissão Examinadora:

Documento assinado digitalmente
gov.br
PAULO ROBERTO BUENO
Data: 21/10/2022 13:28:40-0300
Verifique em https://verificador.iti.br

Prof. Dr. PAULO ROBERTO BUENO (Participaçao Virtual)
Departamento de Engenharia, Fisica e Matematica / Instituto de Quimica - UNESP - Araraquara

SERGI BEÑAT MORAIS EZQUERRO - NIF:16284518N
Firmado digitalmente por SERGI BEÑAT MORAIS EZQUERRO - NIF:16284518N
Fecha: 2022.10.22 14:59:51 +02'00'

Prof. Dr. SERGI MORAIS EZQUERRO (Participaçao Virtual)
Departamento de Química / Universitat Politècnica de València - UPV - Espanha

CAMPUZANO RUIZ SUSANA - DNI 46887040E
Firmado digitalmente por CAMPUZANO RUIZ SUSANA - DNI 46887040E
Nombre de reconocimiento (DN): c=ES, o=UNIVERSIDAD COMPLUTENSE DE MADRID, ou=CERTIFICADO ELECTRONICO DE EMPLEADO PUBLICO, serialNumber=IDCES-46887040E, sn=CAMPUZANO RUIZ, givenName=SUSANA, cn=CAMPUZANO RUIZ SUSANA - DNI 46887040E
Fecha: 2022.10.22 13:00:35 +02'00'

Profa. Dra. SUSANA CAMPUZANO RUIZ (Participaçao Virtual)
Departamento de Química Analítica / Universidad Complutense de Madrid - UCM - Espanha

Digitally signed by Emanuel Carrilho
Date: 2022.10.24 10:27:08 -03'00'

Prof. Dr. EMANUEL CARRILHO (Participaçao Virtual)
Departamento de Química e Física Molecular / Instituto de Química - USP - São Carlos

Documento assinado digitalmente
gov.br
MARCIA REGINA COMINETTI
Data: 24/10/2022 09:58:57-0300
Verifique em https://verificador.iti.br

Profa. Dra. MÁRCIA REGINA COMINETTI (Participaçao Virtual)
Departamento de Gerontologia / Centro de Ciências Biológicas e da Saúde - UFSCar - São Carlos

Araraquara, 21 de outubro de 2022

CURRICULUM VITAE

PERSONAL INFORMATION

Name: Beatriz Lucas Garrote

Birth date: 16/09/1993 – Cieza (Murcia) – Spain

Nacionality: Spanish

Professional address: Instituto Tecnológico de la Energía (ITE). Carrer de Juan de la Cierva y Codorniu, 24, CP: 46980 - Paterna, Valencia (Spain).

EDUCATION

Araraquara, SP (Brazil)	**PhD in Chemistry**
Feb 2019 - Present	São Paulo State University
	PhD Thesis: Label-free electrochemical capacitive biosensors for disease diagnostic
Araraquara, SP (Brazil)	**Biotechnology MSc**
Feb 2016 – Mar 2018	São Paulo State University
	MSc Thesis: The potentiality and limitations of electrochemical impedance spectroscopic methods for molecular film applications
Valencia (Spain)	**Biotechnology BSc**
Sep 2011 – Sep 2015	Polytechnic University of Valencia
	BSc Thesis: Estrategias para la detección directa de ADN genómico en soportes poliméricos

PROFESSIONAL EXPERIENCE

Valencia (Spain)	**R&D Researcher**
Jun 2022 - Present	Instituto Tecnológico de la Energia (ITE)

SCIENTIFIC ACTIVITIES

Events

- XXII Simpósio Brasileiro de Eletroquímica e Eletroanalítica (Ribeirão Preto, 2019). Oral Communication. Role of target-to-receptor size ratio in faradaic resistive and capacitive label-free biosensors.
- IX International Workshop on Sensors and Molecular Recognition (Valencia, 2015). Poster presentation. Detección directa de AND genómico en suportes poliméricos.

Publications

- Lucas Garrote, B. *et al.* Reagentless Quantum-Rate-Based Electrochemical Signal of Graphene for Detecting SARS-CoV-2 Infection Using Nasal Swab Specimens. *ACS Sensors,* doi:10.1021/acssensors.2c01016 (2022).

- Garrote, B. L., Santos, A. & Bueno, P. R. Label-free capacitive assaying of biomarkers for molecular diagnostics. *Nature Protocols*, doi:10.1038/s41596-020-0390-9 (2020).
- Garrote, B. L., Santos, A. & Bueno, P. R. Perspectives on and Precautions for the Uses of Electric Spectroscopic Methods in Label-free Biosensing Applications. *ACS Sensors* **4**, 2216-2227, doi:10.1021/acssensors.9b01177 (2019).
- Garrote, B. L., Fernandes, F. C. B., Cilli, E. M. & Bueno, P. R. Field effect in molecule-gated switches and the role of target-to-receptor size ratio in biosensor sensitivity. *Biosensors and Bioelectronics* **127**, 215-220, doi:10.1016/j.bios.2018.12.018 (2019).
- Lucas-Garrote, B., Morais, S. & Maquieira, Á. Dual signal amplification for highly sensitive hybridization microassays on chemically activated surfaces. *Sensors and Actuators, B: Chemical*, doi:10.1016/j.snb.2016.10.109 (2017).

Patents

- BUENO, P. R. ; GARROTE, BEATRIZ L. ; LOPES, L. C. ; SANTOS, A. ; PINZON, E. F. TRANSDUTOR MODIFICADO, MECANISMO DE TRANSDUÇÃO E MÉTODO DE DETECÇÃO E/OU QUANTIFICAÇÃO DE ESPÉCIES DE INTERESSE ANALÍTICO COM TRANSDUTOR MODIFICADO. 2022, Brasil. Patente: Privilégio de Inovação. Número do registro: BR1020220006300, título: "TRANSDUTOR MODIFICADO, MECANISMO DE TRANSDUÇÃO E MÉTODO DE DETECÇÃO E/OU QUANTIFICAÇÃO DE ESPÉCIES DE INTERESSE ANALÍTICO COM TRANSDUTOR MODIFICADO" , Instituição de registro: INPI - Instituto Nacional da Propriedade Industrial. Depósito: 13/01/2022
- BUENO, P. R. ; GARROTE, BEATRIZ LUCAS ; LOPES, L. C. ; SANTOS, A. ; SANCHEZ, Y. P. . MÉTODO E DISPOSITIVO DE AMPLIFICAÇÃO DE SINAL TRANSDUTOR PARA ENSAIOS CAPACITIVOS. 2021, Brasil. Patente: Privilégio de Inovação. Número do registro: BR1020210238356, título: "MÉTODO E DISPOSITIVO DE AMPLIFICAÇÃO DE SINAL TRANSDUTOR PARA ENSAIOS CAPACITIVOS" , Instituição de registro: INPI - Instituto Nacional da Propriedade Industrial. Depósito: 26/11/2021

ACKNOWLEDGEMENTS

I gratefully acknowledge the financial assistance of FAPESP (grant n° 2018/26273-7), essential for the development of this thesis.

I would like to thank my supervisor Prof. Paulo Bueno for the support, the guidance and the discussion during the development of this thesis.

I want to recognize the support and collaboration of my colleagues from Nanobionics research group, in special Laís, Edgar, Yuliana and Erika (thanks a lot for the help in the peptide synthesis) for the collaboration in the research, the hours working together and the friendship.

I would like to thank Prof. Marco Antonio Schiavon and his research group for providing the quantum dots samples; Prof. Eurico Arruda and Dr. Ronaldo B. Martins for providing the human samples in the SARS-CoV-2 study; Prof. Ronaldo Censi Faria and Prof. Marcia Cominetti for providing their knowledge and the human samples in the ADAM10 study; and Prof. Eduardo Maffud Cilli for the support in the peptide synthesis. Undoubtedly, our collaboration improved the quality of the research developed.

I would like to thank the Chemistry Institute for the facilities and the administrative personnel from the post-graduation and from the LIEC (in special Rose Portasio).

I would like to thank my friends for the support and the advices in the challenging moments; to my family for believe in my potential; and to my girlfriend Gabriela for the unconditional support and the love.

Summary

Abstract

The recent advances in biomedicine and technology have risen the popularization of molecular diagnosis which refers to the use of molecular techniques, such as polymerase chain reaction (PCR) or enzyme-linked immunosorbent assay (ELISA), to analyze biological markers (e.g., proteins, DNA or RNA). Both PCR and ELISA have been improved over the years with a broad range of applications. Nonetheless, both techniques have limitations that complicate their access in developing countries or their application in the field, since both need costly and high-size equipment with a stable source of power, costly reagents, and additional steps, which turn them into time-consuming assays, and high-qualified personnel to run the assays. REASSURED Point-of-care (POC or bedside testing) molecular diagnosis devices appear to overcome those limitations due to the facility to use handheld devices to medically examine a patient during a consultation where doctors and patients are no longer required to wait for lab results to make an appropriate diagnosis. Therefore, POC devices have the potential to become the primary care tool to diagnosis diseases in which the detection time is crucial to initiate the treatment, as is the case in non-communicable diseases (NCDs), and to avoid the spread of infection agents, as it is the case in infectious diseases, reducing the probability of outbreak and multiple deceases. POC molecular diagnosis devices are popularly known as biosensors which are constituted by three elements: receptor, transducer, and output system. Within those, transducer is the main element, since it is responsible to convert the biological/chemical signal of the analyte-receptor interaction into an electrical signal readable by the output system. The recognition of the analyte by the transducer can be directly (i.e., label-free) on only one-step without additional reagents (reagentless) by the variation of an inherent property of the transducer; or indirectly (i.e., label-based) by using additional steps for analyte labeling or additional labeled-molecules. This requirement increases the duration, the cost and the difficult of handling of the assay, so label-free and reagentless methodologies are more appropriate for POC devices. Those requirements are accomplished by using transducers based on electrochemical capacitance which also offers high-sensitivity and the possibility of miniaturization.

Electrochemical capacitive transducers are composed by a redox-active nanostructure immobilized on the electrode surface with discrete energy levels. Those transducers use impedance-derived capacitance spectroscopy as electrochemical technique derived from EIS measurements that measures the electrochemical capacitance (C_μ) of those electroactive nanostructures. C_μ is an intrinsic characteristic of those electroactive nanostructures with thickness < 5nm, related to the energy storage and density-of-states (DOS) of the interface. C_μ biosensors are modelled by the quantum rate theory which resolves the quantum dynamics of the electron transfer (ET) in diffusionless electrochemical reactions, such as one of the electroactive interfaces, given by $k = G/C_\mu$, where k is the electron transfer rate and G is the quantum conductance which measures the charge transport within the electrode and the electroactive interface. This theory demonstrated that in an ideal electron transfer situation,

$G = G_0$, where $G_0 = g_s e^2/h \sim 77.5\ \mu S$ is the quantum of conductance. Moreover, it demonstrated that C_μ is a consequence of the series combination of an electrostatic (C_e) and quantum (C_q) capacitances, such as $1/C_\mu = (1/C_e) + (1/C_q)$, where C_e arises from the charge separation (l) due to the solvation of the electroactive switches and C_q emerges from the occupancy of the energy levels within the charge transfer with the electrode through the backbone of the electroactive molecule (L). In most of the quantum C_μ interfaces, $l \ll L$, so $C_e \gg C_q$, $1/C_e$ is close to zero and $C_\mu \sim C_q$. According to those approximations, $k = G_0/C_q$, demonstrating that electroactive interfaces operate in a purely quantum regime, turning them in high-sensitive transducers for biosensing applications.

The versatility and high-sensitivity of the C_q transducers convert them into promising tool for the development of analytical assays in a vast range of applications qualitative or quantitative. In this Ph.D. project we proposed the use of electrochemical capacitance transducers to develop novel biosensing assays for the diagnosis of relevant diseases: SARS-CoV-2 infection by the detection of spike protein (SP) and nucleocapsid protein (NP) in nasopharyngeal/oropharyngeal samples; Dengue virus infection by the quantification of NS1 protein in serum samples; and Alzheimer's disease (AD) by the quantification of ptau-181 and ADAM10 proteins in human serum samples.

SARS-CoV-2 is the novel circulating member of the family *Coronaviridae* that rapidly spread worldwide and became a global health threat. The development of biosensors became a priority until the development of the vaccines. In this doctoral thesis, the SARS-CoV-2 assay developed detected the presence of the viral proteins S and N in nasopharyngeal/oropharyngeal human samples with 77% of specificity and 80% of sensitivity, higher than the overall commercial rapid assays. Dengue virus also constituted a health threat in some tropical countries, such as Brazil. Efficient POC devices could provide rapid detection of the infection and monitorization of the progression of the disease to more severe haemorrhagic dengue. Thus, in this project we developed a miniaturized and high-sensitive Dengue virus assay for the quantification of the viral protein NS1. A novel amplifier signal methodology was coupled to the assay which increased up to 1000 times its sensitivity, enabling the detection of the virus since the biggening of the infection.

Moreover, in this doctoral thesis, C_q transducers were applied to the first-time label-free quantification of two AD serum biomarkers, ADAM10 and ptau-181. Two ADAM10 assay were developed by using two antibodies that recognized a distinct ADAM10 isoforms. The analytical features of each assay were resolved by measurements on the C_q transducer which enable the determination of the association constant (K_a), limit-of-detection (LOD), limit-of-quantification (LOQ). Both assays demonstrated similar K_a and LODs and LOQs in the nanogram per millilitre range. Also, the specificity of each assay was analysed by the quantification of the protein in serum samples from AD patients and healthy individuals. In the case of the ptau-181 assay, the concentration range in human serum samples was picogram per milliltre, so three different C_q

transducers based on a redox peptide self-assembled monolayer (SAM), the redox peptide SAM coupled to the amplifier signal methodology and a CdTe quantum dot ensemble, were analysed in terms of LOD and LOQ to evaluate which of them would be suitable for the application. The sensitiveness of the rPep SAM was not enough to quantify the protein in such concentration range, while the alternative with the amplifier signal and the QD-based transducers were suitable for the application.

In summary, in this doctoral thesis it was demonstrated the potential of the electrochemical capacitance technique for the development of transducers for POC devices. The versatility of the technique enables a vast range of applications which diverse analytical features requirement. Accordingly, the objectives proposed in the beginning of this project were successfully achieved and new prospect for future research have been created

Resumo expandido

Os recentes avanços em medicina e tecnologia tem aumentado o uso das técnicas de diagnóstico molecular para a análises de marcadores biológicos (proteínas, DNA ou RNA), como as técnicas de reação em cadeia da polimerase (PCR, do inglês *polymerase chain reaction*) e o ensaio de proteínas imuno absorvidas marcadas com enzimas (ELISA, do inglês *enzyme-linked immunosorbent assay*). Estas técnicas apresentam elevada sensibilidade e especificidade que permitem um diagnóstico personalizado mais rápido, sensível e confiável do que técnicas de imagem como a ressonância magnética (MRI). Apesar das vantagens analíticas das duas técnicas, elas apresentam limitações que dificultam o seu acesso em países em desenvolvimento e a sua aplicação fora de laboratórios devido ao fato de que precisam de equipamentos de elevado preço e tamanho, reagentes caros e requerem de múltiplas etapas até o resultado do ensaio. Assim, PCR e ELISA são técnicas demoradas e que precisam ser aplicadas por pessoal qualificado em espaços dedicados a ensaios clínicos. Os dispositivos de *point-of-care* (POC) tem aparecido como uma alternativa para superar as limitações das técnicas tradicionais devido à facilidade de uso e rapidez nos resultados. Dispositivos POC tem o potencial de serem a primeira ferramenta no diagnóstico de doenças não transmissíveis (NCDs em inglês) e de doenças infecciosas, diminuindo a probabilidade de avanço descontrolado do agente infeccioso e de um grande número de óbitos. O interesse pelo desenvolvimento de dispositivos POC levou à Organização Mundial da Saúde (OMS) a estabelecer os critérios de qualidade, analíticos e sociais que os POCs precisavam cumprir para serem usados nos distintos níveis dos sistemas de saúde de países em desenvolvimento e desenvolvidos, além de substituir as técnicas de diagnóstico tradicionais. Esses critérios foram nomeados como ASSURED, que se corresponde ao acrônimo de *affordable*, *sensitive*, *specific*, *user-friendly*, *rapid and robust*, *equipment-free* e *deriverable*. Em 2019, o acrônimo foi atualizado para REASSURED, no qual foram incluídos *real-time connectivity*, *easy of sample collection and environmentally friendly*.

POCs são comummente chamados de biossensores que estão constituídos por três elementos principais: Receptor (molécula que interage especificamente com o analito na amostra); Transdutor (que contém a molécula receptora na sua superfície e converte o sinal biológico/químico da interação entre as moléculas em um sinal elétrico); e o, Sistema de saída (encarregado de traduzir esse sinal elétrico numa informação entendível pelo usuário, como por exemplo, a quantidade de analito na amostra). A detecção ou quantificação do analito na amostra pode ser feita de forma direta, por metodologias sem marcador (*label-free*), que medem uma propriedade do transdutor sem adição de reagentes (*reagentless*); ou de forma indireta, usando moléculas adicionais marcadas que geram o sinal detectado pelo transdutor. Esta última metodologia é chamada de *label-based* e apresenta limitações frente as metodologias *label-free* devido ao número de reagentes e de etapas adicionais necessárias para obter o resultado, o que aumenta o preço e o tempo para a realização do ensaio. Por isso, os ensaios *label-free* são escolhidos para o desenvolvimento de biossensores rápidos e baratos.

Geralmente os biossensores são classificados pelo tipo de transdutor que contêm. Dentre os diferentes tipos (i.e., piezoelétrico, ótico), os biossensores eletroquímicos baseados na técnica de espectroscopia de impedância eletroquímica (EIS em inglês) apresentam vantagens devido à capacidade de miniaturização, portabilidade, elevada sensibilidade, simplicidade, baixo custo e rapidez. Os transdutores de EIS medem variações das funções de imitância complexa, como impedância (Z^*) ou capacitância (C^*), devido à interação entre o receptor e o analito na superfície de um eletrodo, os quais transformam essas variações em sinais elétricos. Apesar das vantagens que apresentam, os estudos e ajustes dos dados com os circuitos elétricos que representam cada biossensor são necessários para a correta interpretação dos dados obtidos nos biossensores que utilizam a técnica EIS. As medidas de EIS são feitas em um eletrodo imerso em eletrólito que contém ou não uma sonda redox (i.e., modo faradaico ou não faradaico, respetivamente). Ambas as configurações podem ser usadas em biossensoriamento, sendo que medidas de EIS não faradaico se modelam com a teoria da dupla camada elétrica e medem variações na carga eletrostática da superfície do eletrodo, tendo aplicações em sensores iónicos. Por outro lado, as medidas de EIS faradaica se modelam com o circuito de *Randles* e medem variações na resistência de transferência de carga entre a sonda redox no eletrólito de suporte e a superfície do eletrodo. O uso de uma sonda redox no eletrólito de suporte pode dificultar a aplicação do biossensor como dispositivo POC. Para resolver essa limitação, a espectroscopia de capacitância derivada da impedância (ECS em inglês) aparece como alternativa à EIS tradicional. ECS é uma técnica derivada das medidas de EIS que mede a capacitância eletroquímica (C_μ) em transdutores eletroativos, que são transdutores que contêm as sondas redox confinadas na superfície do eletrodo, ao invés de em solução. C_μ é uma característica intrínseca das nanoestruturas eletroativas de espessura < 5 nm com estados de energia quantizados, relacionada a sua densidade de estados (DOS em inglês). Diferentemente da EIS tradicional, ECS é *reagentless*, pois não precisa de reagentes adicionais no eletrólito de suporte para realizar a medida eletroquímica. A teoria da taxa quântica de transferência eletrônica (*quantum rate theory* em inglês) descreve os fundamentos eletroquímicos das reações não dependentes de difusão que ocorrem nos biossensores capacitivos baseados em ECS, onde um eletrodo com níveis de energia contínuos é modificado com moléculas eletroativas que apresentam níveis de energia discretos. Nesta situação, a transferência de elétrons entre a moléculas eletroativas e o eletrodo depende do transporte e do armazenamento de carga que são medidos pela condutância quântica (G) e C_μ, respetivamente. Desta forma, a taxa de transferência de elétrons (k) é descrita pela teoria como $k = G/C_\mu = G_0 \sum_{n=1}^{N} T_n(\mu, L)\left(\frac{1}{C_e} + \frac{1}{C_q}\right)$, onde $G_0 = g_s e^2/h \sim 77.5\ \mu S$ é o quantum de condutância, ou seja, G máxima num canal quântico ideal, h é a constante de Planck, g_s é a degenerescência do elétron, e e é a carga do elétron; e $\sum_{n=1}^{N} T_n(\mu, L)$ é a probabilidade de transmitância de um elétron entre dois níveis de energia a certo potencial químico (μ) através de um canal quântico N de comprimento L. O modo mais simples de G é assumir que $T_n(\mu, L)$ de um único elétron em um único canal quântico ($N = 1$) é perfeita. Assim, $T_n(\mu, L) = 1$ e, consequentemente, $G = G_0$. No caso de C_μ, é obtida pela combinação em série

das capacitâncias eletrostáticas (C_e) e quânticas (C_q), sendo $1/C_\mu = (1/C_e) + (1/C_q)$. C_e está relacionada com a separação de cargas (l) na solvatação dos agrupamentos eletroativos na superfície do eletrodo, enquanto que C_q está relacionada com a ocupação dos níveis de energia dos agrupamentos eletroativos devido à transferência de elétrons entre eles e o eletrodo através da estrutura das moléculas que os contêm (L). Na maioria dos sistemas quânticos C_μ , entende-se que $l \ll L$, assim $C_e \gg C_q$, e em consequência $1/C_e$ e $C_\mu \sim C_q$. Assim, as definições de G e C_μ demonstram que ambas têm uma natureza quântica e, por tanto, em processos eletroquímicos não dependentes de difusão, k também a terá, sendo definida por $k = G_0/C_q$ (assumindo as aproximações descritas). Como G_0 é uma constante, k depende únicamente de C_q e esta pode ser acessada experimentalmente por medidas de EIS convertida em capacitância (ECS). Como comentado anteriormente, C_q está relacionada com o armazenamento de energia em estruturas eletroativas e na sua densidade de estados. Essas variáveis mudam quando ocorrem variações nelas ou no ambiente próximo. Dessa forma, pode ser usada como sinal analítico para o desenvolvimento de biossensores, como já foi demostrado em biossensores baseados em monocamadas automontadas (*self-assembled monolayer, SAM,* em inglês) com agrupamentos redox, filmes de óxidos mistos, grafeno ou pontos quânticos (*quantum dost, QD,* em inglês).

Devido à sensibilidade e simplicidade demonstrada pelos biossensores de C_q e à necessidade de novas técnicas analíticas para a detecção de doenças não transmissíveis e infecciosas de forma rápida, precoce e de baixo custo, os objetivos propostos neste projeto foram o desenvolvimento de biossensores para a detecção de infecções causadas pelo vírus da Dengue e o SARS-CoV-2; e o diagnóstico precoce da doença de Alzheimer pela quantificação dos biomarcadores ADAM10 e ptau-181. Para atingir esses objetivos, foram usados novos transdutores e novos processos eletroquímicos que melhoraram as características analíticas (sensibilidade e especificidade) dos biossensores C_q.

As infecções virais são uma ameaça para a saúde em todos os países do mundo, pois emergem até o desenho de vacinas ou o descobrimento de algum medicamento efetivo. Durante o período de emersão, o controle da transmissão do vírus é essencial e pode ser feita através de biossensores específicos e sensíveis. O exemplo mais recente dessa necessidade é a emergência do novo coronavírus SARS-CoV-2 (*severe acute respiratory syndrome 2* em inglês), responsável pela pandemia de Covid-19 que tem causado 610 milhões de casos e 6.5 milhões de óbitos até o dia 21 de setembro de 2022, segundo a OMS. Neste projeto de pesquisa foi desenvolvido um biossensor C_q contendo, pela primeira vez, grafeno como transdutor quântico (o descobrimento está sob proteção intelectual) para a detecção de duas proteínas virais, a proteína S (*spike* em inglês) e a proteína N (*nucleocapsid* em inglês). A prova de conceito do novo transdutor foi realizada em 13 amostras de nasofaringe/orofaringe de pessoas saudáveis e em 15 amostras de pacientes que sofreram infecção pelo vírus SARS-CoV-2. O novo biossensor quântico baseado em uma única camada de grafeno (*single layer graphene, SLG,* em inglês), S/N-SLG, conseguiu

diferenciar as amostras de vírus positivas das negativas com uma especificidade do 77% e uma sensibilidade do 80%, sendo maior do que as que apresentam os ensaios de antígenos rápidos (geralmente baseados em técnicas de imunocromatografia).

O vírus da Dengue é outro exemplo da necessidade de diagnóstico rápido e precoce em infecções virais que ainda não tem vacinas disponíveis. A transmissão do vírus através da picada de mosquitos femininos *Aedes aegypti* ocasiona uma ameaça sanitária cada ano. Segundo a Organização Pan-Americana de saúde (OPAS) ocorreram 975 mil casos no Brasil apenas em 2021. Além do alto número de casos, o risco de sofrer dengue hemorrágica faz com que o diagnóstico rápido para monitorar o avanço da doença seja uma necessidade. C_q já foi usada para o desenvolvimento de um biossensor qualitativo para diferenciar amostras de soro humano positivas para dengue e amostras negativas com elevada especificidade. Porém, o ensaio não era miniaturizado para aplicação POC. Por isso, neste trabalho foi desenvolvido um biossensor quantitativo para detecção da proteína NS1 do vírus da Dengue usando eletrodos de ouro miniaturizados e uma nova metodologia de amplificação de sinal para transdutores capacitivos (o descobrimento está sob proteção intelectual). Esta metodologia de amplificação de sinal consistiu no acoplamento eletroquímico da densidade de estados de duas sondas redox no sistema, sendo que uma se encontra em solução no eletrólito de suporte e outra confinada na superfície do eletrodo, o que permitiu aumentar em até 1000 vezes a sensibilidade do ensaio em termos de mínima concentração detectada (LOD em inglês) e mínima concentração quantificada (LOQ em inglês), que passou de ser $LOD = 0.52\ ng\ mL^{-1}$ e $LOQ = 1.75\ ng\ mL^{-1}$ a $LOD = 0.67\ pg\ mL^{-1}$ e $LOQ = 2.23\ pg\ mL^{-1}$ quando a metodologia de amplificação de sinal foi incluída. Assim, a detecção e quantificação com concentrações tão baixas permitiria a detecção de doenças infecciosas antes da aparição dos sintomas e progressão das doenças.

No caso de doenças não transmissíveis, transdutores de C_q também podem ser usados para desenvolver biossensores que quantifiquem biomarcadores específicos envolvidos nos eventos bioquímicos da doença. Esses transdutores podem ajudar no diagnóstico precoce e agilizar a aplicação dos tratamentos, como é o caso da doença de Alzheimer (AD em inglês). AD é um tipo de demência neurodegenerativa, causada pelo acúmulo de placas de β amiloide e a formação de emaranhamento de proteína tau. Alguns tratamentos baseados no uso de anticorpos monoclonais anti-β amiloide tem aparecido, como o caso do aducanumab e lecanemab, que tem como objetivo diminuir a acumulação de placas de β amiloide. Além das pesquisas sobre tratamentos que revertam os efeitos da doença, há esforços em descobrir novos biomarcadores em sangue ou soro que permitam a monitorização contínua deles e, assim, o diagnóstico precoce. Algumas proteínas já foram reportadas na literatura por apresentarem concentrações diferentes em pessoas com diferentes níveis de AD e pessoas saudáveis, como as proteínas ADAM10 e ptau-181. Na literatura já foram reportados ensaios para a quantificação destas duas proteínas, porém, utilizando estratégias *label-based*, as quais não são apropriadas em aplicações POC. Por isso, neste trabalho foram desenvolvidos biossensores *label-free* para a quantificação desses dois biomarcadores usando diferentes estratégias.

A proteína ADAM10 está envolvida no processo de clivagem do precursor da β amiloide (APP) em fragmentos solúveis que não geram neurodegeneração. Ela é sintetizada em forma de precursor proADAM10 ($\sim$80 kDa), que gera uma proteína madura e ativa de $\sim$65 kDa ou uma isoforma solúvel e inativa de $\sim$55 kDa. Esta isoforma foi reportada na literatura como biomarcador em soro para a progressão de AD, estando em maior concentração quanto maior era o estágio da doença. Dependendo do anticorpo usado para detectar a proteína, pode ser quantificada uma ou várias dessas isoformas. Neste trabalho, dois biossensores de ADAM10 foram desenvolvidos usando dois anticorpos diferentes, Ab1 que reconhece mais de uma isoforma (não especificado pelo fabricante), e Ab2 que reconhece unicamente a isoforma solúvel. Ambos os biossensores foram obtidos usando como transdutor C_q uma SAM de peptídeo eletroativo (i.e., contendo um agrupamento redox), na qual o anticorpo era imobilizado covalentemente. Pela primeira vez um biossensor capacitivo foi usado para a quantificação de uma proteína em amostra complexa e para o diagnóstico de uma doença não transmissível. Os biossensores foram analisados obtendo a constante de afinidade (K_a) do anticorpo e analito, os valores de LOD e LOQ, e quantificando a proteína em amostras de soro de pacientes com AD e de indivíduos saudáveis. O biossensor com o anticorpo Ab1 mostrou elevada afinidade pela proteína ADAM10 ($K_a = (0.022 \pm 0.004)\ mL\ ng^{-1}$) e valores de LOD e LOQ no intervalo de concentração necessário. Porém, esse biossensor mostrou maior concentração de ADAM10 nas amostras de indivíduos saudáveis, contrariando as informações reportadas na literatura e sugerindo a interação com várias isoformas. No caso do biossensor com o Ab2, o valor de K_a do sistema ($K_a = (0.03 \pm 0.008)\ mL\ ng^{-1}$) não foi estatisticamente diferente do biossensor com Ab1. Porém, a concentração de ADAM10 obtida nas análises das amostras de soro de paciente usando o biossensor C_q aumentou com a progressão da doença como nos ensaios reportados na literatura. Ademais, a concentração de ADAM10 em 6 das 10 amostras obtidas pelo biossensor capacitivo coincidiu com os valores calculados usando um kit de ELISA comercial, demonstrando o potencial do biossensor.

A proteína ptau-181 é a proteína tau fosforilada no resíduo 181 que está relacionada com a agregação delas e a agregação de emaranhados que geram neurodegeneração. É produzida pelos neurônios, então está presente numa concentração elevada no líquido cefalorraquidiano (liquor e CSF em inglês). Porém, a concentração em sangue é na faixa de picogramas por mililitro. Por esse motivo, as técnicas de elevada sensibilidade são necessárias para a quantificação nas amostras de soro. Assim, neste trabalho o biossensor de ptau-181 foi desenvolvido usando três tipos diferentes de transdutores C_q, sendo um baseado em SAM de peptídeo eletroativo, outro incluindo a metodologia de amplificação de sinal usando uma sonda redox em solução, e o terceiro baseado numa monocamada de QD. Os QDs são semicondutores zero dimensionais com propriedades quânticas cuja densidade de estados pode ser acessada por medidas de ECS. Estudos recentes publicados pelo nosso grupo de pesquisa demonstrou que os QDs apresentam elevada sensibilidade à variações na sua superfície ou ambiente e podem ser usados como transdutores capacitivos onde sua densidade de estados é o sinal analítico. Assim, os três

transdutores C_q usados para quantificar ptau-181 em amostras de soro humano comercial foram avaliados em termos de LOD e LOQ. O biossensor baseado na SAM de peptídeo eletroativo não apresentou variações significativas nos intervalos de concentrações analisados ($1 - 64\ pg\ mL^{-1}$), enquanto que os transdutores com o sistema de amplificação de sinal e de QDs mostraram valores de LOD e LOQ na faixa de concentrações femtomolar, sendo que o transdutor com amplificação de sinal foi 25 vezes mais sensível que o transdutor baseado em QDs ($LOD_{amplif} = 0.7\ fM$ e $LOD_{QD} = 17.5\ fM$, respetivamente). Assim, esses transdutores mostraram bom potencial em aplicações que requerem altos níveis de sensibilidade.

Em conclusão, neste trabalho foi demostrado o potencial da técnica de capacitância eletroquímica para o desenho de transdutores em biossensores POC. A versatilidade da técnica permite a aplicação em diferentes campos que requerem diferentes características analíticas. Ademais, o estudo fundamental dos transdutores usando a *quantum rate theory* permite a melhora constante dos biossensores já desenvolvidos e o desenho de novos transdutores ou reações eletroquímicas que trazem vantagens sobre os métodos “tradicionais”. Portanto, os objetivos propostos no início do projeto foram atingidos com sucesso e novos caminhos para futuras pesquisas foram iniciados.

List of figures

List of tables

1. Introduction

The recent advances in biomedicine and technology have risen the popularization of molecular diagnosis which refers to the use of molecular techniques, such as polymerase chain reaction (PCR) or enzyme-linked immunosorbent assay (ELISA), to analyze biological markers (e.g., proteins, DNA or RNA). Due to the use of those high-sensitive and high-specific techniques, molecular diagnosis enables personalized, specific, and more rapid diagnosis than image-based diagnosis techniques, such as magnetic resonance imaging (MRI). PCR[1] is a molecular technique used to detect the presence or absence of certain DNA/RNA sequences or nucleotides by the cyclical amplification of the region of interest by applying temperature cycles and using specific reagents, such as Taq polymerase and primers. In molecular diagnosis, PCR enables the diagnosis of genetic human diseases and infectious diseases by detecting genetic mutations or the genome of infectious agents, respectively. On the other hand, ELISA[2] is used to analyze protein biomarkers. ELISA assay consists of the detection or quantification of proteins by their specific interaction with antibodies labeled with enzymes whose reaction with the specific substrate causes a colored product. Both PCR and ELISA have been improved over the years, appearing as variations of the initial assays which have opened a broader range of applications. Nonetheless, both techniques have limitations that complicate their access in developing countries or their application in the field, since both need costly and high-size equipment with a stable source of power, costly reagents, and additional steps, which turn them into time-consuming assays, and high-qualified personnel to run the assays. Point-of-care (POC or bedside testing) molecular diagnosis devices appear to overcome those limitations due to the facility to use handheld devices to medically examine a patient during a consultation where doctors and patients are no longer required to wait for lab results to make an appropriate diagnosis.

POC molecular diagnosis devices have the potential to become the primary care tool to diagnosis diseases in which the detection time is crucial to initiate the treatment, as is the case in non-communicable diseases (NCDs), and to avoid the spread of infection agents, as it is the case in infectious diseases, reducing the probability of outbreak and multiple deceases.[3] The main characteristics of POC devices are simplicity, rapidity, and accessible prize to be applied on-site by qualified or unqualified personnel.[3; 4] Such is the interest in POC devices that in early 2000 the World Health Organization (WHO)[5] established that the POC analytical devices should meet the quality-ASSURED to be used at all level in the health care system in developed and developing countries. ASSURED is the acronym of [6]:

- **Affordable**. Perhaps the main concern on molecular diagnostic devices. To be affordable involves being accessible in any country's healthcare system, i.e., developed or developing.
- **Sensitive**. The sensitivity of an analytical assay measures the probability of obtaining false negative results and it is related to the lower concentration of analyte that the assay can detect or quantify. Thus, the higher the sensitivity, the higher the power to detect lower

concentrations of the biomarkers and therefore, to achieve early diagnosis which is crucial in some diseases.

- **Specific**. Together with sensitivity, the specificity of the assay is related to the accuracy of the device. Specificity measures the false positive results of the assay due to unspecific interaction with the biosensing interface (e.g., cross-reactivity, matrix effect). For some diseases whose treatment is not harmful, lower specificity could be tolerated whether the sensitivity of the assay is considerably high.
- **User-friendly**. POC devices should be simple to handle by an unqualified end-user. The test should be performed with the lowest manipulation possible by the end-user to avoid false results. Moreover, the assay should have easy and well-explained instructions available.
- **Rapid and robust**. Results should be delivered within 5 and 60 minutes after sample collection (and/or incubation on the biosensing interface) to avoid a returning clinical visit that could be challenging in some rural areas or developing countries. Moreover, the performance of the POC device should not be dependent on extreme shipping or storage conditions, such as temperature or humidity.
- **Equipment-free**. The requirement of high-size equipment is one of the limitations of the application of the so-called gold standard analytical techniques (i.e., PCR and ELISA) in the field. Therefore, POC devices should be miniaturized or they should use easy-to-use, portable, or day-to-day devices, such as smartphones, to bring advantages over the traditional and well-established approaches.
- **Deliverable**. Accessibility is one of the aims of POC devices. The delivery strategy of the POC devices should ensure the shipping to low and high resources areas.

Since the establishment of the quality control characteristics, the advances in molecular diagnosis technology and approaches have led to the achievement of successful ASSURED devices. Nonetheless, challenges related to standardization and quality control for surveillance and sample collection and processing remained.[6] Therefore, recently, the criteria were actualized to a new quality level referred to as REASSURED to obtain the next generation of POC devices. The additional letters to the acronym include real-time connectivity, ease of sample collection, and environmentally friendly:

- **Real-time connectivity**. Global connectivity is now a reality due to the advances in technology. The development of artificial intelligence (AI) and the internet of things (IoT) has already simplified daily activities which could also bring advantages to the surveillance systems through the real-time connection of POC devices. By doing so, it would be possible to monitor continuously the device performance; detect faster assay errors; perform remote software actualization, and submit the results to an online database which would enable the corresponding surveillance system to have more accurate control of patients and the spread of infectious diseases.
- **Ease of sample collection and environmentally friendly**. Simplification of molecular diagnostic assays includes simplifying the sample collection. For example, it could be a

handicap to the end-user whether the POC device would require intravenous punction to obtain a blood sample instead of a finger prick since it must be performed by qualified personnel. Therefore, the assay should be designed carefully. On the other hand, the use of environmentally friendly protocols is a recent concern worldwide. Developers should consider the environmental impact of the application of the assays over the years, such as the amount of plastic waste produced per assay or the use of contaminant reagents. In summary, simplicity is the key word of POC devices and their design should meet that.

Ideal POC molecular diagnosis devices will be obtained, insofar, by achieving those characteristics[6] and they will revolutionize the healthcare systems and diagnosis industry.

POC molecular diagnosis devices are popularly known as biosensors which are constituted by three elements: receptor, transducer, and output system (Figure 1). The receptor is the molecule that interacts specifically with the analyte of interest from the sample (e.g., urine, saliva, blood, or serum). Antibodies, DNA/RNA sequences, enzymes, or proteins can be used as receptors. Those molecules are immobilized to the transducer surface which is perhaps the main element in a biosensor since it is responsible to convert the biological/chemical signal of the analyte-receptor interaction into an electrical signal readable by the output system. Finally, the output system translates the electrical signal into a response understandable by the end-user (e.g., the protein is in the sample). The analyte in the sample can be directly (i.e., label-free) or indirectly (i.e., label-based) detected. In general, label-free offers advantages over label-based methodologies, since label-free designs detect the analyte-receptor interaction in only one step by the variation of an inherent property of the transducer, such as mass, temperature, or electrical resistance, while label-based strategies require additional steps to include additional labeled molecules, such as secondary antibodies labeled with enzymes, to detect or quantify the analyte via the label reaction, for example, products from the enzymatic reaction. Contrary to label-based methodologies, label-free, in general, are reagentless, that is, the assays included in the biosensing interface all of the necessary elements for the recognition which enables the autonomous and independent functionality of the assay without any treatment of the samples or additional steps. The requirement of additional steps and reagents increases considerably the duration of the assay and/or the necessity of complicated microfluidics systems to avoid end-user manipulation. Therefore, label-free and reagentless methodologies are more appropriate for POC devices than label-based procedures, since, in general, they are simpler, faster, easier to use, and present a lower prize.[7]

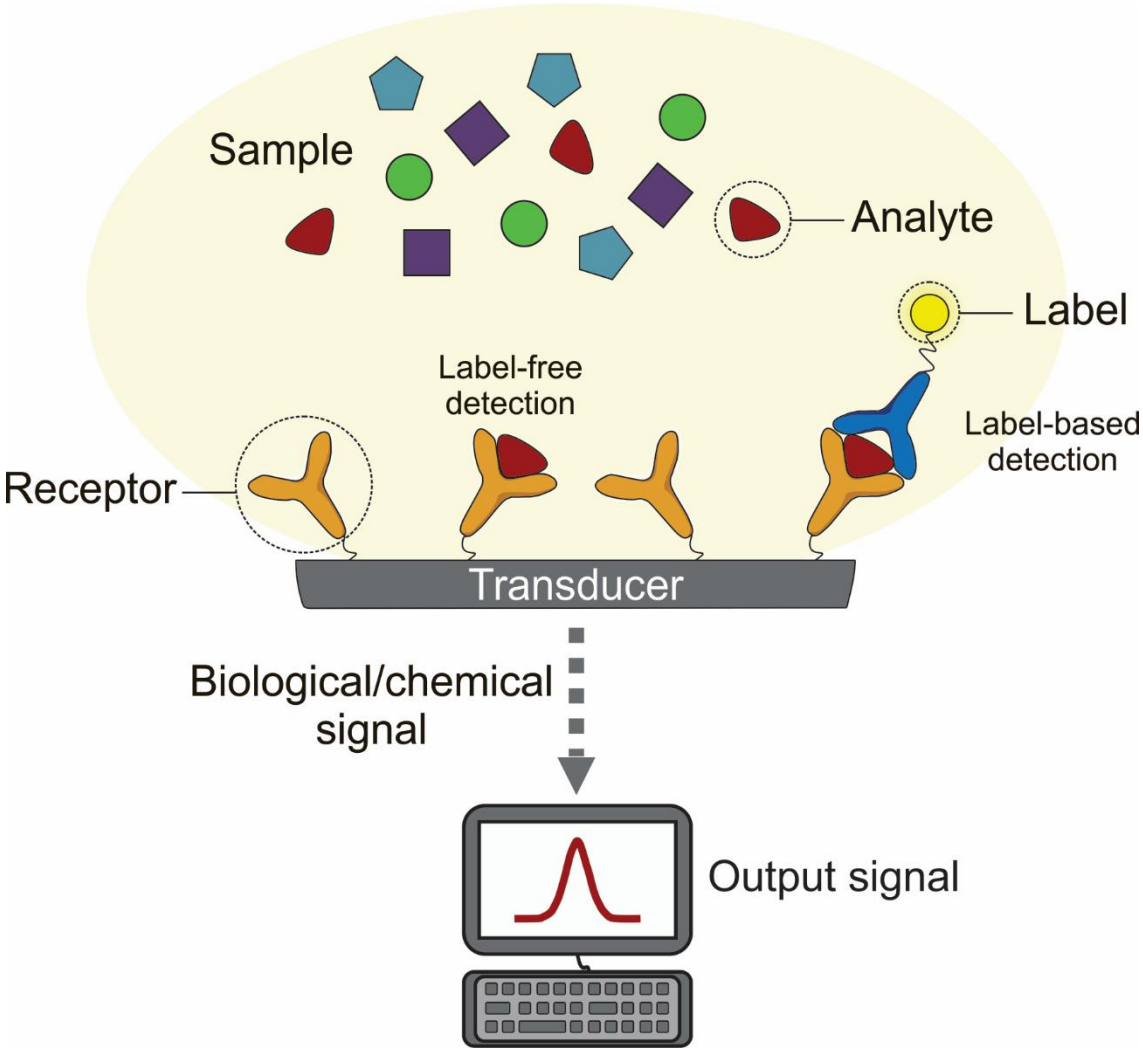

Figure 1. Schematic representation of a biosensor. It includes the complex sample where the analyte of interest is present which interacts with the specific receptor immobilized on the transducer surface. The biological/chemical signal generated by the receptor/analyte interaction is detected by the transducer directly (label-free) or indirectly (label-based) and it is converted into a readable signal by an output system.

Source: Author

Biosensor transducers

As aforementioned, transducers are the main element in a biosensor and so, they are usually used to classify them. According to the analytical signal applied, transducers are optical, piezoelectric, or electrochemical. Each transducer has advantages and limitations that will be discussed. The nature of the analytical signal of optical biosensors can be i) colorimetric, based on the color variation of the solution where analyte-receptor interaction occurs; ii) fluorescence, based on the fluorescent emission at a certain wavelength via fluorescent probes or labels; iii) luminescence, based on luminescent emission from labeled molecules[3]; or iv) spectroscopic, based on variation in the evanescent field.[8] Colorimetric, fluorescence and luminescent approaches require labelled molecules to provide the analytical signal and high-size costly equipment to readout. Therefore, their application as POC devices is challenging. On the other hand, spectroscopic-based optical biosensors are label-free approaches. The most

popularized technique is surface plasmon resonance (SPR). SPR detects in real-time the analyte-receptor interaction via variation in the refractive index from a surface plasmon wave.[8] Although functional in a wide range of applications[9], efforts now are focused on improving the sensitivity and miniaturizing the equipment required. In this matter, alternatives to the traditional SPR have appeared, such as localized surface plasmon resonance (LSPR). Nonetheless, LSPR still struggles with the requirement of costly equipment and labeled reagents, such as gold nanoparticles (AuNP) or fluorescence probes.[8] Likewise, piezoelectric transducers require costly and voluminous equipment that limit its application for the development of POC devices, despite their contribution in analytical chemistry analysis, such as it is the case of quartz crystal microbalance (QCM) for reaction kinetic studies.[10] Consequently, POC optical or piezoelectric devices require further improvements to meet the REASSURED quality level.

In contrast, electrochemical transducers have already proven their potential to be applied as POC molecular diagnosis devices, as it is demonstrated by the portable glucometers available in every drugstore that was first introduced in 1962 by Clark, et al.[11; 12] Moreover, the miniaturization of the commercial potentiostat, such as the Palmsens potentiostats[13; 14], has simplified the development of electrochemical POC assays. Electrochemical transducers convert the biochemical signal due to analyte-receptor interaction on an electrode surface into an electrical signal. The nature of the electrical signal can be potentiometric, amperometric, or impedimetric. Potentiometric transducers measure potential differences within two electrodes whilst maintaining zero current. Those are widely applied in the development of ion-selective electrodes, being pHmeter the most popular example.[15] Commercial portable potentiometric biosensors, besides pHmeters, are now available to perform rapid blood tests on-site, such as some i-STAT cartridges from Abbott.[16] Amperometric transducers measure current variation due to enzymatic catalysis[17], such as glucose oxidase in glucometers, or redox reaction on the electrode, such as the traditional ferri/ferrocyanate redox pair. Amperometric transducers can be modified with specific receptors, opening a wider range of biological, environmental, or food industry applications with high-specificity[18], compared to potentiometric assays. Nonetheless, amperometric techniques suffer from low sensitivity in comparison with impedimetric techniques, requiring, in some situations, label-based procedures. Impedimetric transducers measure complex immittance functions[19], such as impedance or capacitance, of the interface which are not accessible by transient techniques (e.g., amperometry) by employing electrochemical impedance spectroscopy (EIS) measurements. EIS-based biosensors are vastly applied in situations where high sensitivity is required. Nonetheless, the interpretation and electric circuit fitting of the data is sometimes misunderstood, due to the theoretical background complexity.[20] Impedance and capacitance-based transducers will be discussed in more detail in the following section.

Impedimetric and capacitive electrochemical transducers

Impedance or capacitance-based transducers use the electrochemical impedance spectroscopy (EIS) technique. EIS is an alternate current (AC) electrochemical technique that measures the

complex impedance (Z^*) by applying a sinusoidal voltage perturbation in a range of frequencies and measuring the current obtained.[21] EIS measurements are performed with an electrode immersed in an electrolyte solution that contains or does not have a redox probe, i.e., faradaic or non-faradaic modes, respectively. Both modes can be used in biosensing; however, the features measured and the analytical signal employed is different in each one. Non-faradaic mode measures variation in the electrostatic charge of the electrode-electrolyte interface, commonly known as double-layer capacitance (C_{dl}), due to modifications in the electrode surface, such as analyte-receptor interaction. Generally, the electrical circuit that represents those systems is the resistance of the solution (R_s) in series with C_{dl} and in parallel with the capacitance of the monolayer (C_m) whether the electrode is modified.[22] This non-faradaic EIS technique is mainly used for ion sensing.[23; 24] On the other hand, the faradaic EIS mode requires a redox probe in the electrolyte solution to measure variations in the charge transfer resistance (R_{ct}) within the electrolyte and the electrode due to variations in the electrode surface. Usually, faradaic EIS systems are modeled by the Randles circuit which includes the R_{ct} and the Warburg element (W), related to the diffusion of the redox probe in the electrolytic solution towards the electrode for the charge transfer to occurs (Figure 2), in parallel with C_{dl} and all of them in series with R_s.[22] Alternatives to the original Randles circuit have appeared to better fit the variety of faradaic approaches that have been reported in the literature.[20] Faradaic EIS with ferri/ferrocyanide redox pair in solution is the most common application of EIS in biosensing,[20] nonetheless, ferri/ferrocyanide and gold-based EIS biosensor requires carefully control to avoid data misinterpretation due to the destructive etching effect of the redox probe over the gold electrode that causes unspecific R_{ct} variation.[22; 25] Moreover, since the principle of the analytical signal in faradaic EIS biosensor is physical (and/or chemical) hindrance to charge transfer, defective electrode modification could compromise the assay sensitivity and selectivity/specificity due to unmodified electrode regions.[22; 26; 27] In general, the need of a redox probe in solution entails some limitations that hamper the release of commercial faradaic EIS, since, besides the aforementioned limitations, they would require complex microfluidic cartridges for reagent mixing to minimize the manipulation of the end-user. Alternative configurations to the traditional EIS, such as impedance-derived capacitance spectroscopy (for capacitance-based transducers), have appeared to overcome those limitations.

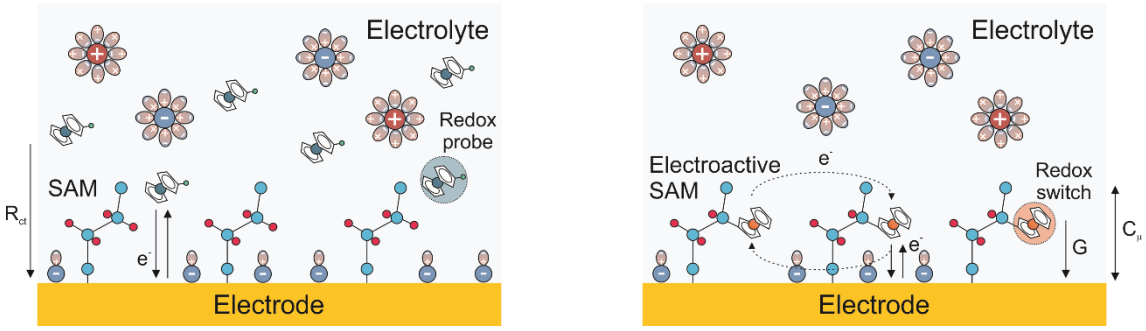

Figure 2. On the left, faradaic electrochemical impedance spectroscopy (EIS) with redox probe in solution, and on the right, impedance-derived capacitance spectroscopy (ECS) with confined redox switches on the electrode surface.

Source: Author

Impedance-derived capacitance spectroscopy is a technique derived from EIS measurements that measures the electrochemical capacitance (C_μ) of electroactive interfaces (i.e., electrodes modified with redox switches instead of being in the supporting electrolyte, such as in traditional EIS – Figure 2). C_μ is an intrinsic characteristic of those electroactive nanostructures with thickness < 5nm, related to the energy storage and density-of-states (DOS) of the interface. The use of nanoscale electroactive interfaces with quantized energy levels converts C_μ biosensors into reagentless quantum devices in which the variation in their quantum properties can be used as a high-sensitive analytical signal without additional redox probes in the solution.[28] C_μ biosensors are theoretically supported by the quantum rate theory which describes a simplistic manner of accessing the quantum characteristics of nanostructures immobilised on an electrode and depicted their application in sensing.[29; 30] The theoretical background is described in the following section.

The theoretical background of the C_μ biosensors: Quantum rate theory

The quantum rate theory has been recently described by our research group.[29; 30; 31] It resolves the quantum dynamics of the electron transfer (ET) in diffusionless electrochemical reactions, such as one of the electroactive interfaces (i.e., an electrode with continuous energy levels and electroactive molecules with discrete energy levels). ET between the electrode and the quantized nanostructures depends on the charge transport and charge storage which is measured by the quantum conductance (G) and C_μ, respectively (Figure 2). Therefore, ET rate (k), according to the quantum rate theory, is given by

$$k = \frac{G}{C_\mu} = G_0 \sum_{n=1}^{N} T_n(\mu, L) \left(\frac{1}{C_e} + \frac{1}{C_q}\right) \quad (1)$$

wherein $G_0 = g_s e^2/h \sim 77.5\ \mu S$ is the quantum of conductance (i.e., the maximum G of an ideal quantum channel), h is the Planck's constant, g_s is the degeneracy of the electron and e is the electron charge; and $\sum_{n=1}^{N} T_n(\mu, L)$ is the electron transmittance probability between two energy levels at a certain chemical potential (μ) through the N quantum channels of length L. The simplest mode of G is obtained by assuming perfect $T_n(\mu, L)$ of a single electron in a single

perfect channel, $N = 1$, where the transmittance probability equals the unity and, consequently, $G = G_0$. Additionally, the reciprocal of G corresponds with the quantum resistance (i.e., $1/G = R_q$), commonly known as R_{ct}. The quantum nature of the charge transfer resistance in diffusionless electrochemical reaction has been recently empirically and theoretically depicted by Sánchez et al.[31] The second term of Eq. 1 corresponds to C_μ which is a consequence of the series combination of an electrostatic (C_e) and quantum (C_q) capacitances, such as $1/C_\mu = (1/C_e) + (1/C_q)$. C_e arises from the charge separation (l) due to the solvation of the electroactive switches, while C_q emerges from the occupancy of the energy levels of the electroactive interface within the charge transfer with the electrode through the backbone of the electroactive molecule (L). Noteworthy is the fact that $l \ll L$ in most of the quantum C_μ interfaces; therefore, $C_e \gg C_q$, $1/C_e$ is close to zero and $C_\mu \sim C_q$ (Figure 3). The definition of G and C_μ demonstrated the quantum nature of the ET in diffusionless electrochemical processes. Assuming the aforementioned approximations, i.e., $G \sim G_0$ and $C_\mu \sim C_q$, Eq. 1 can be rearranged and simplified such as,

$$k = \frac{G_0}{C_q} = g_r g_s \frac{e^2}{hC_q} = g_r g_s \frac{E}{h} \quad (2)$$

where g_r is included as the degeneracy of the electrochemical reaction in the electroactive interface, owing to the two electrochemical states that the electroactive switch can assume, i.e., reduced/oxidized (Figure 3a) or hole/electron (Figure 3b). In Eq. 2, C_q is the single variable that k is dependent and experimentally accessible by EIS measurements converted to capacitance.[29; 31] Thus, C_q can be used as analytical signal in biosensing which, as aforementioned, is related to the energy storage, such as $E = e^2/C_q$ [32], and the DOS of the interface, $C_q = e^2 \cdot (dN/d\mu) = e^2 \cdot DOS$. Moreover, the thermal broadening of the energy levels by statistical mechanics enables a more realistic definition of C_q [33],

$$C_q = \frac{e^2 \cdot N}{k_B T} f(1-f) \quad (3)$$

wherein k_B is the Boltzmann's constant; T is the absolute temperature; N is the ensemble of quantum channels contributing to the charge transfer. Each quantum channel constitutes a single $r_q c_q$ microstate; and $f = n/N = (1 + e^{\mu - E_r/k_B T})^{-1} = (1 + e^{-eV/k_B T})^{-1}$ is the Fermi-Dirac function that describes the occupation of the energy levels, where E_r is the Fermi-level of the interface (or, in the case of redox films, the formal potential E_r/e of the redox molecules ensemble). Note that $-eV = \mu - E_r$ and, therefore, at the Fermi-level, i.e., $\mu = E_r$, $f = 1/2$ (which depicts that half of the levels are occupied and half unoccupied), $f(1-f) = 1/4$ in Eq. 3 and C_q maximizes.

Those statements demonstrate that C_q biosensors operate in a purely quantum regime and by accessing ET in a much simplistic manner, a vast range of applications is possible, not only in biosensing by using as analytical signals k, G or C_μ, but in other research fields. The quantum

rate theory has been suitable for model redox SAMs[29], mixed oxide films[34], graphene[35; 36; 37], and quantum dots (under preparation for publication).

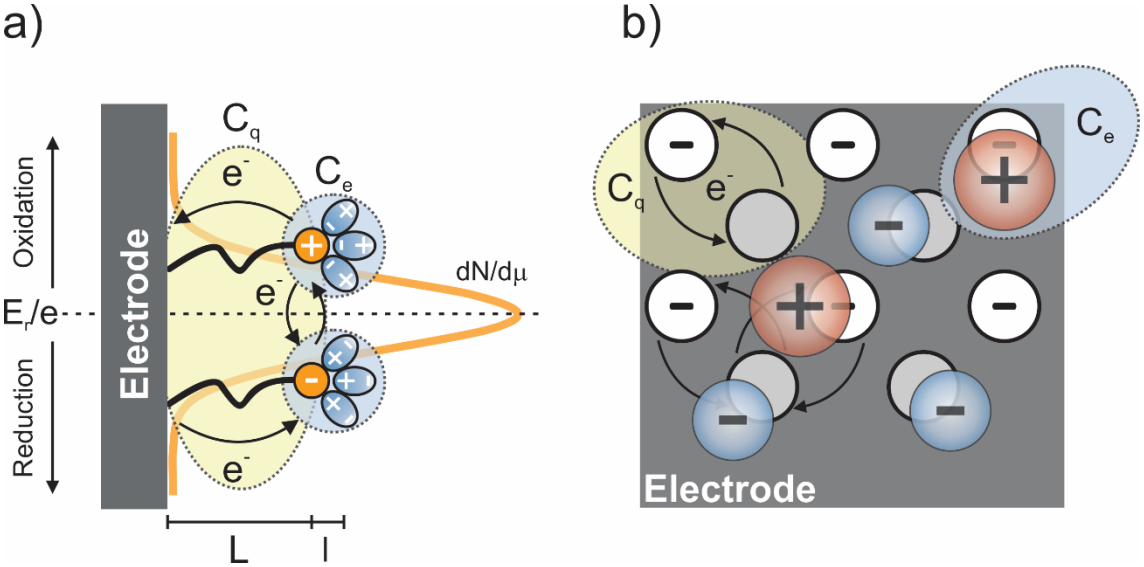

Figure 3. Schematic representation of the electrochemical capacitance (C_μ) of electroactive interfaces of a) a redox SAM and b) a semiconductor. In a), it is represented the charge transfer from/to the electrode to/from the electroactive molecules through the distance L and the non-faradaic contribution due to the ionic solvation around the electroactive centers (l); $dN/d\mu$ is the density-of-state (DOS) of the electroactive interface and E_r/e is the formal potential of the electroactive interface at which half of the electroactive molecules are oxidized and half reduced. In b), it is represented the generation of holes (grey circles) and the occupation of electrons (white circles with a dash) due to the charge transfer within the HOMO-LUMO energy levels. Again, it is generated charge separation due to the (de)occupation of the energy levels (L), related to C_q and the solvation of the charge carriers (l), related to C_e. Note that in both situations $l \ll L$, demonstrating that $C_e \gg C_q$ and $C_\mu \sim C_q$, as discussed in the main text.

Source: Author

Furthermore, the quantum rate theory comprised the equivalent electric circuit to fit the experimental data as additional theoretical background support (Figure 4). Two main branches are identified in the electrical circuit: the non-faradaic (blue in Figure 4a) and the faradaic branch (orange in Figure 4a). The non-faradaic branch comprises C_m, R_t and C_t related to the monolayer capacitance and the ionic relaxation, whilst the faradaic branch contains R_q and C_q related to the quantum ET. R_q and C_q are the average values of the $r_q c_q$ microstates ensemble composed by each electroactive switch in the interface, as illustrated in Figure 4b. The electroactive interfaces are often characterized by cyclic voltammetry, CV (Figure 4c), which delimits the redox active window of the interface and enables the calculation of its Fermi-level (or formal potential), E_r/e. The information provided by CV measurements is applied for impedance-derived capacitance spectroscopy measurements to differentiate between the faradaic C_q and non-faradaic C_{NF} contributions, measured at the E_r/e and E_{out}, i.e., outside the electroactive window, respectively (Figure 4d).

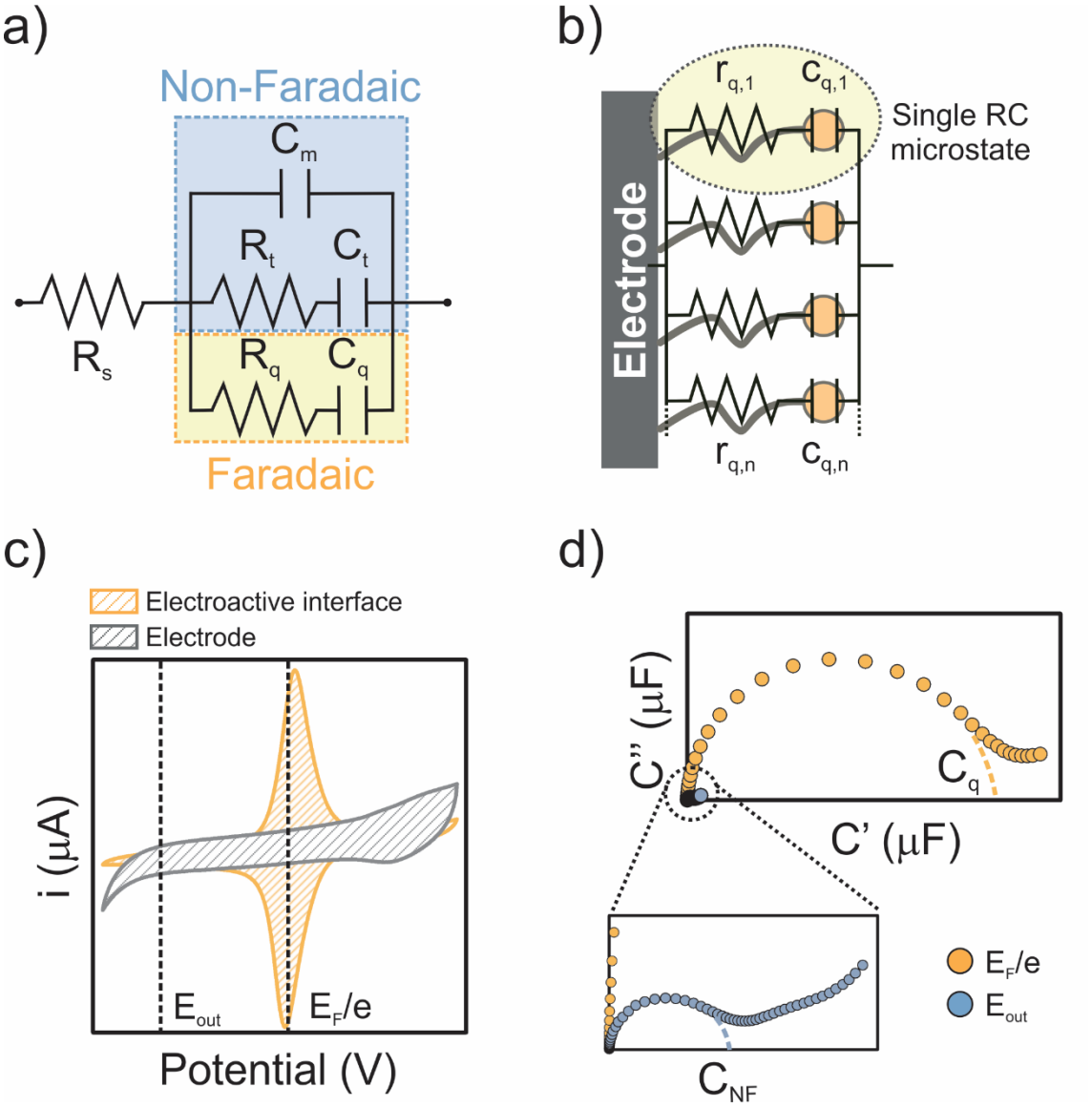

Figure 4. Data modeling and interpretation. a) Electric circuit for impedance-derived capacitance spectroscopy modeling which comprises a non-faradaic (blue) and faradaic branch (orange). R_q and C_q in the faradaic branch represents the average values of the RC microstates ensemble depicted in b). c) Cyclic voltammogram and d) capacitive Nyquist plot of an electroactive interface. In c), E_F/e is the Fermi-level of the interface (or formal potential), obtained as the arithmetical average of the oxidation and reduction potentials (i.e., $(E_{ox} + E_{red})/2$). In d), C_q is the quantum capacitance measured at the E_F/e (orange), whilst C_{NF} is the non-faradaic capacitance measured outside the electroactive window, E_{out} (blue). Both capacitive values are obtained from the semicircle values in the Nyquist plots.

Source: Author

C_q biosensors have been improved through the years to overcome the limitations observed in certain applications in terms of sensitivity, specificity, selectivity, or other analytical features by the incorporation of new electroactive materials for transducer development, such as graphene[38; 39] or quantum dots (under preparation for publication), or by the incorporation of novel electrochemical reactions, such as the coupling of the electrochemical process of two redox switches with similar E_F/e.[40; 41] The later has demonstrated applications as an amplifier signal methodology in C_q transducers. Several signal amplifier strategies coupled to

electrochemical transducers have been reported in the literature, as reviewed by Liu et al.[42] In general, those strategies are based on the use of nanomaterials, enzyme catalysis, or isothermal nucleic acids amplification methodologies; nonetheless, they require additional steps or labeled reagents that increase the assay duration or the end-user manipulation (likewise label-based assays). Within those amplification methodologies, none of them has been described for C_q transducers. In this project, it was proven a novel label-free amplification strategy without additional steps for C_q biosensors, patented by our research group.[40] It will be described in the results section.

As was discussed in this section, the mechanisms involved in C_q transducers are acutely depicted and understood by the quantum rate theory. This knowledge enables the application of C_q transducers in biosensing with higher efficiency, the improvement of their analytical performance, and the continuous discovery and study of new types of C_q transducers and applications.

C_q biosensors applications: Qualitative and quantitative assays

Capacitive biosensors have been applied for the detection or quantification of several analytes[28] which includes analytes from infective agents (e.g. Dengue virus) and human proteins related to non-communicable diseases (NCDs, e.g. Alzheimer's disease). Each application requires different sensing characteristics, for example, in the case of the diagnosis of viral infections just the detection of the viral protein is necessary for diagnostic (qualitative assays), while in the case of NCDs, the concentration of the analyte is the biomarker of the disease and thus, it requires more complex quantitative assays. In any case, C_q biosensors could bring advantages to traditional diagnosis techniques.

Viral infections are a health threat worldwide from their emergence until the design of a vaccine or an effective drug discovery. Throughout that period, disease-spread control is necessary and, as discussed previously, biosensors become one of the most important tool. For example, the emergence of the novel SARS-CoV-2 (severe acute respiratory syndrome 2), responsible of Covid-19 pandemic, at the end of 2019 evidenced this need.

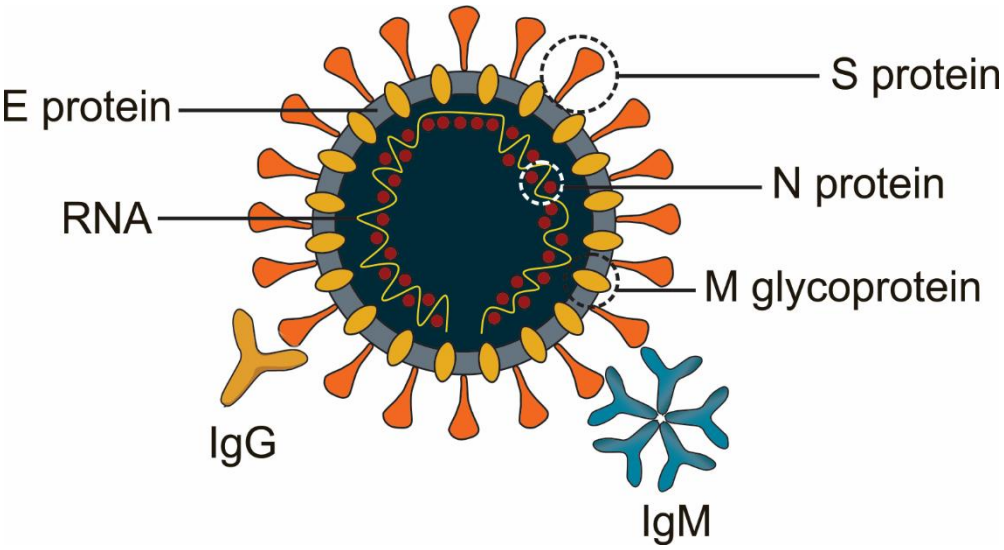

Figure 5. SARS-CoV-2 virion structure and possible targets for biosensor development. S: Spike protein; N: Nucleocapsid protein; M: Membrane glycoprotein; IgM: Immunoglobulin M; IgG: Immunoglobulin G; RNA: viral genome; E: Envelope protein. Adapted from reference Morales-Narváez and Dincer.[43]

Source: Author

SARS-CoV-2 is the novel circulating member of the family *Coronaviridae* that rapidly spread worldwide and became a global health threat. Since the first case, 610 million cases and 6.5 million deaths have been registered as of September 21st, 2022, according to the World Health Organization.[44] The shape of the SARS-CoV-2 virion particles are spherical with spike projections (Figure 5). From the most external to the internal layer, the virion is composed mainly of four structural proteins: spike (S), membrane (M), envelope (E), and nucleocapsid (N) proteins; and a positive sense RNA sequence (+ssRNA). Human cell infections are achieved by the S protein interaction with the human receptor angiotensin-converting enzyme 2 (ACE2).[45] rRT-PCR (reverse real-time PCR) is the gold-standard molecular technique to diagnose SARS-CoV-2 infection by detecting the viral RNA. Nonetheless, besides the already described limitations associated with the technique, the situation was aggravated by reagent shortage. Therefore, efforts were addressed to biosensor development. Biosensors can be designed by targeting:

i) The viral genome, such as the graphene-based electrochemical assay proposed by Alafeef et al.[46] which used gold nanoparticles (AuNP) modified with DNA sequences complementary to the N-gene whose interaction with the virus RNA causes a variation in the electrode voltage; the electrochemical assay based on isothermal rolling circle amplification proposed by Chaibun et al.[47] which used complementary probes to the product resulting from the amplification step with redox labels, increasing the current with the presence of the virus; or the amplifier-free electrochemical biosensor from Kashefi-Kheyrabadi et al.[48] which used a similar approach as Chaibun et al.[47] with complementary probes with redox labels, but avoiding the amplification step. Those approaches aimed to substitute and overcome the limitations associated with rRT-PCR assays. Nonetheless, they still require sample pre-treatment for RNA purification which could compromise the results and increase the duration of the assay.

ii) The human immunoglobulins, IgG and IgM, are produced by the immune system against the viral proteins, such as Elledge et al.[49] which described a luminescent assay to detect anti-SARS-CoV-2 antibodies by using nanoluciferase fragments linked to viral protein fragments. Those fragments interact with the antibodies in the samples and by doing so, the nanoluciferase fragments are close enough to interact with each other, reconstituting the nanoluciferase enzyme with luminescence activity; or the electrochemical graphene-based multiplexed assay proposed by Torrente-Rodríguez et al.[50] which measured current variations after the antibody interaction with the target immobilized on the electrode surface by using redox probe in the supporting electrolyte. Serological assays enable the detection of the immune response after the viral infection or the vaccine application. Nonetheless, they are not a feasible option for the early diagnosis, since IgG and IgM are produced 7 days after the infection.

iii) The viral proteins, such as S or N proteins, are the main alternative to rRT-PCR, since their detection enables the direct and rapid diagnosis of SARS-CoV-2 infection.[43] Several assays have been reported in the literature to detect S and/or N protein, such as the microfluidic magneto electrochemical assay from Li and Lillehoj.[51] The assay used magnetic nanoparticles (MNP) modified with an antibody anti-N protein used to pre-concentrate the sample before its incubation with an electrode modified with a secondary antibody anti-N. The presence of the complex MNP-Ab1-N protein-Ab2 in the electrode was measured by current variation. Likewise, Nascimento et al.[52] used MNP for the detection of the S protein in saliva samples. Although they achieved high sensitivity (50 pg mL^{-1} in Li and Lillehoj[51] and 0.35 ag mL^{-1} in Nascimento et al.[52]), the detection of the analyte was not direct, since it required previous enrichment steps that delayed the result released. On the other hand, Nguyen et al.[53], Raziq et al.[54], Seo et al.[55], and Yousefi, et al.[56] used direct approaches to detect the analytes based on phononic, electrochemical molecular imprinted polymer (MIP), field effect transistor (FET) and electrochemical with tethered redox probe devices, respectively (Table 1). So far, no capacitive biosensor for the detection of SARS-CoV-2 has been described. Nonetheless, electrochemical capacitance would enable the development of a high-sensitive, robust, and direct POC device with low-cost reagents and equipment that compete with the already described devices.

Table 1. Examples of SARS-CoV-2 direct detection devices.

Transducer	Receptor/target	Biosensing interface	LOD	Reference
FET	Ab anti-S / S protein or virion	Graphene-PBASE-Ab	100 fg mL^{-1} (in CTM) 242 copies mL^{-1} (in clinical samples)	[55]
Chronoamperometry	Ab anti-S / S protein or virion	Redox DNA linker-Ab	$4 \cdot 10^3$ virions mL^{-1}	[56]
DPV	N-protein MIP	MIP-redox probe in solution	15 fM	[54]
Phononic	Ab anti-S / S protein or virion	Graphene-PBASE-Ab	1 fg mL^{-1} (in PBS) 3.75 fg mL^{-1} (in saliva)	[53]
Electromechanical FET	Aptamer probe / SARS-CoV-2 RNA	Graphene-tetrahedral dsDNA base-flexible ssDNA-aptamer probe	~0.02 copies μL^{-1}	[57]
EIS	Aptamer / S protein or virion	Au-aptamer-redox probe in solution	-	[58]

LOD: Limit of detection. FET: Field-effect transistor. PBASE: 1-pyrenebutyric acid *N*-hydroxysuccinimide ester. CTM: Clinical transport medium. DPV: Differential pulse voltammetry. MIP: Molecular imprinted polymer. EIS: Electrochemical impedance spectroscopy.

Dengue virus is another example of an infectious disease that requires rapid and specific diagnosis, since, so far, there is no vaccine. Dengue virus is an RNA *Flavivirus* member of the family *Flaviviridae*. It is an arbovirus transmitted by the bite of infected female mosquitoes which causes a huge number of cases throughout countries in the Americas, especially in Brazil where it was registered 975 thousand cases in 2021, according to the Pan American Health organization.[59; 60] Moreover, several serotypes of Dengue virus have been described and re-infection could increase the severity of the disease to dengue haemorrhagic fever. Therefore, the rapid diagnosis of Dengue virus infection could monitor the progression of the disease and decrease the number of deceases.

The Dengue virion consists of a spherical particle composed of structural proteins from the envelop (E) and membrane (M) embedded in a lipidic bilayer. Inside the envelope, it is placed the nucleocapsid composed of capsid proteins (C) and the RNA genome (Figure 6). Besides the structural proteins, the RNA genome codifies non-structural (NS) proteins that are involved in the virus replication and virion assembly.[61]

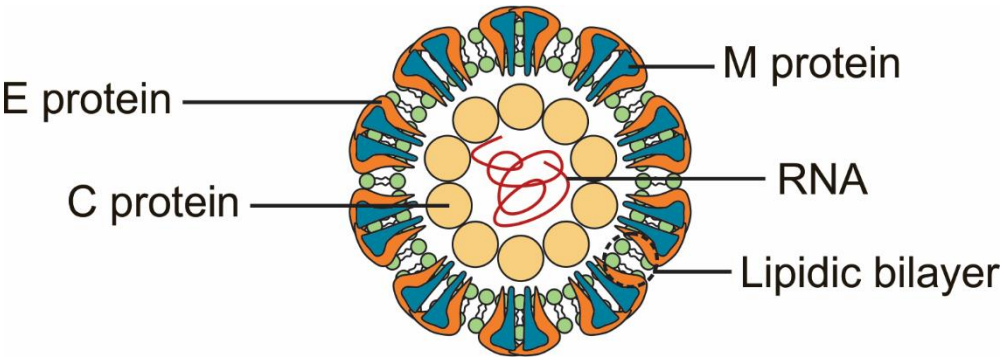

Figure 6. Dengue virion particle. E: Envelope protein (in orange); C: Capsid protein; M: Membrane protein (in blue); RNA: viral genome. Adapted from references [61] and [62].

Source: Author

The gold standard molecular techniques to diagnose the infection are rRT-PCR to detect the viral genome and ELISA to detect the viral protein NS1 or the immunoglobulins IgG and IgM.[63] Again, due to the limitations aforementioned associated with PCR and ELISA, electrochemical POC devices are being developed with similar molecular targets (i.e., RNA and NS1 protein), as reviewed by Anusha, et al.[64] and Nicolini, et al.[65] Some of the assays developed are summarized in Table 2. Moreover, electrochemical capacitance has been used to develop a qualitative biosensor for the detection of NS1 in serum samples with high specificity by using a redox-peptide self-assembled monolayer and antibody anti-NS1 as a molecular receptor.[66] Nonetheless, the device was not miniaturized for application in the field and it needed improvements, such as using miniaturized gold microfabricated electrodes and lower limit of detection (LOD) in neat serum samples.

Table 2. Examples of electrochemical biosensors for Dengue virus detection.

Transducer	Receptor/target	Biosensing interface	LOD	Reference
EIS	Ab anti-NS1 / NS1	Au-MUA/6-MH SAM-Ab and redox probe in solution	30 ng mL^{-1}	67
ECS	Ab anti-NS1 / NS1	Au-11-Fc/16-MHA SAM-Ab	0.05 ng mL^{-1}	68
Amperometry	Ab anti-NS1 / NS1	GCE-MWCNT-PAH-Ab and HRP labeled Ab	0.035 µg mL^{-1}	69
Cyclic voltammetry DPV	DNA probe / DENV RNA	FTO-ZnO/Pt-Pd nanocomposites-DNA probe and methylene blue	$4.3 \cdot 10^{-5}$ M	70
EIS	DENV2 NS1 / Ab anti-DENV2	GCE-MWCNT-polypyrrole amide linker-DENV2 NS1 and redox probe in solution	10^{-12} g mL^{-1}	71
DPV	DENV3 DNA probe / DENV3 RNA	PGE-DENV3 DNA probe	3.09 nM	72
ECS	Ab anti-IgG / IgG Ab anti-NS1 / NS1	Au-11-Fc/PEG thiol SAM	231 pg mL^{-1} 340 pg mL^{-1}	73

MUA: 11-mercaptoundecanoic acid. 6-MH: 6-mercaptohexanol. ECS: Electrochemical capacitance spectroscopy. 11-Fc: 11-ferrocenyl-undecanethiol. 16-MHA: 16-mercaptohexadecanoic acid. GCE: Glassy carbon electrode. MWCNT: Multi-walled carbon nanotubes. PAH: poly(allylamine). DENV: Dengue virus. FTO: Fluorine-doped tin oxide. DENV2: Dengue virus serotype 2. DENV3: Dengue virus serotype 3. PGE: Pencil graphite electrode. PEG: Polyethylene glycol thiol.

As aforementioned, C_μ transducers are also adequate for the quantification of analytes in complex samples, being a high-sensitive tool for the early diagnosis of NCDs whose biomarkers are concentration-dependent, such as Alzheimer's disease (AD).

AD is a neurodegenerative type of dementia (represents 60-70% of the overall cases[74]) that causes cognitive deterioration. Although AD is a complex disease with a complex aetiology, two main molecular events characterized it: i) the deposition and accumulation of amyloid β plaques due to the misprocessing of the amyloid β precursor protein; and ii) the formation of tau neurofibrillary tangles (Figure 7). Both events contribute to neuroinflammation and neuron and synapsis degeneration.[75]

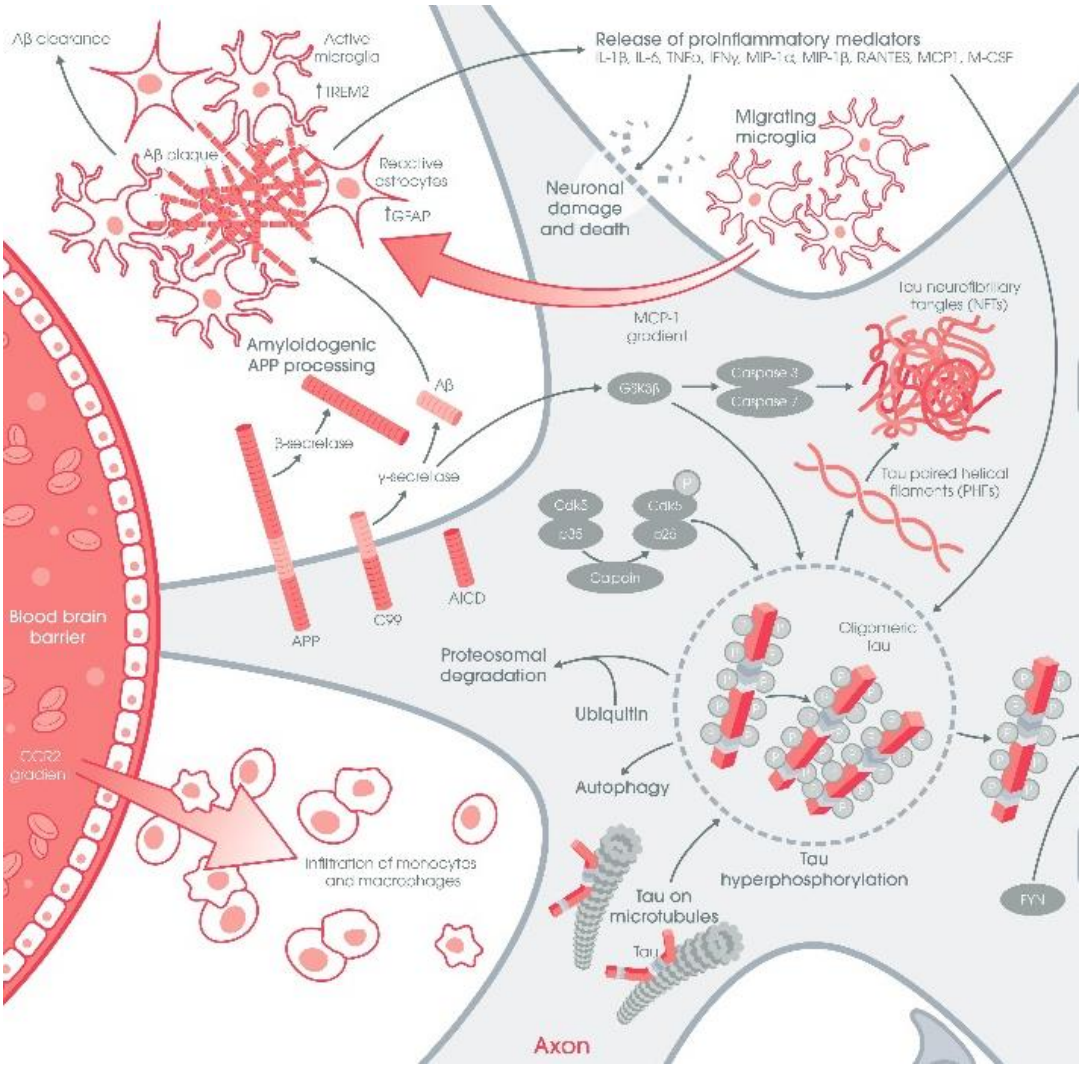

Figure 7. Schematic representation of the formation of $A\beta$ plaques and tau neurofibrillary tangles responsible for neuroinflammation and neuron degeneration in Alzheimer's disease. Adapted from [76].

Source: Abcam plc.

AD diagnosis is based on cognitive tests, image techniques, and the concentration of tau and amyloid β proteins in cerebrospinal fluid (CSF).[77] Regarding treatment against AD, there are symptomatic treatments available, such as the one based on acetylcholinesterase inhibitors to slow down cognitive deterioration,[78] and treatments to reduce the accumulation of Aβ plaques, such as it is the case of the monoclonal antibodies anti-Aβ aducanumab, approved in 2021, and lecanemab, which still requires further analysis, but it has appeared as the most promising alternative.[79] Many research groups worldwide are still focused on developing a successful treatment; nonetheless, because the causes of AD are unknown and the difficulties associated with an early diagnosis at which the neural damage is not critical yet, that is not an easy achievement.[75] Therefore, the discovery of new biomarkers related to the early stages of the disease and the development of high-sensitive analytical approaches to monitor those biomarkers could contribute to the discovery and evaluation of new treatments.

As aforementioned, tau and amyloid β proteins are already accepted biomarkers in CSF, as reviewed by Huynh et al.[80] and Molinuevo et al.[75] Nonetheless, the use CSF biomarkers

complicate the periodic control of the proteins and thus, the early diagnosis, since invasive methodologies are required to collect the sample. For that reason, the use of biomarkers in the blood is preferred, although the biomarkers are in a lower concentration. Similar AD CSF biomarkers are found in blood, such as the Aβ-42/Aβ-40 rate and tau isoforms. Specifically, from the latter group, ptau-181 (phosphorylated tau 181) has been recently analyzed as a potential premature biomarker.[81] Moreover, other types of proteins have been described as candidates to compose a panel of AD biomarkers to facilitate the early AD diagnosis, such as the protein ADAM10 (a disintegrin and metalloproteinase 10).[82]

On the other hand, ADAM10 is a ~55-65 kDa α-secretase involved in the cleavage of the amyloid β precursor protein into a soluble fragment (i.e., not involved in neurodegeneration).[83] Colciaghi et al.[84] reported a difference in the ADAM10 concentration in platelets between healthy individuals and early-stage AD patients which was also observed in blood serum by Vatanabe et al.[85] and Oliveira et al.[86] Moreover, Oliveira et al.[86] developed the first analytical device for the quantification of ADAM10 in serum samples. The amperometric device was composed of graphite electrodes modified with PDDA (poly-(diallyldimethylammonium chloride), AuNP and antibody anti-ADAM10. Magnetic nanoparticles (MNP) modified with a secondary antibody anti-ADAM10 were used for the detection (or quantification) of the analyte. Nonetheless, the device was label-based, so it also had time and cost limitations as well as the ptau-181 quantification methodology described by Karikari et al.[87] Electrochemical capacitance can be applied for the label-free quantification of ADAM10 in patient samples with high-sensitivity.

Tau protein is a microtubule-associated protein, predominantly expressed in neurons. Their phosphorylation reduces the affinity for microtubules and promotes aggregation and the formation of the neurofibrillary tangles. Several phosphorylation patterns have been studied for potential AD biomarkers in blood, as is the case of tau protein phosphorylated at the 181 reside.[81; 87] Tatebe et al.[81] depicted for the first time that ptau-181 was significantly increased in patients with AD in blood. Likewise, Karikari et al.[87] reported an increase by using a label-based methodology to quantify the ptau-181concentration in AD patients, patients with mild cognitive impairment (MCI), and healthy individuals. Although they depicted a high-sensitive methodology, it was label-based, so it had limitations associated with the number of steps, reagents, and assay duration. High sensitivity can be achieved with label-free techniques and direct detection methodologies, such as electrochemical capacitance.

According to the information discussed, in this Ph.D. project we proposed the use of electrochemical capacitance transducers to develop novel biosensing assays for the diagnosis of relevant diseases: SARS-CoV-2 infection by the detection of spike protein (SP) and nucleocapsid protein (NP) in nasopharyngeal/oropharyngeal samples; Dengue virus infection by the quantification of NS1 protein in serum samples; and to diagnose AD and to evaluate the effects of the treatments by the quantification of ptau-181 and ADAM10 proteins in human serum samples.

2. Objectives

The general objective of this Ph.D. project was to develop novel capacitive biosensors for the rapid diagnosis of relevant diseases. This main objective was separated into several specific objectives:

i. To develop a qualitative biosensor for the detection of SARS-CoV-2 infections with high sensitivity and specificity by detecting the presence of the viral proteins Spike and Nucleocapsid in nasopharyngeal/oropharyngeal patient samples.

ii. To develop a miniaturized high-sensitivity quantitative biosensor for the diagnosis of Dengue virus infections by quantifying the viral protein NS1 in serum samples for the premature diagnosis of dengue fever.

iii. To develop for the first time a label-free quantitative biosensor for the quantification of the concentration of ADAM10 in patient serum samples for the premature diagnose of AD or the disease screening.

iv. To develop for the first time a label-free quantitative biosensor for the quantification of the protein ptau-181 in neat serum samples for the premature diagnose of AD or the disease screening.

3. Material and methods

Chemical reagents and proteins.

The list of chemical reagents and proteins used in the development of the Ph.D. project is compiled in Table 3.

The ferrocene-tagged peptide used as a redox self-assembled monolayer (of thickness ~ 1.4 nm in aqueous solutions) was Fc-Glu-Ala-Ala-Cys, synthesized by solid phase peptide synthesis using Fmoc protocols on rink amide resin (0.48 mmol g^{-1}). Coupling was performed at a 2-fold molar excess relative to the amino component in the resin, using diisopropylcarbodiimide (Dic)/ 1-hydroxybenzotriazole (HOBt). Fmoc groups were deprotected using 20% 4-methylpiperidine/dimethylformamide (DMF) for 20 min. The ferrocene redox probe was introduced at the N-terminus by reaction with one molar equivalent 3-ferrocenylpropionic anhydride in 5 mL DMF (1:1) for 24 h. Peptide cleavage was performed by removing side chain protecting groups with 95% trifluoroacetic acid (TFA), 2.5% H_2O, and 2.5% triisopropylsilane for 2 h. The peptide was then precipitated with diethyl ether and separated from the reaction solution by centrifugation. Then, it was solubilized with acetonitrile/H_2O (v/v) and separated by centrifugation.

The cadmium telluride quantum dots (CdTe QD) of size 2.23 nm were synthesized and provided by Prof. Marco Antonio Schiavon research group.

The antibody solutions were prepared in 12 mM phosphate buffer (PB) containing 3.59 g L^{-1} $Na_2HPO_4 \cdot 12H_2O$ and 0.27 g L^{-1} KH_2PO_4. All the solutions were prepared using deionized water from the Milli-Q system (18.2 MΩ.cm at 25°C) from Millipore.

Table 3. List of chemical reagents and proteins used in the Ph.D. project.

Reagent	Company	Catalog number
0.3μm alumina suspension	Buehler	40-6363-006
0.05μm alumina suspension	Buehler	40-10083
Polishing cloth	Buehler	40-7738
Sodium hydroxide (NaOH)	Sigma-Aldrich	S5881
Sulfuric acid (H_2SO_4)	Qhemis	QHA008
Ethyl alcohol, pure	Sigma-Aldrich	E7023
Isopropyl alcohol	Synth	A1078
Acetonitrile (ACN) for HPLC	Sigma-Aldrich	34851
Tetrabutylammonium perchlorate ($TBAClO_4$)	Sigma-Aldrich	86893
Sodium phosphate dibasic dodecahydrate	Sigma-Aldrich	71650
Potassium dihydrogen phosphate	Sigma-Aldrich	P5655
Phosphate buffered saline (PBS) tablets	Sigma-Aldrich	P4417
Ferrocenecarboxylic acid (FcA)	Sigma-Aldrich	46264
N-(3-Dimethylaminopropyl)-N'-ethylcarbodiimide hydrochloride (EDC)	Sigma-Aldrich	03450
N-Hydrosuccinimide (NHS)	Sigma-Aldrich	130672
SuperBlock blocking buffer in PBS	Thermo Fisher	37515
Human serum	Sigma-Aldrich	H4522
Monoclonal anti-ADAM10 antibody (Ab1)	Abcam	ab59482
Polyclonal anti-ADAM10 antibody – middle region (Ab2)	Aviva System Biology	OAGA02442
Human recombinant ADAM10	Prospec	PRO-476
Phospho-Tau (Thr181) monoclonal antibody	Thermo Fisher	MN1050
Tau-441, GSK3beta-phosphorylated	Signal Chem	T08-50FN
Monoclonal anti-Dengue virus NS1 glycoprotein antibody	Abcam	ab41616
Recombinant Dengue virus 1 NS1 protein	Abcam	ab181950
Polyclonal anti-SARS-CoV-2 spike protein antibody	RheaBiotech	IM-0828
Monoclonal anti-SARS-CoV-2 nucleocapsid protein antibody	Abcam	Ab272852

Equipment and electrodes.

Electrochemical measurements were performed in a portable PalmSens potentiostat equipped with a frequency response analysis (FRA) module by using a 3 electrodes electrochemical cell containing a working electrode, Ag|AgCl (3 M KCl) as reference electrode, and a platinum disc as the counter electrode (Figure 8a).

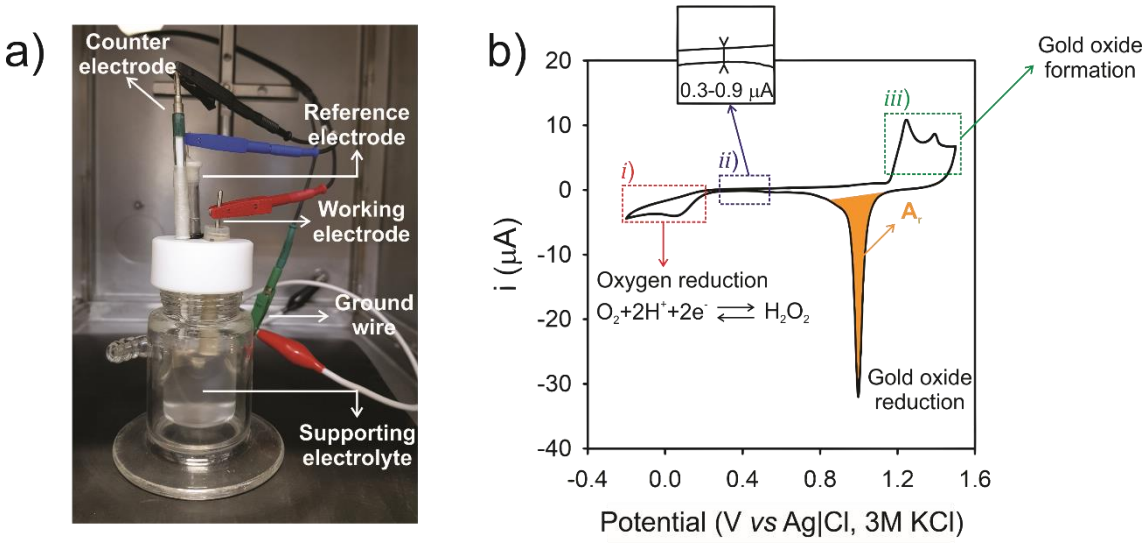

Figure 8. Experimental setup and representative gold characterization. a) Electrochemical cell used during the experiments. b) Representative voltammogram of the electrochemical characterization of gold Metrohm electrodes in 0.5 M H_2SO_4. The insets depict the regions of the CV where essential information about the gold surface state is observed. i) Region of reduction of oxygen. ii) Is indicative of contaminants adsorbed on the gold surface. On a clean surface, a minimum capacitive current (within 0.3-0.9 µA) is observed. iii) In this region between c.a. 1.2-1.6 V (*versus* Ag|AgCl; 3 M KCl) gold oxide is formed in the interface. The peaks represent the orientation or the shape of the crystalline gold lattice of the polycrystalline electrode exposed to the solution phase. They are, respectively from reduction to oxidation direction, cubic, octahedric, or rhombic dodecahedric.[88]

Source: Adapted from Garrote et al.[28]

The electrodes used in the experiments developed in this project were: Au electrodes purchased from Metrohm (diameter 2mm, cat. No. 6.1204.140), miniaturized Au electrodes fabricated on Si/SiO_2 wafers, and single-layer graphene (SLG) obtained via chemical vapor deposition (CVD) on 90 nm SiO_2 over a Si substrate purchased from Graphenea.

Working electrodes pre-treatment.

The pre-treatment protocol was different for each working electrode. Each protocol is detailed below.

- *Au Metrohm electrode pre-treatment*.

Au Metrohm electrodes were slightly polished by 0.3 and 0.05 µm alumina suspension on the polishing cloth. After each alumina, the electrodes were sonicated for 2min in deionized water to remove the alumina residues. After the mechanical polishing, the electrodes were electrochemically polished under basic conditions by cyclic voltammetry (CV) in 0.5 M NaOH (100 cycles from -1.7 to -0.7 V *versus* Ag|AgCl, 3 M KCl at 0.1 V s^{-1}). Afterward, the electrodes

were immersed for 30 min in stirring ethanol solution to remove the remaining oxide residues. Finally, the electrodes were electrochemically polished under acidic conditions by CV in 0.5 M H_2SO_4 (50 cycles from -0.2 to 1.5 V *versus* Ag|AgCl, 3 M KCl at 0.1 V s^{-1}). The area of the reduction peak obtained in the sulphuric acid CV (Figure 8b) was used to calculate the electro-active area of the polished gold surface by using a conversion factor of 410 µC cm^{-2}.[89] The ratio of the electro-active area to the geometric electrode area (0.03142 cm^{-2}) corresponded to the electrochemical surface roughness. The surface roughness was maintained below 1.5 to ensure reproducible and stable molecular film properties. This protocol is described in detail in Garrote et al.[28]

- *Miniaturised Au electrode pre-treatment*.

The miniaturized gold electrodes were fabricated on Si/SiO_2 wafers. Firstly, the wafers were patterned using lase-writer photolithography, and then the Ti adhesion layer (10 nm thickness) was deposited before the deposition of the Au layer (100 nm thickness). The electroactive area of the working electrode (SiO_2/Au) was 1 mm^2. The pre-treatment of the Au electrodes consisted of immersing the miniaturized electrodes in several solvents (isopropyl alcohol, acetone, isopropyl alcohol, and deionized water) and sonicating for 12 min in each solvent. Then, the electrodes were dried with nitrogen and kept for 30 min in UV/Ozone radiation.

- *Single-layer graphene (SLG) pre-treatment*.

The SLG electrodes were electrochemically pre-treated to generate functional groups for receptor immobilization. This protocol is under patenting process, so the details will not be revealed here.

Electrochemical capacitive immunosensor fabrication.

Immunosensors were obtained from freshly pre-treated working electrodes (protocols depicted in the previous subsection). Au electrodes (either from Metrohm or miniaturized electrodes) were modified with ferrocene-tagged peptide self-assembled monolayer (SAM) by immersing them in 2 mM redox peptide solution in ACN/deionized water (1:1, v/v) for 16h at room temperature (25 °C). After the chemical modification, the electrodes were rinsed in acetonitrile/water and deionized water, and characterized by cyclic voltammetry (CV) to ensure the correct formation of the SAM and to calculate its formal potential ($E_F/e = (V_{ox} + V_{red})/2$, wherein V_{ox} is the oxidation potential and V_{red} is the reduction potential - Figure 4c). The CV was performed from -0.0 to 0.7 V *versus* Ag|AgCl, 3 M KCl at a scan rate of 0.1 V s^{-1} in 20 mM of $TBAClO_4$ dissolved in ACN/deionized water (1:4 v/v) as a supporting electrolyte. In the assay with an amplifier signal, E_F/e is the potential at which the electronic coupling is achieved between the states of the redox active sites confined on the electrode and that of the diffusive redox probe in solution. To obtain that value, CV was performed with the same parameters but using 100 µM FcA in 20 mM of $TBAClO_4$ dissolved in ACN/deionized water (1:4 v/v) as a supporting electrolyte. In those assays, the redox-peptide SAM was used as a signal transducer, owing to the quantum features of the ferrocene confined on the electrode (coupled with the redox probe

in solution, in the case of amplifier signal, Figure 9b), and as a linker for receptor immobilization, owing to the carboxylic acid functional group from the Glu of the peptide backbone (Figure 9a).

CdTe quantum dots (QDs)-based assays were performed with miniaturized Au electrodes. Firstly, the electrodes were modified with a monolayer of L-cysteine by immersing the electrodes in 50 mM L-cysteine aqueous solution for 16h at room temperature (25 °C). Then, the electrodes were rinsed with deionized water and immersed in an aqueous solution containing 0.2 mM CdTe QDs, 0.1 g mL^{-1} EDC and 0.1 g mL^{-1} NHS for 3h at room temperature (25 °C) in the dark for QDs immobilization by the carbodiimide reaction[90] between the amine groups in the L-cysteine and the carboxylic acid groups in the CdTe QD surface. After the immobilization, the electrodes were rinsed with deionized water. Note that some of the -COOH groups from the QDs surface reacted with the L-cysteine monolayer for immobilization on the electrode, but there were still available functional groups for receptor immobilization (Figure 9c).

In the case of the SLG electrodes, the carboxylic acid functional groups were obtained directly from the electrochemical pre-treatment (Figure 9d).

Once the carboxylic acids were available on the electrode surface, the protocol was similar for any electrode type. This functionalization protocol was depicted in detail in Garrote et al.[28] Briefly, the carboxylic acid groups from the electrodes were activated by the carbodiimide reaction[90] in an aqueous solution containing 0.2 M EDC and 0.05 M NHS (50 mg. mL^{-1} EDC and 50 mg. mL^{-1} NHS in the case of QDs transducer). The electrodes were incubated for 30 min at room temperature (25 °C). Then, the electrodes were rinsed with deionized water and PB (pH 7.4) and incubated for 1h at room temperature (25 °C) in the specific antibody solution prepared in PB (pH 7.4). After the incubation, the electrodes were rinsed with PB (pH 7.4) and deionized water. The remaining ester-carboxylic acid groups were blocked by immersing the electrodes in undiluted Superblock™ solution in PBS for 30 min at room temperature (25 °C). Each step of fabrication of the immunosensor was characterized by electrochemical impedance spectroscopy (EIS) measurements at the E_F/e (in the case of redox-peptide modified Au electrodes) or OCP potential (in the case of SLG or Au electrodes modified with QDs) in a frequency range of 100 kHz to 0.1 Hz and 10 mV peak-to-peak amplitude. As a supporting electrolyte, in redox-peptide modified Au electrodes assays, it was used 20 mM of $TBAClO_4$ dissolved in ACN/deionized water (1:4 v/v); and in SLG or QD-Au electrodes assay, it was used PB (pH 7.4).

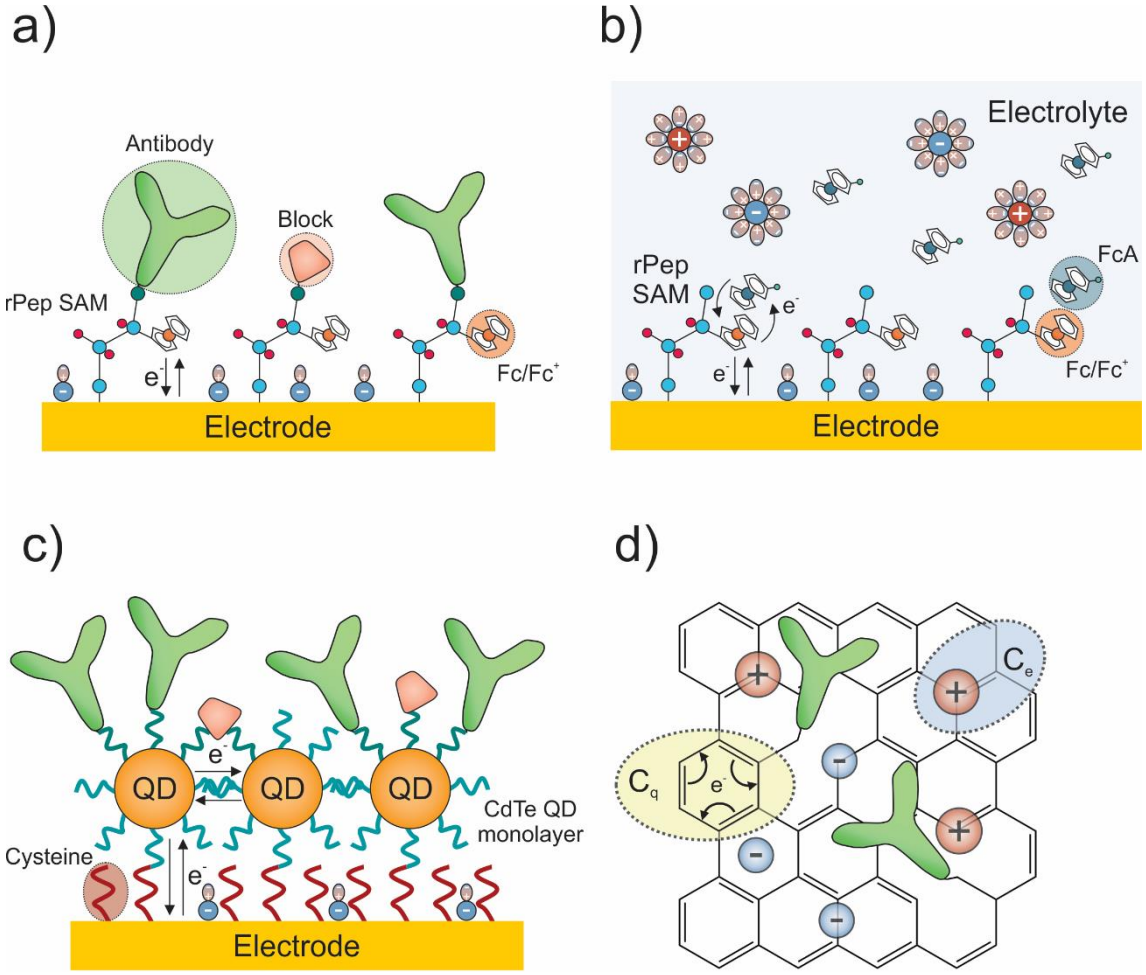

Figure 9. Schematic representation of the C_μ~C_q transducers and biosensing interfaces used in this project, being a) Au electrode modified with redox peptide SAM (rPep SAM) and b) with amplifier signal methodology with redox probe in solution; c) Au electrode modified with L-cysteine monolayer and CdTe quantum dots, and d) single-layer graphene (SLG).

Source: Author.

Impedance Spectroscopy and Capacitive Spectra

The obtained raw EIS data were converted into real (C') and imaginary (C") capacitive components of the complex capacitance function $C^*(\omega)$, using the mathematical equations $C' = \phi Z$" and C" $= \phi Z'$, wherein Z' and Z" correspond to the real and imaginary impedance components, respectively; and $\phi = 1/\omega|Z|^2$, where $\omega = 2\pi f$ is the angular frequency, $|Z|$ is the modulus of the complex impedance $Z^*(\omega)$, and f as the linear frequency. Throughout the thesis, EIS measurements converted to capacitance will be referred to as impedance-derived electrochemical capacitance spectroscopy (ECS).

Quantitative analytical assay

After the formation of the biosensing interface, the analytical assay was performed. Before the incubation with the specific samples, at least one blank measurement was recorded to quantify the matrix effect of the samples. The biosensing interfaces were incubated for 30 min at room temperature (25°C) in 25 - 50 µL neat human serum or PB (pH 7.4) samples without the specific analyte, and then, washed with PB and deionized water and characterized by ECS. This step was

repeated until achieved stability, that is when the variation of the analytical signal was lower than 5%. Afterward, the immunosensor was consecutively incubated with 25 - 50 µL of the samples containing increasing concentrations of the specific analyte. Each sample was incubated for 30 min at room temperature (25°C). Then, the electrodes were rinsed with PB and deionized water and characterized by ECS. From those measurements, an analytical curve was obtained by plotting the relative response percentages ($RR\%$) of each sample *versus* the logarithmic concentration range of the target. $RR\%$ was obtained by

$$RR\% = [(S_n - S_0)/S_0] \cdot 100 \quad (4)$$

where S_0 is the analytical signal of the blank and S_n is the analytical signal of each sample.

The correlation between $RR\%$ and analyte concentration was statistically analyzed by linear regression or Langmuir isotherm fitting.

Quantitative assays were statistically analyzed by linear regression or Langmuir isotherm fitting and evaluated by the analytical parameters limit of detection (LOD) and limit of quantification (LOQ). LOD and LOQ denoted the lower analyte concentration detected or quantified, respectively, by the assay developed. Those values are obtained from the linear regression by using Eq. 5 and 6.

$$LOD = (3 \cdot SD/b) \quad (5)$$

$$LOQ = (10 \cdot SD/b) \quad (6)$$

where SD is the standard deviation of the blanks and b is the slope of the analytical curve.

Spike assay

The accuracy of the quantitative assays was evaluated by spike assay, that is, to calculate the analyte concentration in a known-concentration sample by interpolation in the analytical curve. The samples containing a certain concentration of analyte were prepared in neat human serum and incubated for 30 min at room temperature (25°C) on the biosensing interface (25 - 50 µL). Then, the electrodes were rinsed with PB and deionized water and characterized by ECS. The $RR\%$ values were calculated by Eq. 4 and by interpolation in the analytical curve, the analyte concentration in each sample was calculated. The accuracy of the quantification was evaluated by the recovery value, being $Recovery\ (\%) = ([analyte]/[analyte]_{Calculated}) \cdot 100$, wherein $[analyte]$ is the analyte concentration prepared and $[analyte]_{Calculated}$ is the concentration calculated by the analytical curve. Recovery values close to 100% represent more accurate results.

Qualitative analytical assay

The biosensing interface for qualitative assays was evaluated by positive and negative samples, that is, containing or not the specific analyte. Firstly, the sensitivity, specificity, and stability of the biosensing interface were analyzed by incubating it for 30 min at room temperature (25°C) with 50 µL of the negative or positive samples, buffer, and buffer containing the specific analyte,

respectively. After each incubation, the immunosensors were rinsed with deionized water, characterized by ECS, and the $RR\%$ (Eq. 4) was calculated compared with the block measurements (i.e., measurements before and after the sample incubation). The immunosensor was optimized to be incubated with human samples when the $RR\%$ of the positive samples was statistically different from the negative samples $RR\%$. Afterward, the sensitivity and specificity were reanalyzed by negative and positive human samples, following the same protocol.

Qualitative assays were evaluated by the sensitivity of the analytical parameters (related to the truly positive results, Eq. 7), specificity (related to the true negatives results, Eq. 8), and accuracy. Those values were obtained by the statistical analysis of receiver operating characteristic (ROC). ROC validates the power of qualitative assays to distinguish positive and negative samples in terms of their sensitivity and specificity at different cut-off (CO) values (that is, the limit value of the analytical signal that separates negative and positive samples). The accuracy of the assay is represented by the area under the ROC curve (AUC), wherein < 0.5 is for random assay; 0.5-0.6 is for low accuracy; 0.7-0.8 is medium accuracy; 0.8-0.9 is good accuracy, and > 0.9 is excellent accuracy.

$$Sensitivity = TP/(TP + FN) \quad (7)$$

$$Specificity = TN/(TN + FP) \quad (8)$$

where TP is true positive results, FN is false positive results, TN is true negative results and FP is false positive results.

4. Results and discussion

Qualitative SARS-CoV-2 graphene assay

The reagentless and label-free SARS-CoV-2 quantum capacitive assay was developed by a novel graphene quantum transducer patented by our research group[39] and published in Lucas Garrote et al.[38] Graphene is a single carbon-atom-thick sheet sp^2-hybridized with notable intrinsic electric properties[36] which makes graphene a promising tool in a vast of applications. Within those, graphene is gaining attention as a transducer in electrochemical biosensors; nonetheless, this is challenging, due to the high sensitivity associated with the high quantization of the energy levels of graphene.[91] For the development of the SARS-CoV-2 assay, that limitation was overcome by the proper modification of the graphene surface.

The graphene-based transducer for the SARS-CoV-2 assay was designed by using two analytical signals related to the quantum ET rate frequency (k), an intrinsic property of the single layer graphene (SLG) interface. The chemical immobilization of the receptor on the SLG (Figure 10a) and its interaction with the analyte influence the conductivity of the electrons in the plane and thus, k, as stated in Eq. 1. From the ECS measurements (Figure 10b), a frequency range is accessed, enabling multiple frequency possibilities as analytical signal. In the SARS-CoV-2 assay, the relative variation of the resonant, f_r, and equilibrium, f_e, frequencies were used as analytical signals. f_e corresponds to the charge equilibrium regime of the interface, where theoretically $f \to 0$. On the other hand, f_r corresponds to a dynamic or resonance rate regime (maximum of conductance). Both were sensitive to changes in the surrounding environment owing to receptor-target interaction because G and C_q were affected (Eq.1). f_r and f_e analytical signals were named as S_1 and S_2, respectively. This analytical strategy was applied for the development of a high-sensitive SARS-CoV-2 assay in nasopharyngeal/oropharyngeal swab patient samples as a substitute for a PCR assay.

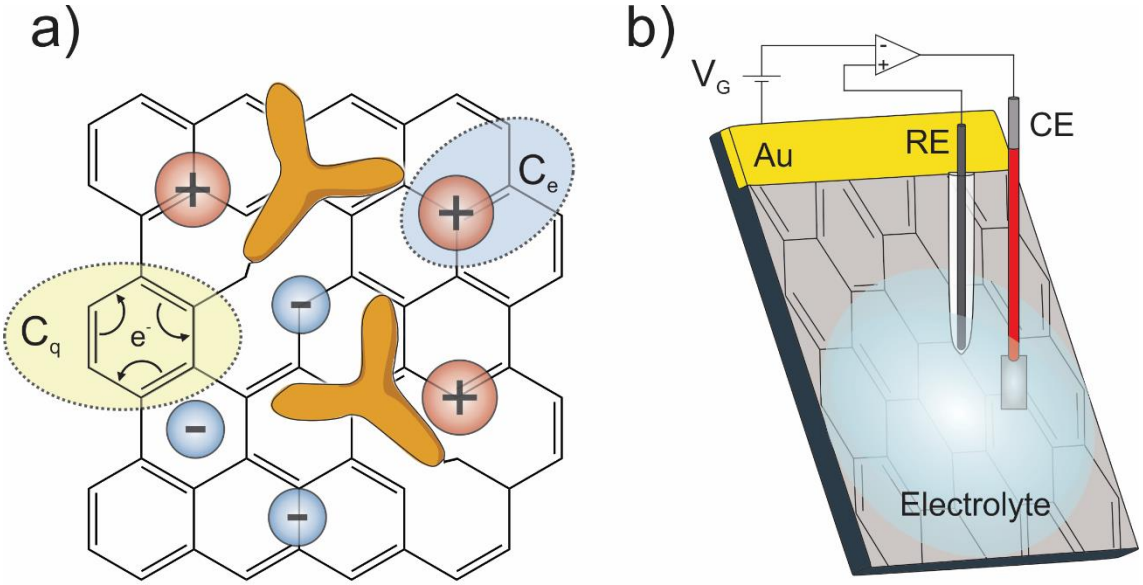

Figure 10. a) Schematic representation of C_e and C_q contributions in an SLG electrochemical interface modified with specific antibodies. b) Setup of the ECS measurements of the SLG biosensing interface. It corresponds to an AC mode of operation of a GFET in an electrochemical environment.

Source: Adapted from Lucas Garrote et al. [38]

Firstly, the SLG electrode was modified with the specific antibody for the detection of the SARS-CoV-2 spike (S) protein in inactivated virus samples produced in cell culture for optimization. ECS measurements of the biosensing interface (i.e, SLG modified with Ab anti-S - Figure 10a) were recorded before and after the incubation with the sample and the S_1 and S_2 $RR\%$ was calculated (Eq. 4). The $RR\%$ of seven positive samples (that is, inactivated virus samples produced in cell culture) was compared to the $RR\%$ of seven samples of the cell supernatant without the virus (i.e., negative samples). The results were represented by a Box plot and statistically analyzed by t-Student (Figure 11). The S_1 $RR\%$ of the positive samples was not statistically different from the $RR\%$ of the negative samples ($p = 0.08$), probably because of the small number of samples (n) analysed; nonetheless, the S_1 was considered promising and including in further analyses. Contrary to S_1, the S_2 $RR\%$ statistically differentiated between positive and negative samples ($p < 0.05$). The cut-off value for each analytical signal, CO_1 and CO_2, was calculated by the $RR\%$ average of the negative samples plus one ($x = 1$) standard deviation ($CO = \overline{RR\%} + x \cdot SD$).

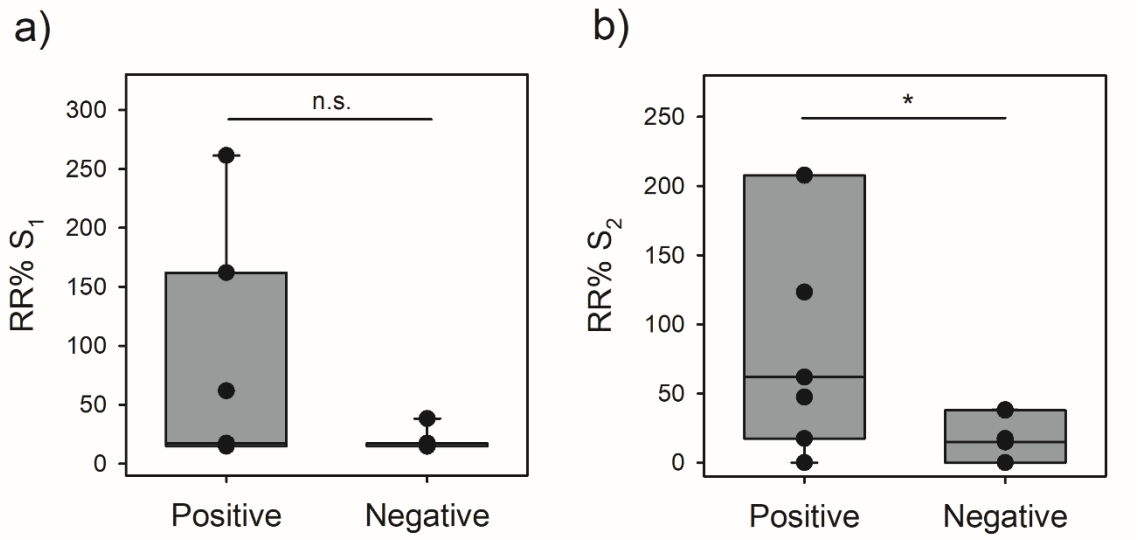

Figure 11. S protein-SLG assay optimization with inactivated virus samples produced in cell culture (positive samples) and cell culture supernatant (negative samples). a) Boxplot of the analytical signal S_1 comparing positive and negative samples ($n = 7$). n.s. denotes no significant ($p < 0.08$) in t-Student statistical analysis; b) Box-plot of the analytical signal S_2 comparing positive and negative samples ($n = 7$). * denotes $p < 0.05$ in t-Student statistical analyze.

Source: Adapted from Lucas Garrote et al. [38]

The combination of the S_1 and S_2 $RR\%$ and their CO values delimited graphically the negative ($RR\% < CO$, in green) and positive areas ($RR\% > CO$), as depicted in Figure 12. Samples with S_1 and S_2 $RR\%$ lower than CO_1 and CO_2, respectively, was in the green area from Figure 12 and then, considered negative. On the other hand, samples with either S_1 or S_2 $RR\%$ higher than CO_1 or CO_2, respectively, was outside the green area in Figure 12 and hence, considered positive. The analysis of the samples considering these criteria arose in two false negatives (FN) and two false positives (FP) results, where FN denotes a positive sample considered negative by the S protein-SLG assay (i.e., S_1 and S_2 $RR\% < CO_1$ and CO_2), and FP denotes a negative sample considered positive by the S protein-SLG assay (i.e., S_1 or S_2 $RR\% > CO_1$ or CO_2). Therefore, the sensitivity (i.e., rate of true positive, TP, results) and specificity (i.e., rate of true negative, TN, results) of S protein-SLG assays were 71%, obtained by Eq. 7 and 8.

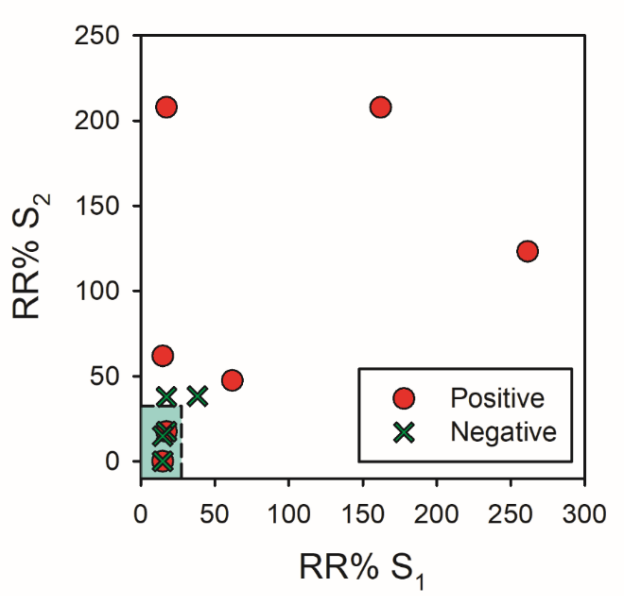

Figure 12. S_1 and S_2 $RR\%$ in positive and negative samples. The vertical and horizontal dashed lines represent the CO values of S_1 and S_2, respectively, obtained as the average $RR\%$ of the negative samples plus standard deviation ($\overline{RR\%} + SD$) of each analytical signal. The green area represents the $RR\%$ of the samples considered negatives by the S protein-SLG assay, where the S_1 and S_2 $RR\%$ was lower than their CO values. Samples outside the green area (that is, S_1 and S_2 $RR\%$ was higher than their CO values) was considered positive by the S protein-SLG assay.

Source: Adapted from Lucas Garrote et al. [38]

This preliminary analysis with inactivated virus samples demonstrated that the SLG C_q transducer enabled the detection of relevant biomarkers, proven here by the S protein from SARS-CoV-2, with appropriate sensitivity and specificity. Therefore, the assay was suitable for the detection of viral infection in nasal swabs from patient samples.

The S protein-SLG assay was analyzed in 13 nasopharyngeal/oropharyngeal human samples from healthy individuals and 15 SARS-CoV-2-infected patients. Note that all samples were confirmed by rRT-PCR at the Clinical Virology Laboratory of the Clinical Hospital (HC-FMRP) of Sao Paulo University (USP) in Ribeirão Preto during the patient primary diagnosis. The accuracy of the results obtained from the patient samples was statistically analyzed by the ROC test which validates qualitative assays, as described in the experimental section. The accuracy of the S protein-SLG assay was 86.7%, related to good accuracy assays, according to the ROC criteria (experimental section). Moreover, the sensitivity and specificity of the assay obtained from the ROC test were 93% and 62%, respectively. Although the accuracy and sensitivity values were close to 100%, related to a reliable assay, the specificity obtained almost corresponded to a random assay with low reliability and robustness (that is, close to 50%). To increase the specificity, a second SARS-CoV-2 viral protein, the nucleocapsid (N) protein, was added as a target to the assay, achieving a *quasi*-multiplexed assay (Figure 13).

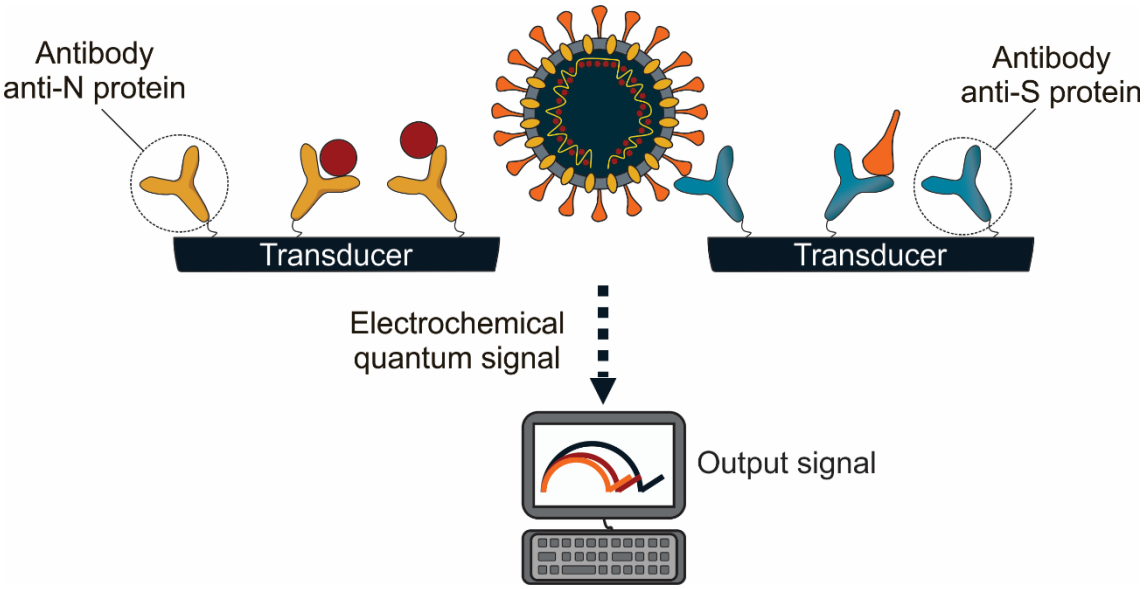

Figure 13. *Quase*-multiplex SLG-based C_q transducer for the detection of the S and N SARS-CoV-2 proteins.

Source: Author

Therefore, following the methodology adopted for the S-SLG assay, the 13 negative and 15 positive samples were also analyzed by the N protein-SLG assay which consisted of the SLG electrode modified with the antibody anti-N protein. The results of the *quasi*-multiplexed S/N-SLG assay were analyzed by the ROC test (Figure 14), resulting in 83.8% of accuracy, 80% of sensitivity, and 77% of specificity. Although the sensitivity of the assay decreased by almost 14% with the analysis of both viral proteins, the specificity increased by almost 20%, while maintaining almost constant the accuracy of the assay. Despite the slight decrease in sensitivity, the dual detection of the S and N viral proteins for the diagnosis of SARS-CoV-2 infections increased the specificity and reliability, while ensuring the robustness of the assay strategy and enabling the development of a high-sensitive and specific biosensing device. The multiple assays developed overcame the limitations of the analysis of each analyte separately, such as the related to high number of mutations depicted in the S gene which could affect the antigenicity of the receptor[92], compromising the specificity of the assay in a long-term period. Moreover, the ROC curve provided the COs values for each analytical signal, S_1 and S_2, for each analytical assay, S and N, corresponding with the point in the curve which is the closest to the left corner of the ROC graph (that is, $sensitivity = 1$ and $(1 - Specificity) = 0$). In Figure 14, the most suitable CO was obtained by assuming $x = 0.7$ (yellow crossed-square) in the equation $CO = \overline{RR\%} + x \cdot SD$. Accordingly, the CO values of the S-SLG assay were $CO\ S_1 = 28.2\%$ and $CO\ S_2 = 42.8\%$; and the N-SLG assay CO vales were $CO\ S_1 = 21.8\%$ and $CO\ S_2 = 30.6\%$.

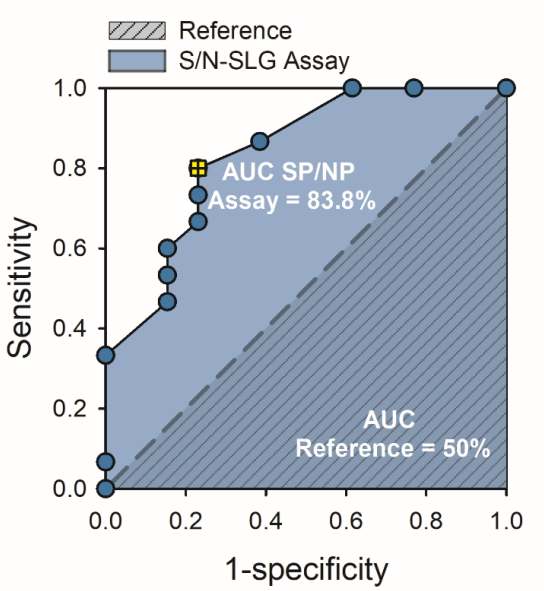

Figure 14. ROC analysis of the S/N-SLG assay. The area under the reference curve (AUC = 50%) represents the result of a random assay. The S/N-SLG assay AUC was 83.8% (labelled in blue). The most suitable S_1 and S_2 CO was obtained by assuming $x = 0.7$ (crossed-square labelled in yellow), corresponding to 80% and 77% of sensitivity and specificity, respectively.

Source: Adapted from Lucas Garrote et al. [38]

Likewise in the optimization assay, criteria to consider negative or positive results by the S/N-SLG assay were established, being a negative result when none of the analytical signals were higher than their CO value (that is, $RR\%\ SP\ S_1 < CO\ SP\ S_1 = 28.2\%$, $RR\%\ SP\ S_2 < CO\ SP\ S_2 = 42.8\%$, $RR\%\ NP\ S_1 < CO\ NP\ S_1 = 21.8\%$, and $RR\%\ NP\ S_2 < CO\ NP\ S_2 = 30.6\%$); and a positive result when at least one of the analytical signals was higher than their CO (that is, $RR\%\ SP\ S_1 > CO\ SP\ S_1 = 28.2\%$ and/or $RR\%\ SP\ S_2 > CO\ SP\ S_2 = 42.8\%$ and/or $RR\%\ NP\ S_1 > CO\ NP\ S_1 = 21.8\%$ and/or $RR\%\ NP\ S_2 > CO\ NP\ S_2 = 30.6\%$). By utilizing these criteria, the analysis of the 13 rRT-PCR negatives and the 15 rRT-PCR positive patient samples resulted in 3 false positives, 10 true negatives, 12 true positives, and 3 false negative results, as summarised in Table 4. Therefore, the sensitivity and specificity calculated in Eq. 7 and 8 were 80% and 77%, in agreement with the values obtained by the ROC analysis.

Table 4. Sensitivity and specificity of the S/N-SLG quantum assay proposed using AC mode of a GFET (Figure 10) compared with the rRT-PCR gold standard methodology.

		rRT-PCR	
		+	-
S/N-SLG ASSAY	+	12	3
	-	3	10
	Total	15	13
		Sensitivity[a] 80%	Specificity[b] 77%

[a] Sensitivity of the S/N-SLG assay was calculated by $true\ positive\ results/total\ positives$

[b] Specificity of the S/N-SLG assay was calculated by $true\ negative\ results/total\ negatives$

The S/N-SLG assay developed demonstrated higher sensitivity than the overall rapid antigen detection assays which, in general, is around 70% of sensitivity in samples with C_T values higher than 27 (obtained from rRT-PCR).[93; 94] On the other hand, the specificity should be slightly improved, nonetheless, in an emergency, the specificity value would be suitable. In summary, the proof-of-concept of the S/N-SLG assay using the novel quantum-rate transducer methodology demonstrated to be a promising technology in diagnosis, owing to the high-sensitive obtained with high-simplicity.

High-sensitive quantitative NS1 Dengue virus assay

Previous works from our research groups demonstrated the application of C_q transducers for the detection of NS1 Dengue virus protein in human serum samples.[66] Nonetheless, the assay consisted of Metrohm Au electrodes modified with redox peptide SAM that did not enable the application in the field, owing to the size of the working electrode and the electrochemical cell. Moreover, the assay did not quantify the amount of NS1 in the samples that could be helpful for the disease treatment. Therefore, the C_q NS1 Dengue virus assays needed improvements to become a POC device.

During the development of this doctoral thesis, it was demonstrated the application of a charge transfer mediated mechanism through the energy levels of a redox switch confined on the electrode surface and the energy levels of a redox probe in solution described by Sánchez et al.[41] as an amplifier signal methodology for C_q transducers. The amplifier signal strategy consisted on the coupling of two redox-active switches with similar E_F/e which arises the coupling of their DOS (Figure 15). The electroactive interface mediates the ET between the redox probe in solution and the electrode, deriving in a more efficient diffusionless ET process with high sensitivity to variations in the surroundings. This tool was applied for the development of an ultrasensitive NS1 Dengue virus by using gold miniaturized electrodes modified with redox-peptide SAM and FcA in the supporting electrolyte as an amplifier signal probe.

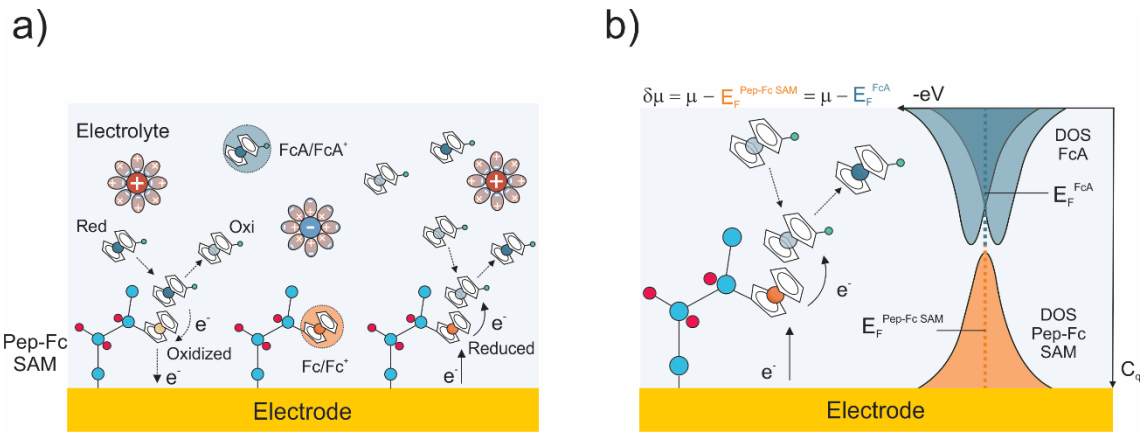

Figure 15. a) Schematic representation of the redox switches Fc (confined on the electrode) and FcA (in solution) electrochemical process coupling. b) depicts the electronic coupling between the redox states from both redox switches, experimentally accessed by ECS, which are in the same Fermi level, i,e, $\delta\mu = \mu - E_F^{FcA} = \mu - E_F^{SAM}$.

Source: Author.

The electrochemical mechanism obtained from the redox switches coupling was characterized by CV and ECS measurements, which demonstrated that the presence of the redox probe in the solution increases C_q and the current density (j) (Figure 16). The rPep SAM was well-formed on the Au electrode, denoting a reversible oxidation/reduction mechanism from the ferrocene confined on the electrode by $\Delta V = V_{ox} - V_{red} < 20\,mV$, $j_{ox}/j_{red} \sim 1$ and a formal potential $E_F/e \sim 0.36\,V$, as shown in orange in Figure 16a. Moreover, the quantum capacitance C_q of the interface was $\sim 150\ \mu F\ cm^{-2}$ (orange circles in Figure 16b) in concordance with previous

experiments. An electrochemical enhancement was favored by a suitable electronic coupling by the presence of FcA redox probe, which has a similar E_F/e that rPep SAM, in the supporting electrolyte, that is, 20 mM $TBAClO_4$ and 100 μM FcA in ACN/H_2O (1:4, v/v). The electrochemical coupling between the redox switches, i.e., confined and in solution, induced a slight shift ($\sim 10\ mV$) of the E_F/e, a 2-fold increase in the current density (Δj_{ox} and Δj_{red}), as shown in blue in Figure 16a; and increased 60% C_q value of the interface (blue triangles in Figure 16b). This gain in C_q and j is consequence of the redox switches coupling which arises in an increase in the number of energy states (N) available or DOS since both are in resonance (note that this is true when both electroactive compounds have similar E_F/e). As a consequence of the increase in N, the electroactive interface was more susceptible to variations in the surroundings, suggesting an amplifier signal effect. To corroborate this hypothesis, the sensitivity of the rPep SAM-based assay with and without a redox probe in solution was compared for the quantification of Dengue virus NS1 protein in neat human serum samples.

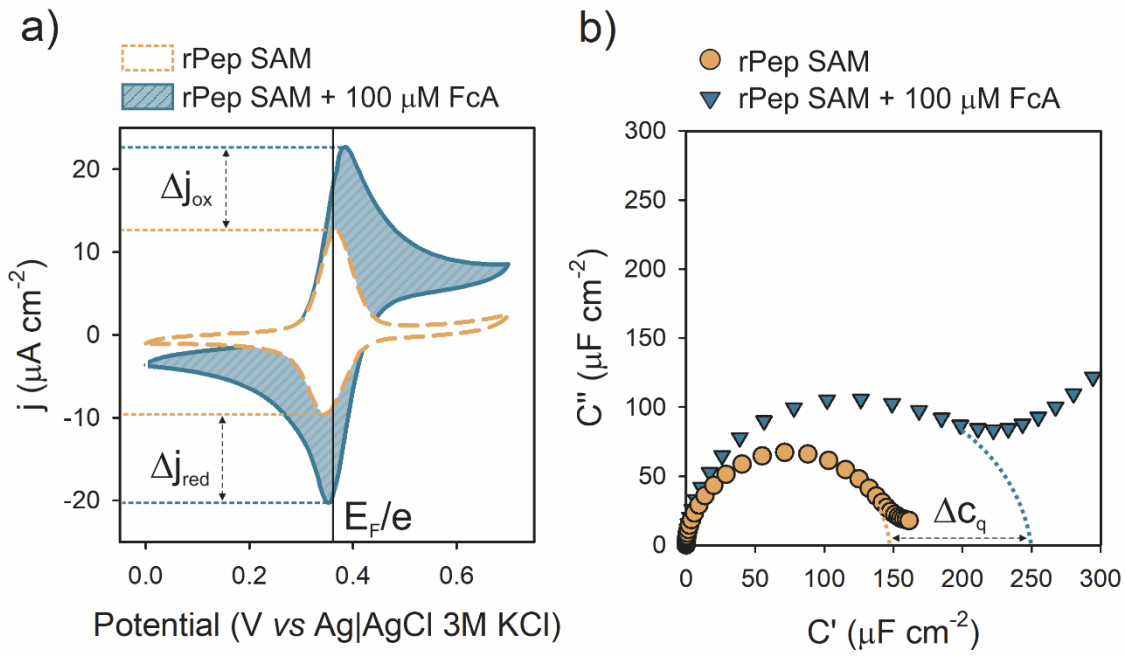

Figure 16. Electrochemical characterization of the coupled electrochemical mechanism between the redox peptide SAM (rPep SAM) and 100 μM FcA. a) Cyclic voltammogram and b) capacitive Nyquist plot of the electroactive interface with (rPep SAM + FcA colored in blue with diagonal lines in a) and blue triangles in b) and without (rPep SAM dashed line in orange in a) and orange circles in b) the redox probe FcA in solution. In a), Δj_{ox} and Δj_{red} depict the density current gain with the amplifier signal. In b), ΔC_q depicts the quantum capacitance gain by using the amplifier signal technology developed.

Source: Author.

The construction of the biosensing interface, including the immobilization of the specific antibody anti-NS1, was performed following the protocol depicted in the experimental section and reference Garrote et al.[28] Each step was characterized by ECS in 20 mM $TBAClO_4$ in ACN/H_2O (1:4, v/v) in the absence (Figure 17a) or presence (Figure 17b) of 100 μM FcA. The immobilization of the Ab anti-NS1 and the block of the unreactive carboxylic groups decreased by almost 10% and 20% C_q in the non-amplifier and amplifier signal assay, respectively. The blank

measurements were performed with a neat human serum which demonstrated higher instability in the assay based on the redox peptide SAM ($\sim 10\%$) than in the assay with amplifier signal ($\sim 3\%$). Nonetheless, the rPep SAM was stable after several blank measurements and the biosensing interfaces were incubated with the human serum samples containing increasing concentrations of NS1 protein (Figure 18).

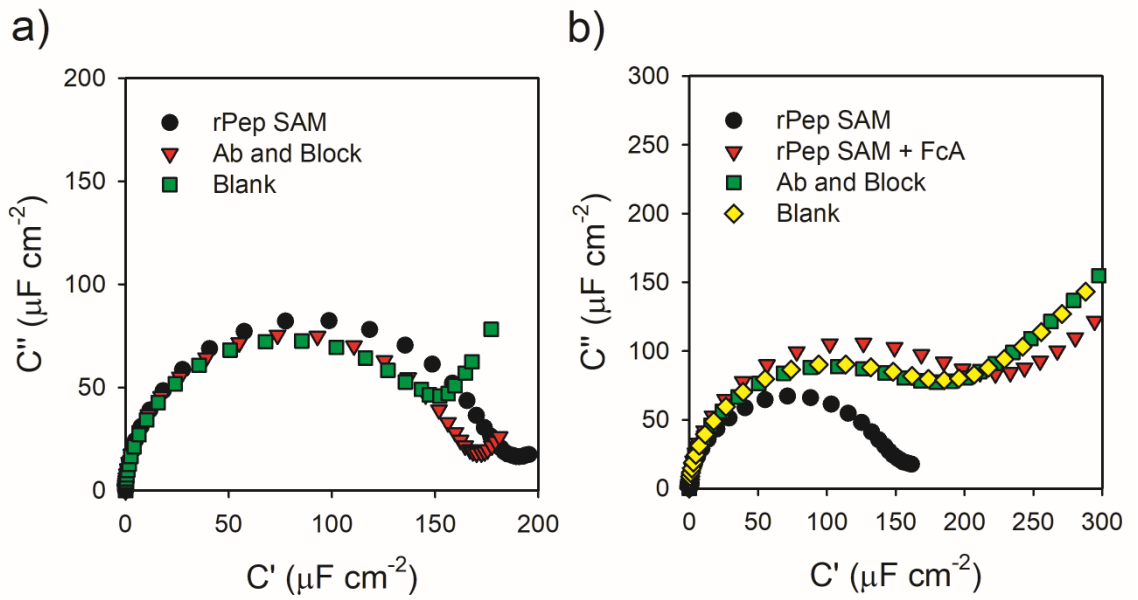

Figure 17. Capacitive Nyquist plot of the biosensing interface fabrication process measured in a) 20 mM $TBAClO_4$ in ACN/H_2O (1:4, v/v) as supporting electrolyte, and b) 20 mM $TBAClO_4$ in ACN/H_2O (1:4, v/v) containing 100 µM FcA redox probe as supporting electrolyte. rPep SAM in b) (black circles) was measured in 20 mM $TBAClO_4$ in ACN/H_2O (1:4, v/v) as a supporting electrolyte (that is, without redox probe in solution) for comparison.

Source: Author.

The $RR\%$ (Eq. 4) of the NS1 assay based on rPep SAM (without amplifier signal) after the incubation with the samples containing NS1 concentration in the pg mL^{-1} range was a drift of $\pm$ 5% (Figure 18a), whereas the $RR\%$ of the assay with amplifier signal was higher than the variation of the blanks and it was correlated to the increase in NS1 concentration (Figure 18b). Therefore, the analytical curve was obtained by plotting the $RR\%$ of the analytical signal $1/C_q$ against NS1 concentration (Figure 19).

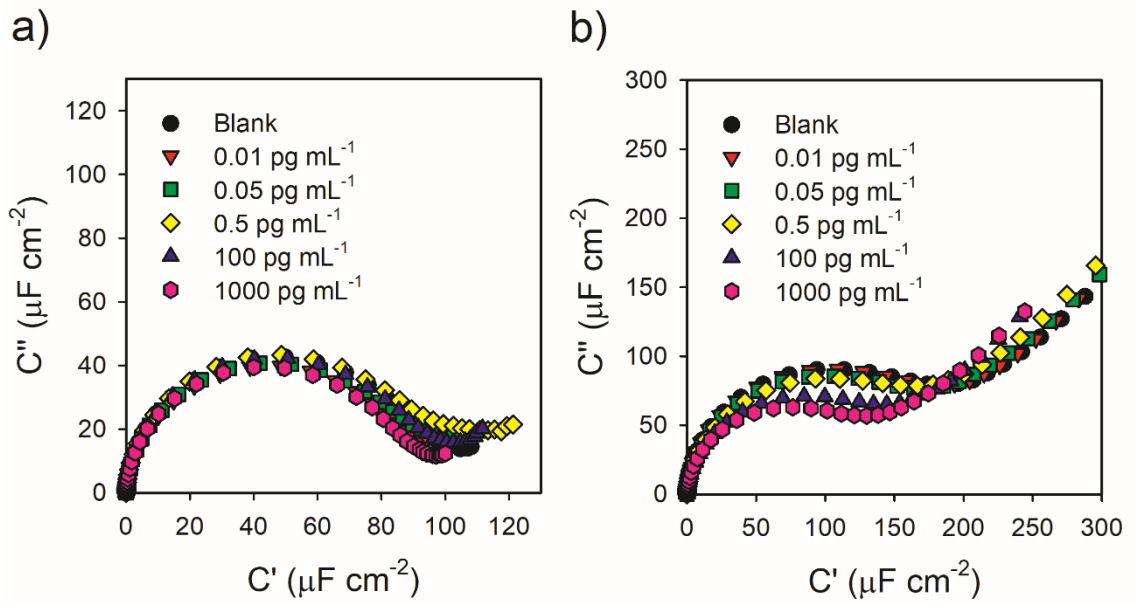

Figure 18. Capacitive Nyquist plot of the NS1 assay measured in a) 20 mM $TBAClO_4$ in ACN/H_2O (1:4, v/v) as supporting electrolyte, and b) 20 mM $TBAClO_4$ in ACN/H_2O (1:4, v/v) containing 100 µM FcA redox probe as supporting electrolyte.

Source: Author.

The non-amplifier signal NS1 assay presented a linear variation in the incubation with the NS1 concentration range 10^3 – 10^6 pg mL^{-1} with $r^2 = 0.98$ (orange circles in Figure 19a), while the assay with the amplifier signal methodology demonstrated two linear regressions (blue circles in Figure 19a): i) at the concentration range 10^{-2} – $10^3\ pg\ mL^{-1}$ ($r^2 = 0.99$), corresponding with the lower concentrations where the assay without the amplifier signal methodology did not present sensitivity enough to detect the analyte (Figure 19b); and ii) in the higher concentration range $5 \cdot 10^4$ – $10^6\ pg\ mL^{-1}$. The analytical parameters LOD (Eq. 5) and LOQ (Eq. 6) were calculated for each assay to quantify the increase in sensitivity due to the amplifier signal methodology. The LOD and LOQ of the rPep SAM-based assay (without signal amplifier) were $0.5\ ng\ mL^{-1}$ and $1.7\ ng\ mL^{-1}$, respectively, while the LOD and LOQ with the amplifier signal were $0.7\ pg\ mL^{-1}$ and $2.2\ pg\ mL^{-1}$, respectively. Therefore, it was observed an almost 1000-fold increase in the assay sensitivity in terms of the lower concentration detected and quantified by using FcA redox probe in the supporting electrolyte. This result demonstrated that the improvement in the electron transfer efficiency by the coupling of the electrochemical processes from both redox switches (that is, a redox switch confined on the electrode and a redox probe in solution) constituted an amplifier signal methodology that increase the sensitivity of capacitive biosensors.

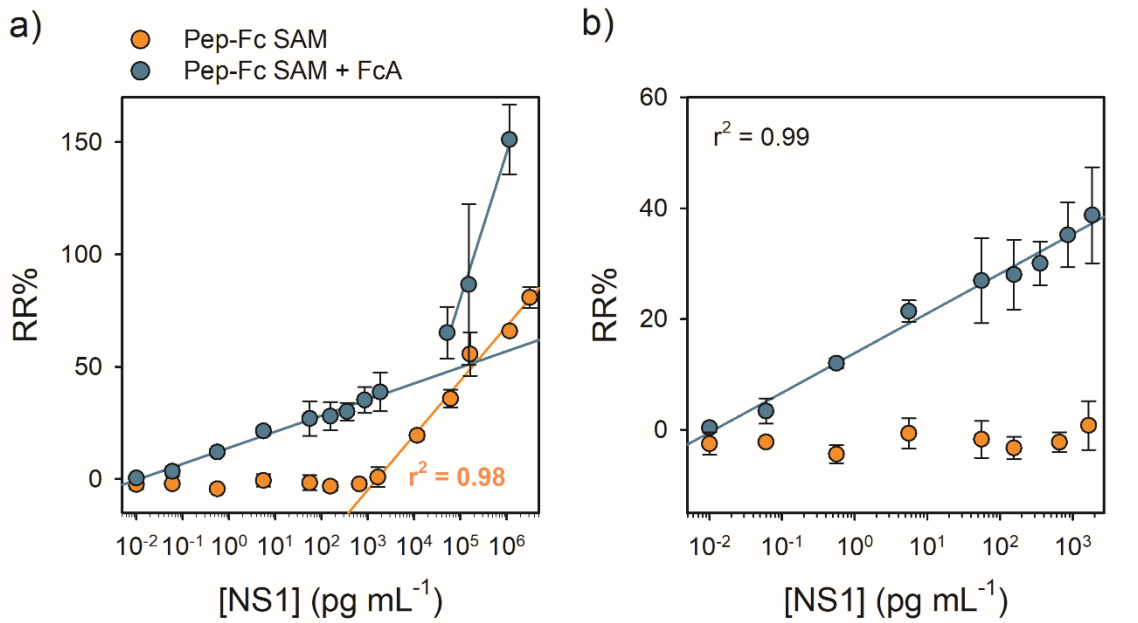

Figure 19. a) Analytical curves (relative response, $RR\%$, against NS1 concentration) of the assay with redox-peptide SAM (rPep SAM in orange) and the assay with the amplifier signal mechanism with redox probe in solution (rPep SAM + FcA in blue). NS1 concentration range 10^{-2} – $10^{6}\ pg\ mL^{-1}$. rPep SAM (in orange) linear regression in the range 10^{3} – $10^{6}\ pg\ mL^{-1}$ with $r^2 = 0.98$. In b), linear regression of the lower NS1 concentration range (10^{-2} – $10^{3}\ pg\ mL^{-1}$) of the analytical curves comparing the $RR\%$ of the assay with amplifier signal (in blue, $r^2 = 0.99$) and the drift of the assay without the amplifier signal.

Source: Author.

The accuracy of the analytical curve of the high-sensitive assay with the amplifier signal for the quantification of the analyte NS1 in neat serum samples was analyzed by a spike assay. Three human serum samples containing 2.5, 17, and 35 $pg\ mL^{-1}$ NS1 was prepared and incubated on the biosensing interface. By the interpolation in the equation of the analytical curve (Eq.9) from Figure 19b, the NS1 concentration was calculated. The accuracy was quantified by the recovery value in percentage. The results of the spike assay are compiled in Table 5.

$$RR\% = 13.9 + 7.2 \cdot log\ [NS1] \qquad (9)$$

Table 5. NS1 spike assay ($n = 2$) using the $1/C_q$ analytical curve with the amplifier signal methodology in Figure 19b.

[NS1] (pg mL^{-1})	[NS1] Calculated$^{(*)}$ (pg mL^{-1})	% Recovery$^{(**)}$
2.5	3.5 ± 0.5	141.3 ± 17.8
17.0	16.4 ± 4.9	96.7 ± 28.6
35.0	36.0 ± 2.9	102.9 ± 8.3

$^{(*)}$ Calculated by interpolation in Eq. 9

$^{(**)}$ Calculated by $Recovery\ (\%) = ([NS1]/[NS1]_{Calculated}) \cdot 100$

The recovery value of the quantification of the samples containing 17 and 35 $pg\ mL^{-1}$ NS1 was close to 100%, denoting high accuracy of the analytical curve. Nonetheless, the recovery of the sample with the lowest concentration, 2.5 $pg\ mL^{-1}$ NS1, was ($141.3\ \pm\ 17.8$) %, that is, it was calculated by Eq. 9 as a higher concentration than the real concentration in the sample. This

inaccuracy could be related to the proximity to the LOQ of the assay ($LOQ = 2.2\ pg\ mL^{-1}$) where the error of the linear regression is higher. Moreover, errors during the preparation of the samples, such as pipetting, could increase the inaccuracy.

In summary, in this section, it was demonstrated that the use of two redox switches with electrochemical processes coupled (that is, redox probes with similar E_F/e) improved the efficiency in the electron transfer and it serves as an amplifier signal methodology in electrochemical capacitive biosensors by the high-sensitive quantification of NS1 Dengue virus protein in neat serum samples. This discovery opens vast applications of C_q biosensors where the detection of a trace amount of analyte is required.

ADAM10 quantification assay for Alzheimer's disease diagnosis in serum samples

One of the main objectives of the Ph.D. thesis was to develop, for the first time, a C_q biosensor for the quantification of ADAM10 in human serum samples of healthy individuals and patients with Alzheimer's disease (AD). In this regard, the first step was to obtain an analytical curve that correlated the relative variation or relative response, $RR\%$ (Eq. 4), of the analytical signal with the concentration of analyte ADAM10.

The electrochemical capacitive biosensing interfaces were prepared and characterized as described in Garrote, et al.[28] and in the experimental section of this thesis. The impedance-derived electrochemical capacitance spectroscopy measurements of the modification of the electrode with the redox peptide SAM, the antibody anti-ADAM10 (Ab1), and the blocking procedure is depicted in Figure 20a. The immobilization of the Ab ADAM10 on the redox-peptide SAM decreased by 13.8% the C_q signal due to the variation of the tagged ferrocene density-of-states (DOS) electron occupancy of the peptide SAM interface. The remaining available carboxylic acid groups from the SAM were blocked by using a blocking solution, where 2.8% of the variation was obtained. The stability of the assay was analyzed by at least one blank measurement with a commercial human serum. The assay was considered stable whether the drift caused was lower than 5%. In this case, as is observed in Figure 20a, the drift was 0.1%.

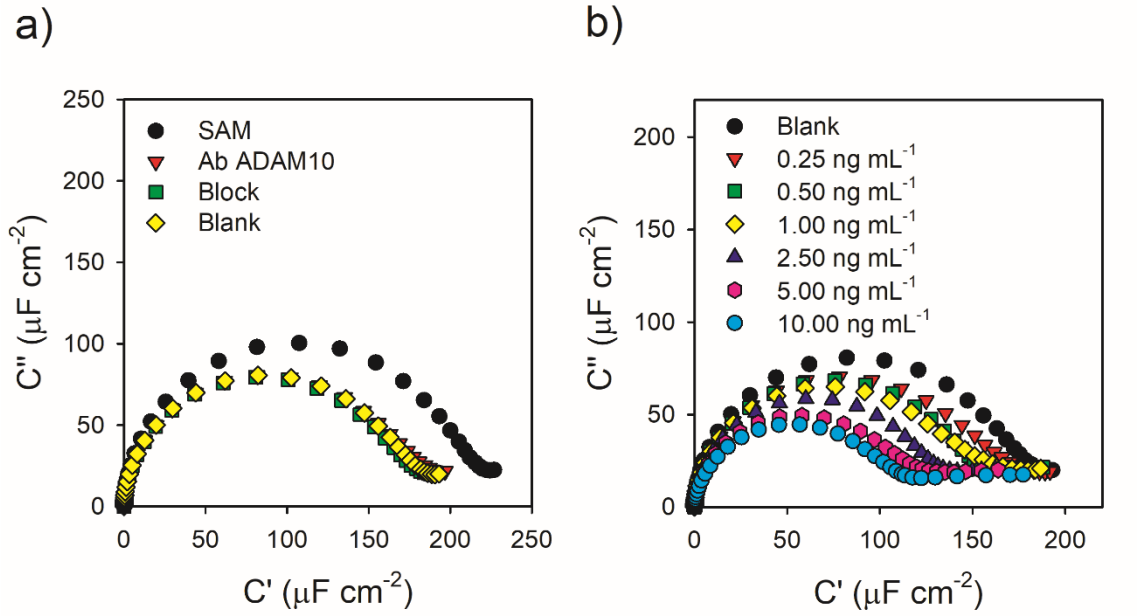

Figure 20. Capacitive Nyquist plot of a) modification of the electrode for the biosensing interface construction and b) incubation in the neat serum samples containing ADAM10 protein ranging $0.25 - 10\ ng\ mL^{-1}$.

Source: Author.

The stable biosensing interface was consecutively incubated with commercial human serum samples containing increasing ADAM10 concentrations in the range of $0.25 - 10\ ng\ mL^{-1}$. Likewise, for each sample, the C_q value was obtained from the Nyquist plot (Figure 20b). The variation due to Ab ADAM10 and ADAM10 analyte interaction was quantified by the $RR\%$ given by Eq. 4.

The analytical signals analyzed from the Nyquist plot were C_q, maximum of C'' and $1/C_q$, wherein the maximum of C'' is related to the conductance of the charge transfer process (such as $G = \omega C'' = 2\pi f C''$) and $1/C_q$ is related to the energy storage in the electroactive interface (such as $E \propto e^2/C_q$). The analytical curve of each analytical signal (Figure 21) was obtained by plotting the $RR\%$ of each sample compared to the blank against the accumulative value of the concentrations incubated (i.e., the $RR\%$ of the second sample incubated is consequence of the first and the second samples incubation since the incubation of the samples is consecutive).

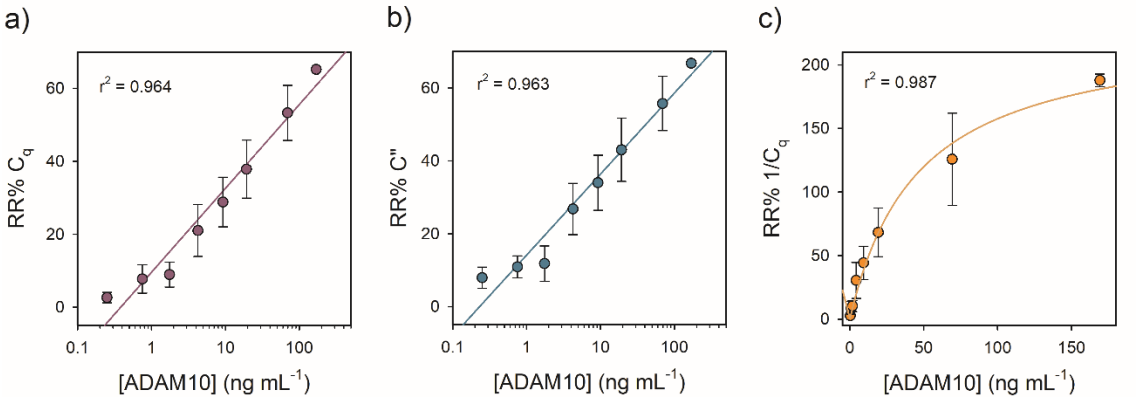

Figure 21. ADAM10 analytical curves with the Ab1 anti-ADAM10 biosensing interface by using as analytical signal a) C_q, b) maximum of C'' and c) $1/C_q$. The error bars depicted the standard error from 4 independent assays ($n = 4$).

Source: Author.

The analytical curves of C_q (Figure 21a) and maximum of C'' (Figure 21b) presented a linear correlation through all the intervals of concentrations analyzed, being $r^2 = 0.964$ and $r^2 = 0.963$, respectively. The equation of the C_q linear regression was $RR\% = 9.62 + 23 \cdot log[ADAM10]$ and $RR\% = 14.18 + 22.22 \cdot log[ADAM10]$ in the case of the maximum of C''. The analytical curve of the analytical signal $1/C_q$ was fitted using the Langmuir isotherm (Figure 21c), given by

$$RR\% = \frac{RR\%_{max} \cdot K_a \cdot [ADAM10]}{1 + K_a \cdot [ADAM10]} \qquad \text{Eq. 10}$$

wherein K_a is the apparent binding affinity constant between ADAM10 and the used antibody. The regression with Eq. 10 was statistically validated by $R^2 = 0.987$. The value of $RR\%_{max}$ and K_a obtained were $(229.9 \pm 16.8)\%$ and $(0.022 \pm 0.004)\ mL\ ng^{-1}$, respectively. The dissociation constant K_d was calculated by $K_d = 1/K_a$, being $7 \cdot 10^{-10}\ M$. As a mere comparison of the K_d value of the streptavidin/biotin interaction, one of the highest-affinity, and the most stable protein interactions in nature is of $\sim 10^{-14}\ M$.[95] Although, the ADAM10/Ab K_d was 10^4 times higher than the streptavidin/biotin value, it can still be considered low, and

therefore, a high ADAM10/Ab interaction was observed. Additionally, the LOD (Eq. 5) and LOQ (Eq. 6) values of the analytical curves were calculated and they are compiled in Table 6.

Table 6. Limit-of-detection (LOD) and limit-of-quantification (LOQ) values of the analytical curves from Figure 21. LOD and LOQ were calculated by Eq. 5 and Eq. 6.

Analytical signal	LOD (ng mL^{-1})	LOQ (ng mL^{-1})
C_q	0.3	1.1
maximum of C''	0.3	1.0
$1/C_q$	0.1	0.4

A spike assay was performed to analyze the accuracy of the analytical curves. The concentrations analyzed were 1.2, 1.7, and $3\ ng\ mL^{-1}$ prepared in neat commercial human serum. The results obtained were analyzed with the three analytical signals from Figure 21. Nonetheless, more accurate results were obtained with the $1/C_q$ analytical curve (Figure 21c). The results are compiled in Table 7. Although the percentage of recovery of the concentration of $1.7\ ng\ mL^{-1}$ was not as close to 100% as the other concentrations, the results obtained applying Eq. 10 were in good agreement. The error observed in the results could be related to inaccuracy in the sample preparation procedure.

Table 7. ADAM10 spike assay ($n = 2$) using the $1/C_q$ analytical curve in Figure 21c.

[ADAM10] (ng mL^{-1})	[ADAM10] Calculated (ng mL^{-1})	% Recovery[a]
1.20	1.1 ± 0.2	92.7 ± 14.4
1.70	1.3 ± 0.2	75.4 ± 12.9
3.00	2.8 ± 0.3	93.9 ± 11.1

[a] Calculated by $Recovery\ (\%) = ([ADAM10]/[ADAM10]_{Calculated}) \cdot 100$

After the validation with commercial human serum, the performance of the capacitive biosensing assay was analyzed in human samples from healthy individuals ($n = 8$), patients with mild cognitive impairment (MCI) ($n = 7$), and patients with advanced Alzheimer's disease (AD) ($n = 5$). Those experiments were performed in collaboration with Prof. Ronaldo Censi Faria and Prof. Marcia Regina Cominetti from UFSCAR (São Carlos, SP). The quantification of ADAM10 in those samples using the $1/C_q$ analytical curve (Figure 21c) demonstrated a decrease in ADAM10 with the progression of the disease, wherein the average values obtained were $1.1 \pm 0.7\ ng\ mL^{-1}$ for the healthy individuals, $0.6 \pm 0.4\ ng\ mL^{-1}$ for the MCI patients and $0.6 \pm 0.4\ ng\ mL^{-1}$ for the AD patients. It was observed a statistical difference in the ADAM10 concentration between the healthy and the AD patients ($p = 0.045$, Figure 22a) and between the healthy group and the combination of MCI and AD patients ($p = 0.028$, Figure 22b).

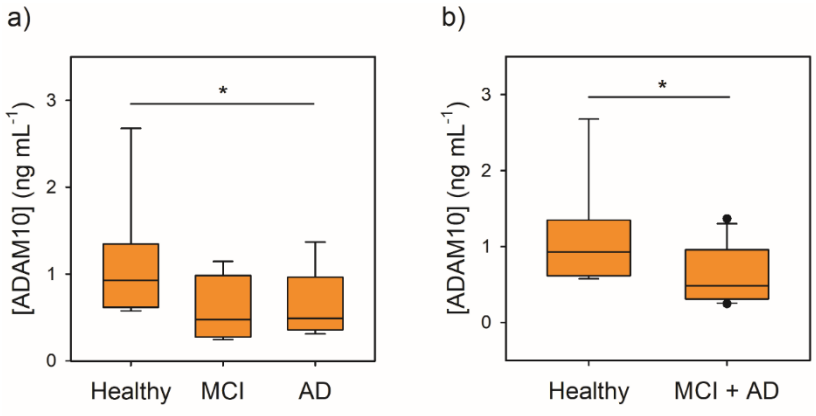

Figure 22. Box plot of the quantification of ADAM10 samples of a) healthy individuals, patients with mild cognitive impairment (MCI), and patients with advanced AD. In b) the samples from the MCI and AD patients were grouped. *Denotes statistical difference ($p < 0.05$). The quantification of ADAM10 in each sample was obtained by applying the $1/C_q$ analytical curve from Figure 21c.

Source: Author.

To validate statistically the assay, the results were analyzed by the receiver operating characteristic (ROC) analysis. ROC is a statistical methodology to validate qualitative clinical tests (i.e., positive or negative samples for AD) by analyzing the performance of the assay in terms of its sensitivity (i.e., rate of true positive results) and its selectivity (i.e., rate of true negative results) in different cut-off values. Therefore, this analysis enables us to estimate the accuracy of the assay by the area under de curve (AUC); and the most suitable cut-off (CO) to differentiate negative samples (i.e., healthy samples) from positive samples (i.e., AD or MCI samples). The ROC analysis (Figure 23) determined that the accuracy of the ADAM10 assay distinguishing between healthy and AD patient samples was 76.3% (AUC in orange squares), whilst the accuracy decreases to 74.5% (AUC in blue circles) when it was included the MCI samples. Moreover, it was possible to estimate the sensitivity, specificity, and the most suitable CO value to differentiate between healthy samples and AD, being 80%, 63%, and $1.38\ ng\ mL^{-1}$ (cross-square labelled in Figure 23), respectively. Whilst the sensitivity of the assay was close to 100%, the specificity/selectivity was closer to a random assay (i.e., 50%). This inaccuracy could be related to the low number of samples used in the assay.

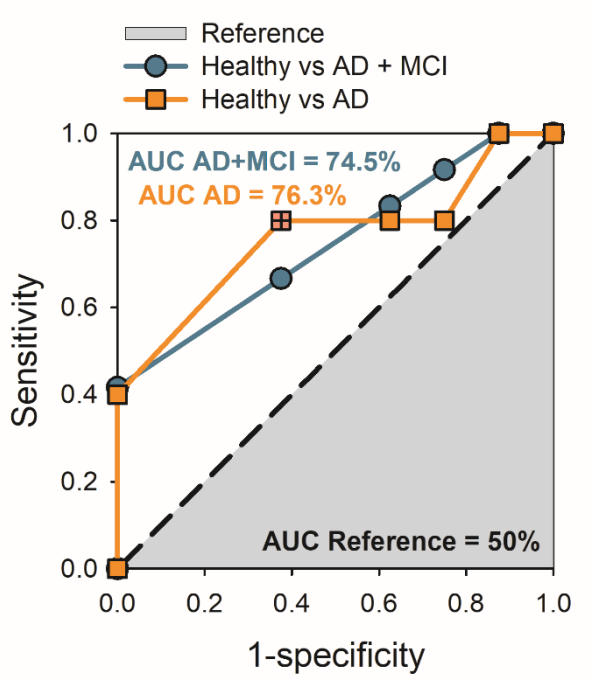

Figure 23. ROC analysis of the ADAM10 assay. The area under the reference curve (AUC = 50%) represents the result of a random assay (i.e., an assay incapable of differentiating between positive and negative samples). This reference was compared with the AUC of the healthy vs AD assay (squares in orange) and the AUC of the healthy vs AD+MCI assay (circled in blue). The most suitable cut-off (cross-square labeled) was assuming $x = 0.375$, corresponding to 80% and 63% of sensitivity and specificity, respectively. The CO value calculated was $1.4\ ng\ mL^{-1}$.

Source: Author.

As it was mentioned before, it is the first time that C_q the transducer is applied to the quantification of a molecular biomarker in human serum samples. The biosensor developed presented 80% and 63% of sensitivity and specificity, respectively, resulting in a very promising for a first quantitative C_q biosensor. Nonetheless, the variation of the ADAM10 concentration in serum observed with the progression of AD was different than the variation reported in the literature. In previous works, Oliveira et al.[86] and Vatanabe et al.[85] reported an increase in ADAM10 concentration in serum with the progression of AD, whilst we observed a decrease in the concentration.

Our initial hypothesis to explain the divergence observed is that our C_q biosensor is quantifying a distinct ADAM10 isoform from the one detected by Oliveira et al.[86] and Vatanabe et al.[85], since the antibody of our biosensor is different to the one used by Vatanabe et al. and, also, it is different to the capture antibody used in Oliveira et al. which used a label-based methodology with two antibodies. This hypothesis is based in the fact that ADAM10 is presented in several isoforms in the cells, i.e., proADAM10 (~ 80 kDa), mature and active (~65 kDa), and soluble and inactive (~55 kDa).[85] Oliveira et al.[86] and Vatanabe et al.[85] confirmed the detection of the soluble isoform whose concentration was increased in the AD patients. Since each antibody could be specific to an isoform and the concentration of each isoform can vary differently with the progression of the disease, we need to confirm the isoform that our antibody detects. Therefore,

to confirm our hypothesis, we developed a second biosensing interface with the antibody anti-ADAM10 (Ab2) used in Vatanabe et al.[85] that is specific to the soluble isoform of ADAM10.

Again, an analytical curve in the ADAM10 concentration range $0.25 - 50\ ng\ mL^{-1}$ with $1/C_q$ as analytical signal was obtained by using Ab2 anti-ADAM10 (Figure 24). The $RR\%_{max}$ and K_a values of the Ab2 anti-ADAM10 was obtained from the Langmuir isotherm (Figure 24a), being $RR\%_{max} = (155.3 \pm 19.5)\%$ and $K_a = (0.03 \pm 0.008)\ mL\ ng^{-1}$. The K_a values of the Ab2 anti-ADAM10 were slightly higher than the one of Ab1 anti-ADAM10; nonetheless, the values were not statistically different. The LOD and LOQ values were obtained from the linear range from the analytical curve (Figure 24b), being $LOD = 0.3\ ng\ mL^{-1}$ and $LOQ = 0.9\ ng\ mL^{-1}$.

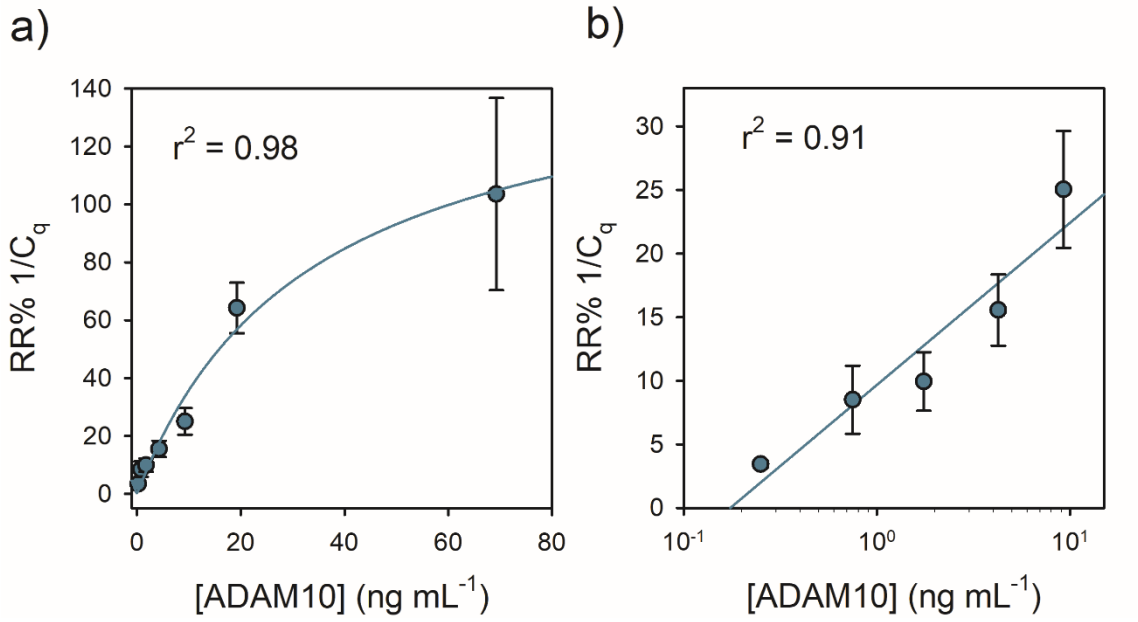

Figure 24. ADAM10 analytical curves with the Ab2 anti-ADAM10 biosensing interface by using as analytical signal $1/C_q$. a) Langmuir isotherm fitting and b) linear range of a). The error bars depicted the standard error from 4 independent assays ($n = 4$).

Source: Author.

Afterward, the serum samples from healthy individuals ($n = 10$) and AD patients ($n = 6$) were incubated in the Ab2 biosensing interface and quantified with the Ab2 analytical curve from Figure 24b. The results are depicted in Figure 25a. The quantification of ADAM10 in the Ab2 biosensing interface indicated higher ADAM10 concentration in the serum of patients with AD (average AD samples concentration $1.7 \pm 0.8\ ng\ mL^{-1}$) than in the samples of healthy individuals (average healthy samples concentration $1.0 \pm 0.6\ ng\ mL^{-1}$), similar as the findings reported by Oliveira et al.[86] and Vatanabe, et al.[85] Nonetheless, although the tendency of the data suggested an increase in ADAM10 concentration with the progression of AD, the results obtained did not present a statistically significant difference that could be related to the low number of samples analyzed, likewise in Vatanabe, et al.[85] study. The difference in the results obtained from the Ab1 and Ab2 assays confirmed the hypothesis that each assay detected different ADAM10 isoforms. While the technical description from Abcam of the Ab1 did not inform the region of interaction with the target, Aviva informs that Ab2 recognizes the middle

region of ADAM10, corresponding to the inactive ~55 kDa ADAM10 isoform, as elucidated by Vatanabe, et al.[85]

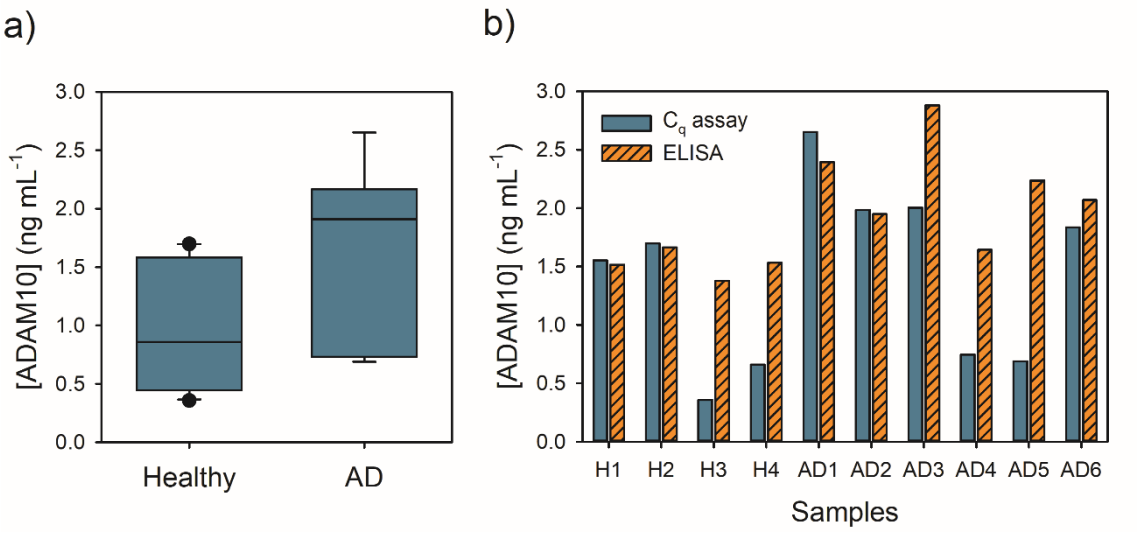

Figure 25. Results of the quantification of ADAM10 in human serum samples with the Ab2 anti-ADAM10 biosensing interface applying the $1/C_q$ analytical curve from Figure 24b. a) Box plot of the quantification of healthy individuals ($n = 10$) and AD patient samples ($n = 6$). t-Student statistical test: $p = 0.063$. b) Comparison of the ADAM10 concentration measured by our C_q assay and ELISA in healthy samples (H1-H4) and AD patient samples (AD1-AD6).

Source: Author.

Moreover, the results from our C_q assay was compared with the concentration calculated by a commercial ELISA kit for ADAM10 quantification (data provided by Prof. Ronaldo C. Faria's research group reported in Oliveira et al.[86]). The ADAM10 concentration in samples H1-H4 and AD1-AD6 were measured by ELISA and C_q assay (Figure 25b) and the values obtained by each method were, in general, in good agreement. In the case of samples H3, H4, AD4, and AD5, the ADAM10 concentration calculated by the C_μ assay was almost half of the concentration calculated by ELISA. This discordance could be related to experimental errors in the construction of the biosensing interface, such as a lower amount of available antibody molecules; or degradation of the protein in the sample during the storage time within the execution of both assays.

In this section, it was demonstrated that C_q biosensors can be applied in the quantification of relevant biomarkers in complex samples for the diagnosis of dementia diseases. Here, we presented two biosensing interfaces for the detection of the analyte ADAM10 by using two different antibodies specific to different ADAM10 isoforms (Ab1 and Ab2) that enabled the quantification of the analyte in serum samples with high accuracy, as indicated by the spike assay in Ab1 assay and by the comparison with ELISA data in Ab2 assay. Moreover, it was demonstrated that the selection of the receptor molecule is important in the interpretation of the assay results because divergences could occur whether different analyte isoforms are analyzed. This is the first time that a C_q transducer is applied to the quantification of analytes in complex samples and the results were very promising.

ptau-181 quantitative assay

The protein ptau-181, as discussed in the introduction, is involved in the neurodegeneration process observed in AD via self-aggregation due to phosphorylation of the protein residues and it has been reported several studies that demonstrated an increase in the protein concentration from 1 to 50 $pg\ mL^{-1}$ in blood with the progression of AD.[81; 87] Due to the low concentration range, high-sensitive C_q transducers were required to achieve the objective proposed in the project, that is, to develop, for the first time, a label-free capacitive biosensor for ptau-181. Therefore, three C_q interfaces based on rPep SAM, rPep SAM with amplifier signal methodology, and CdTe quantum dots (QD) were analyzed and compared in terms of their performance as evaluated through LOD and LOQ values.

The rPep SAM-based assay was developed by using an Au electrode from Metrohm, which was modified with redox peptide SAM where the Ab anti-ptau-181 was immobilized over, as depicted in the experimental section and in more detail in reference Garrote et al.[28] The formation of the redox-peptide capacitive interface was characterized by CV and ECS (Figure 26 in grey dashed lines in a) or grey circles in b)), denoting reversible oxidation/reduction process by $\Delta V = V_{ox} - V_{red} < 20\ mV$ and $j_{ox}/j_{red} \sim 1$.

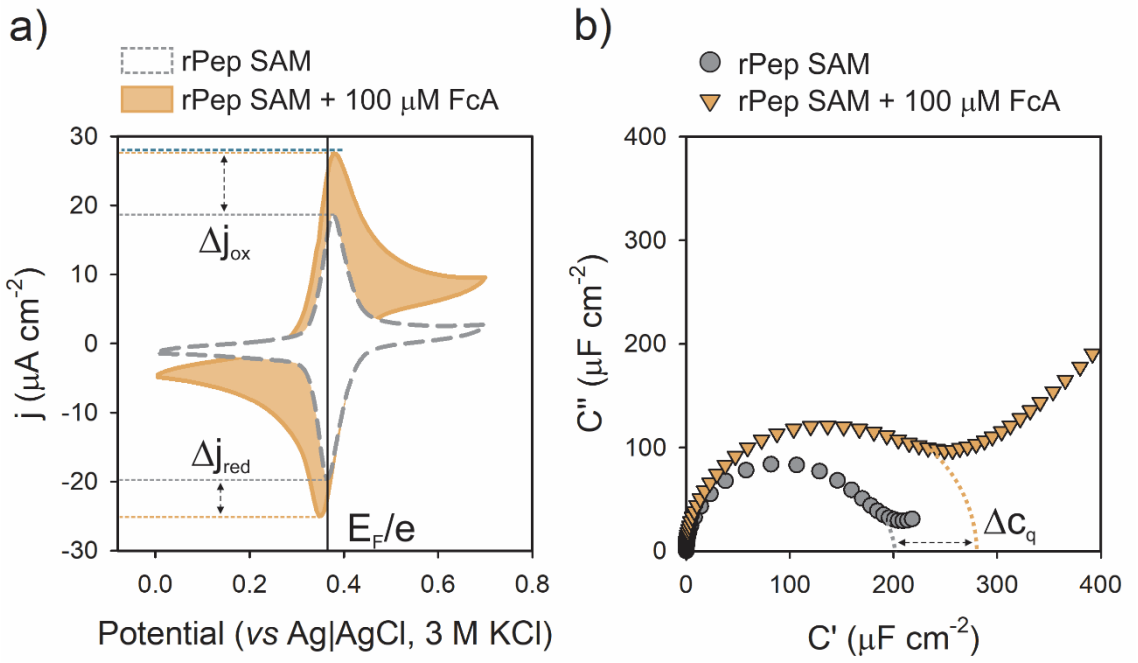

Figure 26. a) Cyclic voltammogram and b) capacitive Nyquist plot of the redox-peptide SAM (rPep SAM) in the presence (colored in orange in a) and orange triangles in b)) and absence (in dashed grey lines in a) and grey circles in b)) of the redox probe FcA in solution. In a), Δj_{ox} and Δj_{red} depict the density current gain with the amplifier signal. In b), ΔC_q depicts the quantum capacitance gain by using the amplifier signal technology developed.

Source: Author.

The immobilisation of the receptor and the construction of the biosensing interface was characterized by ECS (Figure 27a). Note that in the analysis of experimental results, C_q decreased 30% after the immobilization of the antibody and varied $< 1\%$ after the blocking procedure of

the interface, denoting a suitable occupation of the carboxylic acid groups by the antibody blocking molecules. The blank measurements served as a quantification of the drift related to the unspecific interaction of the human serum. Nonetheless, the relative variation of the blanks was $< 3\%$ which indicated a high selectivity and stability. After this analysis, the biosensing interface was consecutively incubated with human serum samples containing increasing concentrations of ptau-181 in the range of $1 - 64\ pg\ mL^{-1}$. Although the electrochemical capacitance is high-sensitive, the $RR\%$ of the assay developed after the incubation with each sample was lower than the $RR\%$ of the blanks, denoting that the redox peptide-based C_q interface was not enough sensitive to detect the analyte in the required concentration range (see Figure 28a).

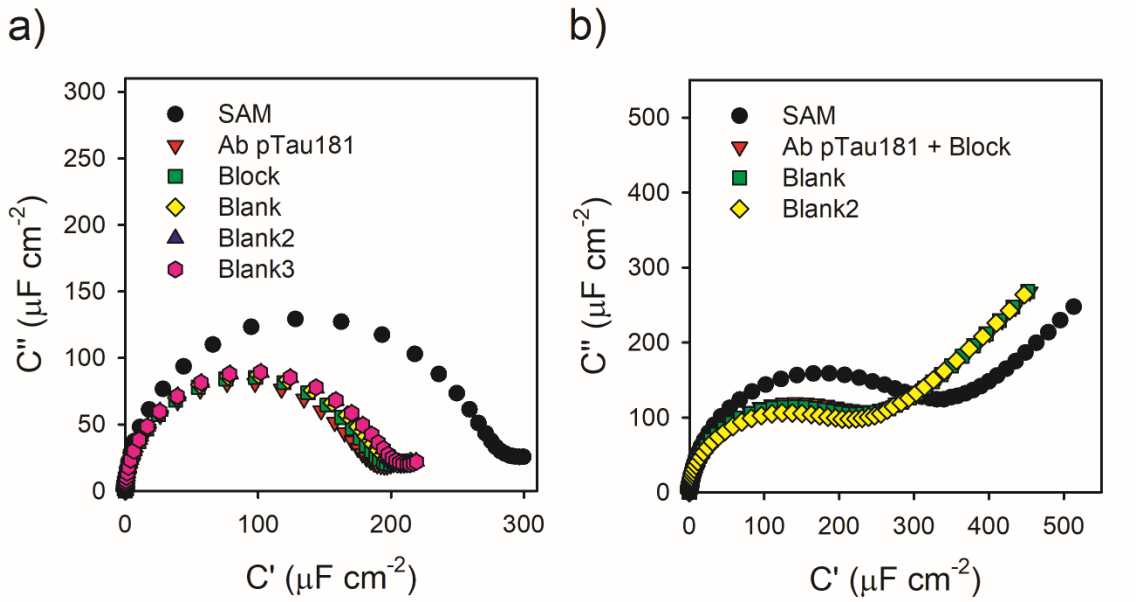

Figure 27. Capacitive Nyquist plots of the formation of the biosensing interface for a) the assay without the redox probe in solution and b) the assay with the redox probe in solution as an amplifier signal.

Source: Author.

The sensitiveness of C_q biosensors depend on three factors: the target-to-receptor size ratio[96], the used transducing signal, and the concentration range of the target in the samples. Considering these aspects, neither the target-to-receptor size ratio nor the concentration range can be varied; therefore, the C_q transducer mechanism can be improved based on an adjustment of rPep SAM by adding an amplifier redox probe in solution[41]; or by modifying the components responsible for C_q with higher sensitiveness to surroundings modifications, such as the consideration of a novel quantum dot (QDs)-based C_q interface (under preparation for publication).

As was depicted in the section reporting the development of the high-sensitive quantitative NS1 Dengue virus assay, it was developed a novel amplifier signal methodology for C_q biosensors that consist in improving quantum rate efficiency of the C_q transducer charge transfer by coupling the density-of-states of electroactive molecules confined to the electrode (that is, for

instance, those of the redox peptide SAM) and that of the redox probe in solution (FcA, 110 μM).[41] In sensing application it enables an enhancement of the sensitivity of the interface to variations in the surrounding environment with the binding process (such as antibody/analyte interaction), as demonstrated in the NS1 Dengue virus biosensor. Likewise, the presence of FcA in the supporting electrolyte in the ptau-181 assay promoted a 1.5-fold and 1.3-fold increase in the oxidative (j_{ox}) and reductive (j_{red}) current densities, respectively, and a 1.3-fold increase in C_q of the interface (Figure 26 colored in orange in a) and orange triangles in b)). Following preceding methodologies, the construction of the biosensing interface was characterized to evaluate the fabrication process step-by-step, but in the present case, the analysis was conducted in a supporting electrolyte containing a redox probe in solution (Figure 27b). Overcoming the assay without the amplifier redox probe, the incubation with undiluted human serum samples containing an increasing concentration of ptau-181 decreased progressively the C_q value (Figure 28b), denoting a higher sensitiveness and successful demonstration of the amplification of the capacitive signal of the interface.

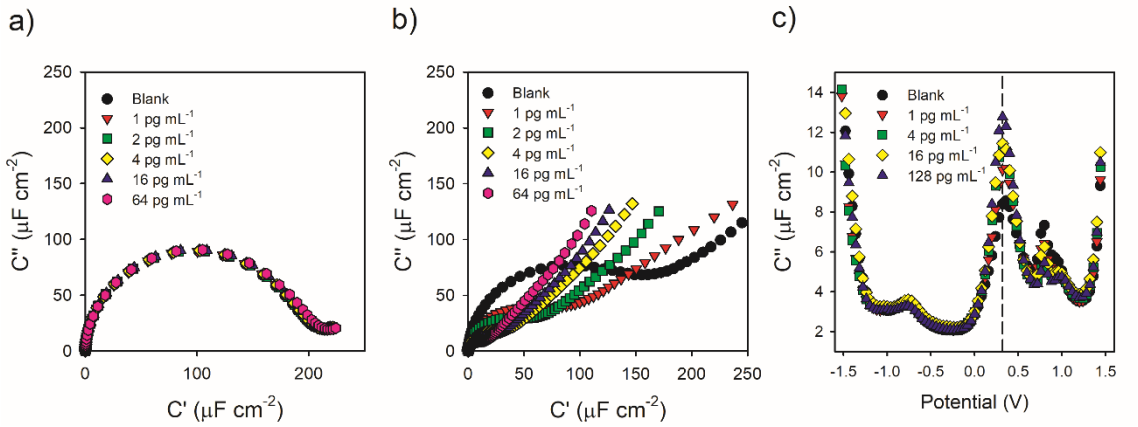

Figure 28. ptau-181 assay by using the following transducer interfaces a) redox peptide SAM and b) redox peptide SAM with redox probe in solution as amplifier signal, and c) CdTe QDs.

Source: Author.

As an alternative to rPep SAM, quantum dots (QDs) C_q-based transducing interface was analyzed. QDs are zero-dimensional (size < 10 nm) semiconductor materials (or artificial atoms) with discrete quantized energy levels that provides excellent optical and electronic properties. Thus, they comprised a promising alternative in the vast possibilities of applications in biological, chemical, and physical research, especially in the diagnosis and detection of diseases.[97; 98] Recently, our research group has demonstrated that QDs can be used as quantum capacitive centers which formed C_q transducers with 4-fold higher sensitivity than C_q assays obtained by rPep SAM or Fc-thiol-based SAM transducers (manuscript under preparation for publication). The mechanism of the QD-based transducer is based on measuring variations in the electron transfer to/from the electrode from/to the QD ensemble (electron transport and charging processes) due to molecule interaction in the surrounding environment. This variation in the electronic properties is obtained by measuring the density-of-states of the QD ensemble accessed in a simple manner by ECS measurements which resolves the energy levels, its

distribution and its variation against surface modifications. Therefore, because of the promising analytical features observed in the QD transducer based on an ensemble of CdTe QD, it was applied to improve the sensitiveness of the ptau-181 assay. The CdTe QD-based assay consisted in miniaturized Au electrodes modified with L-cysteine to which the QDs and formerly the Ab ptau-181 were immobilized (more details about the protocol are depicted in the experimental section). ECS measurements to characterize the modifications were conducted at a potential range of $-1.6 - 1.6\ V$ and a fixed frequency that corresponds to the equilibrium frequency, f_e (that is, $f \to 0$ at which a charge equilibrium regime exists in the interface). The biosensing interface was incubated with ptau-181 serum samples and the DOS of the interface was measured after each incubation (Figure 28c). The interaction between the Ab ptau-181 and the analyte varied the imaginary capacitive (C'') component of the complex capacitance which is associated to the conductance (G, such as $G = 2\pi f C''$) of the energy states associated to this charge equilibrium regime in which there is a communication between CdTeQD states and those of the electrode. Specifically, C'' of the LUMO (lowest unoccupied molecular orbital) energy level ($\sim 0.32\ V$) increased linearly with the target concentration (dashed line in Figure 28c). This increase in C'' as a function of the target immobilization is related to the increase in the charge carriers in the biosensing interface due to the negatively charged phosphorylated residues in the ptau-181 structure.

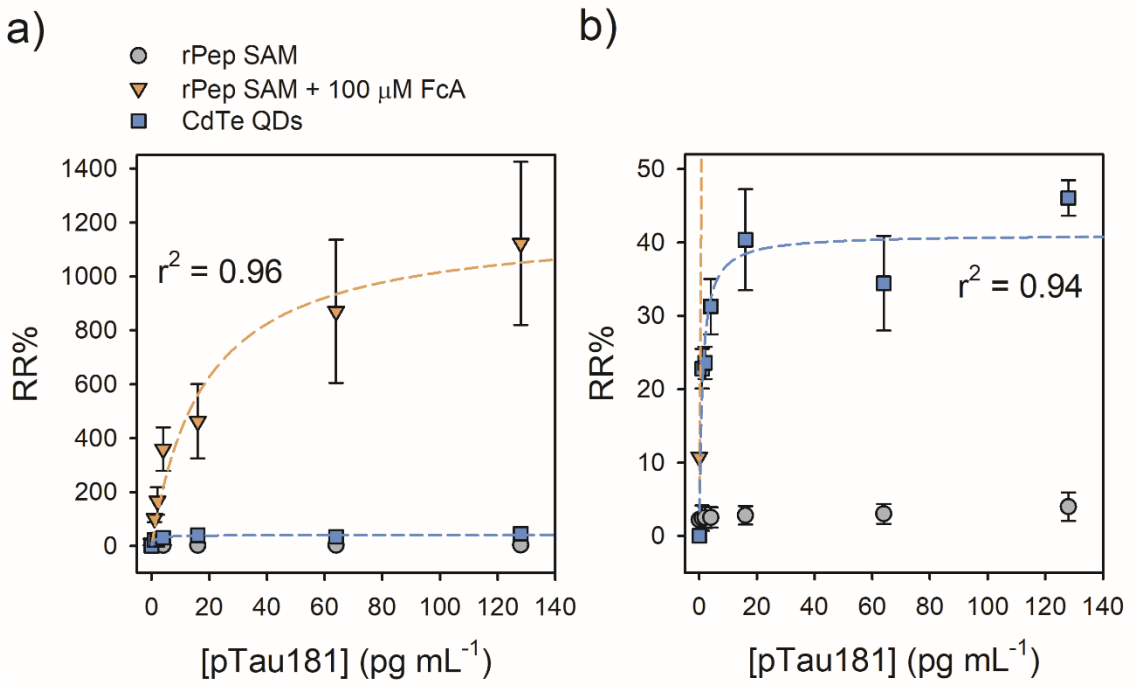

Figure 29. a) Analytical curve of the ptau-181 assay with redox peptide SAM with amplifier signal methodology (orange triangles), that is, redox probe in the supporting electrolyte. b) Zoom from a) to show the analytical curve of the ptau-181 assay with CdTe QDs (blue squares) transducing interface and the unspecific drift of the redox peptide SAM (grey circles). Redox peptide SAM with amplifier signal and CdTe QDs results that were fitted to a Langmuir isotherm providing statistics with $r^2 = 0.96$ and $r^2 = 0.94$, respectively. Error bars represent the standard error of at least 3 independent assays.

Source: Author.

The analytical curves of the rPep SAM with FcA in the supporting electrolyte and the CdTe QDs assays were obtained by plotting the $RR\%$ (Eq. 4) of each ptau-181 sample in neat human serum against the protein concentration. The analytical signal used in the amplifier signal-based assay was $1/C_q$ (orange triangles in Figure 29), related to the energy of the interface, such as $E \propto e^2/{C_q}^{32}$, whereas in the QD-based assay it was used C'' of the LUMO energy level (blue squares in Figure 29), related to G. The on-site analyte-antibody interaction in both assays was demonstrated by fitting the response to a Langmuir isotherm with statistics $r^2 = 0.96$ and $r^2 = 0.94$, respectively for amplifier signal assay and QD-based. From the linear regression of the analytical curve obtained by fitting the $RR\%$ signal with respected to the logarithm of the analyte concentration, we obtained the LOD (Eq. 5) and LOQ (Eq. 6) values, which is compiled in Table 8. The ptau-181 assay based on rPep SAM with the amplifier signal methodology was 25-fold more sensitive than the QD-based assay; nonetheless, the QD-based assay presented suitable LOD and LOQ values for ptau-181 analysis in serum samples in the required analytical range. Both assays improved considerably the results obtained in "pure" rPep SAM-based capacitive assay which only presented a drift signal when incubated in samples containing ptau-181. Moreover, QD and rPep SAMs with FcA assays achieved LOD and LOQ values in the fM range, which is much lower than others C_q biosensors reported in the literature.[99; 100; 101; 102; 103; 104]

Table 8. Limit-of-detection (LOD) and limit-of-quantification (LOQ) of the ptau-181 assays based on rPep SAM, rPep SAM with FcA and CdTe QD C_q transducers.

C_q Transducer	LOD (fM)	LOQ (fM)
rPep SAM	NA	NA
rPep SAM + FcA	0.7	2.3
CdTe QD	17.5	58.4

In summary, the assays based on the rPep SAM with FcA as amplifier signal and the CdTe QD transducer were suitable to quantify the AD biomarker ptau-181 in serum samples with high sensitivity, achieving the objective proposed at the beginning of this thesis. The improvements and the sighting of new C_q transducers have enabled us to overcome the limitations in detection limits and applicability of traditional C_q transducers, such as redox-peptide SAM, and to bring new applications and possibilities to capacitive biosensing technologies.

5. Conclusion

In this doctoral thesis, it was proposed the application of electrochemical capacitance transducers as a high-sensitive, easy-to-use and a miniaturizeble tool for the premature or rapid diagnostic of relevant infectious or non-communicable diseases as an alternative or a complementary screening tool to time-consuming, and complex analytical techniques. As an proof of concept, C_q assays were developed for the detection of SARS-CoV-2 infection, the detection and quantification of Dengue virus infection and the quantification of the AD serum biomarkers ADAM10 and p-tau181, by using well-established C_q transducers, such as the redox-peptide SAM; analytical-improved C_q transducers, such as the redox-peptide SAM coupled with the amplifier signal methodology; or new C_q transducers applied for the first time in this Ph.D. project, such as the single-layer graphene (SLG) and the CdTe quantum dot (CdTe QD) based transducers. The conclusions achieved from those assays were:

i. SLG is an atom-thick molecular layer ultrasensitive to variations in the ionic composition of the medium. The ultrasensitiveness compromises the application of SLG in biosensing, because it causes low-specific and random variation. Nonetheless, here, it was demonstrated that the proper modification of the SLG electrodes enabled to control it and to develop of sensitive and specific qualitative biosensors, as demonstrated in the SARS-CoV-2 assay proof-of-concept.

ii. The electrochemical reaction of C_q transducers operate in a pure quantum diffusionless regime. Here, it was demonstrated that the electron transfer efficiency of this reaction in the redox-peptide SAM was improved by coupling the electrochemical mechanism of the redox-active peptide confined on the electrode with that of a redox probe in solution which induced a 1000-fold improvement in the sensitivity of biosensing assays, as it was observed in the NS1 Dengue virus and p-tau181 assays. This discovery has brought a new level of applications of C_q biosensors that require very low sensitivity.

iii. Redox-peptide SAM is a well-established C_q transducer, used as a standard for the development of new analytical assays. In this Ph.D project for the first time, it was applied for the label-free quantification of ADAM10 in serum samples from healthy individuals and patients with different stages of Alzheimer's disease (AD), demonstrating high accuracy and selectivity due to the high correlation with the concentrations values obtained by the gold-standard analytical technique ELISA.

iv. QDs are zero-dimensional semi-conductors with quantum characteristics and, therefore, with potential as C_q transducers. CdTe QD-based C_q transducer was successfully applied for the quantification of the AD biomarker p-tau181 in commercial serum samples with high sensitivity (23 fM). Together with the redox-peptide SAM coupled with the amplifier signal methodology, CdTe QD-based C_q transducer was the most sensitive C_q transducer improving considerably the analytical features of the redox-peptide SAM (standard). Therefore, it was demonstrated in this Ph.D project that

QD-based C_q transducers were suitable for the development of quantitative biosensing assays with high sensitivity and selectivity.

v. The quantum rate theory describes diffusionless charge transfer mechanisms involved in biological systems. This comprehension of the highly efficient biological processes enables us to develop C_q transducers characterized by their high-efficient electron transfer rate and analytical features by mimicking the biological reactions. Therefore, the quantum rate theory established the fundamentals of the C_q transducers and serves as an analytical tool to measure their potential and to provide the know-how for improving the already developed transducers or for the discovery of new nanostructures or electrochemical reactions that will constitute potential new C_q transducers.

The advantages and limitations of the C_q transducers applied in this Ph.D. project are compiled in Table 9 for better comprehension of the analytical contributions.

As a final remark, this doctoral thesis demonstrated the potential of the electrochemical capacitance technique for the development of transducers for POC devices. The versatility of the technique enables a vast range of applications which diverse analytical features requirements. Noteworthy that the results presented here have derived in two patent applications. Accordingly, the objectives proposed at the beginning of this project were successfully achieved and new prospects for future research have been created.

Table 9. Summary of the advantages and the limitations of the C_q transducers analysed in this Ph.D project.

C_q transducer	Advantages	Limitations
rPep SAM	Well-studied Non-fouling High-reproducibility Sensitivity in the ng per mL range Label-free Reagentless Suitable for qualitative or quantitative assays	Requires high-quality electrode surfaces for self-assembling. Low stability in extreme temperature or long-term storage conditions (organic molecules). Hard to synthetise
rPep SAM with amplifier signal	Sensitivity in the picograms per mL range. Label-free. Suitable for qualitative or quantitative assays	Requires perfect coupling within the redox components. No reagentless. Requires high-quality electrode surfaces for self-assembling. Low stability in extreme temperature or long-term storage conditions (organic molecules). Hard to synthetise
SLG graphene	High-sensitivity. High-specificity (when properly modified). Easy-to-produce. Easy-to-handle. Label-free Reagentless Suitable for qualitative assays	Not suitable for quantitative assays. Ultrasensitive to variations in the ionic environment. Modifications are highly dependent on the initial state of the SLG electrode.
Inorganic quantum dots	Sensitivity in the femtomolar range. High stability in extreme temperatures or long-term storage conditions (inorganic molecules). Label-free Reagentless Suitable for qualitative or quantitative assays	Time-consuming protocol for the formation of the biosensing interface.

.

6. References

[1] NCBI. Polymerase chain reaction (PCR). 2017. Disponível em: < https://www.ncbi.nlm.nih.gov/probe/docs/techpcr/ >. Acesso em: 02/04/2020.

[2] HOSSEINI, S. et al. Advantages, Disadvantages and Modifications of Conventional ELISA. In: HOSSEINI, S.;VÁZQUEZ-VILLEGAS, P.*, et al* (Ed.). **Enzyme-linked Immunosorbent Assay (ELISA): From A to Z**. Singapore: Springer Singapore, 2018. p.67-115. ISBN 978-981-10-6766-2.

[3] DEROCO, P. B.; WACHHOLZ JUNIOR, D.; KUBOTA, L. T. Recent advances in point-of-care biosensors for the diagnosis of neglected tropical diseases. **Sensors and Actuators B: Chemical,** v. 349, p. 130821, 2021/12/15/ 2021. ISSN 0925-4005. Disponível em: < https://www.sciencedirect.com/science/article/pii/S0925400521013897 >.

[4] VAZ, R.; FRASCO, M. F.; SALES, M. G. F. Chapter 4 - Biosensors: concept and importance in point-of-care disease diagnosis. In: KHAN, R.;PARIHAR, A.*, et al* (Ed.). **Biosensor Based Advanced Cancer Diagnostics**: Academic Press, 2022. p.59-84. ISBN 978-0-12-823424-2.

[5] KETTLER, H.; WHITE, K.; HAWKES, S. Mapping the landscape of diagnostics for sexually transmitted infections. **Special programme for research and training in tropical diseases**, https://www.who.int/tdr/publications/documents/mapping-landscape-sti.pdf, 2004. Disponível em: < https://www.who.int/tdr/publications/documents/mapping-landscape-sti.pdf >.

[6] LAND, K. J. et al. REASSURED diagnostics to inform disease control strategies, strengthen health systems and improve patient outcomes. **Nature Microbiology,** v. 4, n. 1, p. 46-54, 2019/01/01 2019. ISSN 2058-5276. Disponível em: < https://doi.org/10.1038/s41564-018-0295-3 >.

[7] LOPES, L. C.; SANTOS, A.; BUENO, P. R. An outlook on electrochemical approaches for molecular diagnostics assays and discussions on the limitations of miniaturized technologies for point-of-care devices. **Sensors and Actuators Reports**, p. 100087, 2022/02/22/ 2022. ISSN 2666-0539. Disponível em: < https://www.sciencedirect.com/science/article/pii/S2666053922000145 >.

[8] CHEN, C.; WANG, J. Optical biosensors: an exhaustive and comprehensive review. **Analyst,** v. 145, n. 5, p. 1605-1628, 2020. ISSN 0003-2654. Disponível em: < http://dx.doi.org/10.1039/C9AN01998G >.

[9] NGUYEN, H. et al. Surface Plasmon Resonance: A Versatile Technique for Biosensor Applications. **Sensors,** v. 15, n. 5, p. 10481-10510, 2015. ISSN 8252217532. Disponível em: < http://www.mdpi.com/1424-8220/15/5/10481/ >.

[10] LIM, H. J. et al. Quartz crystal microbalance-based biosensors as rapid diagnostic devices for infectious diseases. **Biosensors and Bioelectronics,** v. 168, p. 112513,

2020/11/15/ 2020. ISSN 0956-5663. Disponível em: < https://www.sciencedirect.com/science/article/pii/S0956566320305054 >.

[11] CLARK, L. C.; LYONS, C. Electrode systems for continuous monitoring in cardiovascular surgery. **Annals Of The New York Academy Of Sciences,** v. 102, n. 1, p. 29-45, 1962. ISSN 0077-8923 (Print)\r0077-8923 (Linking). Disponível em: < http://onlinelibrary.wiley.com/doi/10.1111/j.1749-6632.1962.tb13623.x/full%5Cnhttp://doi.wiley.com/10.1111/j.1749-6632.1962.tb13623.x >.

[12] HEINEMAN, W. R.; JENSEN, W. B. Leland C. Clark Jr. (1918–2005). **Biosensors and Bioelectronics,** v. 21, n. 8, p. 1403-1404, 2006. Disponível em: < http://linkinghub.elsevier.com/retrieve/pii/S0956566305004094 >.

[13] PALMSENS. PalmSens4: Compact, versatile and powerful. Disponível em: < https://www.palmsens.com/product/palmsens4/ >. Acesso em: 26/01/2022.

[14] PALMSENS. Sensit Smart: Smartphone potentiostat. Disponível em: < https://www.palmsens.com/product/sensit-smart/ >. Acesso em: 26/01/2022.

[15] BRATOV, A.; ABRAMOVA, N.; IPATOV, A. Recent trends in potentiometric sensor arrays—A review. **Analytica Chimica Acta,** v. 678, n. 2, p. 149-159, 2010/09/30/ 2010. ISSN 0003-2670. Disponível em: < https://www.sciencedirect.com/science/article/pii/S0003267010010962 >.

[16] ABBOTT. i-STAT 1. Disponível em: < https://www.globalpointofcare.abbott/en/product-details/apoc/i-stat-system-us.html >. Acesso em: 20/01/2022.

[17] BOLLELLA, P.; GORTON, L. Enzyme based amperometric biosensors. **Current Opinion in Electrochemistry,** v. 10, p. 157-173, 2018/08/01/ 2018. ISSN 2451-9103. Disponível em: < https://www.sciencedirect.com/science/article/pii/S2451910318301005 >.

[18] LOJOU, É.; BIANCO, P. Application of the electrochemical concepts and techniques to amperometric biosensor devices. **Journal of Electroceramics,** v. 16, n. 1, p. 79-91, 2006/02/01 2006. ISSN 1573-8663. Disponível em: < https://doi.org/10.1007/s10832-006-2365-9 >.

[19] PATIL, A. V. et al. Immittance electroanalysis in diagnostics. **Analytical Chemistry,** v. 87, n. 2, p. 944-950, 2015.

[20] BERTOK, T. et al. Electrochemical Impedance Spectroscopy Based Biosensors: Mechanistic Principles, Analytical Examples and Challenges towards Commercialization for Assays of Protein Cancer Biomarkers. **ChemElectroChem,** v. 6, n. 4, p. 989-1003, 2019/02/15 2019. ISSN 2196-0216. Disponível em: < https://doi.org/10.1002/celc.201800848 >. Acesso em: 2022/01/26.

[21] LISDAT, F.; SCHÄFER, D. The use of electrochemical impedance spectroscopy for biosensing. **Analytical and Bioanalytical Chemistry,** v. 391, n. 5, p. 1555-1567, 2008. ISSN 1618-2642.

[22] GARROTE, B. L.; SANTOS, A.; BUENO, P. R. Perspectives on and Precautions for the Uses of Electric Spectroscopic Methods in Label-free Biosensing Applications. **ACS Sensors**, 2019.

[23] BUENO, P. R. et al. The nanoscopic principles of capacitive ion sensing interfaces. **Physical Chemistry Chemical Physics**, 2020. ISSN 1463-9076. Disponível em: < http://dx.doi.org/10.1039/C9CP05543F >.

[24] HEIN, R. et al. A halogen-bonding foldamer molecular film for selective reagentless anion sensing in water. **Chemical Communications,** v. 55, n. 33, p. 4849-4852, 2019. ISSN 1359-7345. Disponível em: < http://dx.doi.org/10.1039/C9CC00335E >.

[25] VOGT, S. et al. Critical view on electrochemical impedance spectroscopy using the ferri/ferrocyanide redox couple at gold electrodes. **Analytical Chemistry,** v. 88, n. 8, p. 4383-4390, 2016.

[26] LEE, L. Y. S.; LENNOX, R. B. Ferrocenylalkylthiolate labeling of defects in alkylthiol self-assembled monolayers on gold. **Physical Chemistry Chemical Physics,** v. 9, n. 8, p. 1013-1020, 2007. Disponível em: < http://xlink.rsc.org/?DOI=B613598F >.

[27] BOUBOUR, E.; LENNOX, R. B. Insulating properties of self-assembled monolayers monitored by impedance spectroscopy. **Langmuir,** v. 16, n. 9, p. 4222-4228, 2000. ISSN 07437463 (ISSN).

[28] GARROTE, B. L.; SANTOS, A.; BUENO, P. R. Label-free capacitive assaying of biomarkers for molecular diagnostics. **Nature Protocols**, 2020/10/26 2020. ISSN 1750-2799. Disponível em: < https://doi.org/10.1038/s41596-020-0390-9 >.

[29] ALARCÓN, E. V. G.; SANTOS, A.; BUENO, P. R. Perspective on quantum electrochemistry. A simple method for measuring the electron transfer rate constant. **Electrochimica Acta,** v. 398, p. 139219, 2021/12/01/ 2021. ISSN 0013-4686. Disponível em: < https://www.sciencedirect.com/science/article/pii/S0013468621015097 >.

[30] BUENO, P. R. Electron transfer and conductance quantum. **Physical Chemistry Chemical Physics,** v. 22, n. 45, p. 26109-26112, 2020. ISSN 1463-9076. Disponível em: < http://dx.doi.org/10.1039/D0CP04522E >.

[31] SÁNCHEZ, Y. P.; SANTOS, A.; BUENO, P. R. Quantum Mechanical Meaning of the Charge Transfer Resistance. **The Journal of Physical Chemistry C**, 2022/02/03 2022. ISSN 1932-7447. Disponível em: < https://doi.org/10.1021/acs.jpcc.1c07801 >.

[32] MIRANDA, D. A.; BUENO, P. R. Density functional theory and an experimentally-designed energy functional of electron density. **Physical Chemistry Chemical Physics,** v. 18, n. 37, p. 25984-25992, 2016. Disponível em: < http://xlink.rsc.org/?DOI=C6CP01659F >.

[33] BUENO, P. R. et al. The density-of-States and equilibrium charge dynamics of redox-active switches. **Electrochimica Acta,** v. 387, p. 138410, 2021/08/10/ 2021. ISSN 0013-4686. Disponível em: < https://www.sciencedirect.com/science/article/pii/S0013468621007003 >.

[34] PINZÓN, E. F.; SANTOS, A. D.; BUENO, P. R. Density of States of a Nanoscale Semiconductor Interface as a Transduction Signal for Sensing Molecules. **ACS Applied Electronic Materials,** v. 3, n. 8, p. 3411-3417, 2021/08/24 2021. Disponível em: < https://doi.org/10.1021/acsaelm.1c00387 >.

[35] LOPES, L. C.; BUENO, P. R. Sensing the quantized reactivity of graphene. **Analytica Chimica Acta,** v. 1177, p. 338735, 2021/09/08/ 2021. ISSN 0003-2670. Disponível em: < https://www.sciencedirect.com/science/article/pii/S0003267021005614 >.

[36] LOPES, L. C.; SANTOS, A.; BUENO, P. R. Measuring quantum conductance and capacitance of graphene using impedance-derived capacitance spectroscopy. **Carbon,** v. 184, p. 821-827, 2021/10/30/ 2021. ISSN 0008-6223. Disponível em: < https://www.sciencedirect.com/science/article/pii/S0008622321008472 >.

[37] BUENO, P. R.; MIRANDA MERCADO, D. A. Quantum Rate Theory for Graphene. **The Journal of Physical Chemistry C**, 2022/09/01 2022. ISSN 1932-7447. Disponível em: < https://doi.org/10.1021/acs.jpcc.2c02419 >.

[38] LUCAS GARROTE, B. et al. Reagentless Quantum-Rate-Based Electrochemical Signal of Graphene for Detecting SARS-CoV-2 Infection Using Nasal Swab Specimens. **ACS Sensors**, 2022/09/01 2022. Disponível em: < https://doi.org/10.1021/acssensors.2c01016 >.

[39] BUENO, P. R. et al. **Transdutor modificado, mecanismo de transdução e método de detecção e/ou quantificação de espécies de interesse analítico com transdutor modificado**. INPI. Brazil 2022.

[40] BUENO, P. R. et al. **Método e dispositivo de amplificação de sinal transdutor para ensaios capacitivos**. INPI. Brazil 2021.

[41] SÁNCHEZ, Y. P.; SANTOS, A.; ROBERTO BUENO, P. Quantum rate efficiency of the charge transfer mediated by quantum capacitive states. **Electrochimica Acta**, p. 141194, 2022/09/15/ 2022. ISSN 0013-4686. Disponível em: < https://www.sciencedirect.com/science/article/pii/S0013468622013512 >.

[42] LIU, Y. et al. Advances in signal amplification strategies for electrochemical biosensing. **Current Opinion in Electrochemistry,** v. 12, p. 5-12, 2018/12/01/ 2018. ISSN 2451-9103. Disponível em: < https://www.sciencedirect.com/science/article/pii/S245191031830098X >.

[43] MORALES-NARVÁEZ, E.; DINCER, C. The impact of biosensing in a pandemic outbreak: COVID-19. **Biosensors and Bioelectronics,** v. 163, p. 112274, 2020/09/01/ 2020. ISSN 0956-5663. Disponível em: < https://www.sciencedirect.com/science/article/pii/S0956566320302694 >.

[44] WHO, W. H. O. WHO Coronavirus (COVID-19) Dashboard. Disponível em: < https://covid19.who.int/table >. Acesso em: 07/12/2021.

[45] HOFFMANN, M. et al. SARS-CoV-2 Cell Entry Depends on ACE2 and TMPRSS2 and Is Blocked by a Clinically Proven Protease Inhibitor. **Cell,** v. 181, n. 2, p. 271-280, 2020. ISSN 0092-8674. Disponível em: < https://doi.org/10.1016/j.cell.2020.02.052 >. Acesso em: 2020/04/01.

[46] ALAFEEF, M. et al. Rapid, Ultrasensitive, and Quantitative Detection of SARS-CoV-2 Using Antisense Oligonucleotides Directed Electrochemical Biosensor Chip. **ACS Nano,** v. 14, n. 12, p. 17028-17045, 2020/12/22 2020. ISSN 1936-0851. Disponível em: < https://doi.org/10.1021/acsnano.0c06392 >.

[47] CHAIBUN, T. et al. Rapid electrochemical detection of coronavirus SARS-CoV-2. **Nature Communications,** v. 12, n. 1, p. 802, 2021/02/05 2021. ISSN 2041-1723. Disponível em: < https://doi.org/10.1038/s41467-021-21121-7 >.

[48] KASHEFI-KHEYRABADI, L. et al. Rapid, multiplexed, and nucleic acid amplification-free detection of SARS-CoV-2 RNA using an electrochemical biosensor. **Biosensors and Bioelectronics,** v. 195, p. 113649, 2022/01/01/ 2022. ISSN 0956-5663. Disponível em: < https://www.sciencedirect.com/science/article/pii/S0956566321006862 >.

[49] ELLEDGE, S. K. et al. Engineering luminescent biosensors for point-of-care SARS-CoV-2 antibody detection. **Nature Biotechnology,** v. 39, n. 8, p. 928-935, 2021/08/01 2021. ISSN 1546-1696. Disponível em: < https://doi.org/10.1038/s41587-021-00878-8 >.

[50] TORRENTE-RODRÍGUEZ, R. M. et al. SARS-CoV-2 RapidPlex: A Graphene-Based Multiplexed Telemedicine Platform for Rapid and Low-Cost COVID-19 Diagnosis and Monitoring. **Matter,** v. 3, n. 6, p. 1981-1998, 2020/12/02/ 2020. ISSN 2590-2385. Disponível em: < https://www.sciencedirect.com/science/article/pii/S2590238520305531 >.

[51] LI, J.; LILLEHOJ, P. B. Microfluidic Magneto Immunosensor for Rapid, High Sensitivity Measurements of SARS-CoV-2 Nucleocapsid Protein in Serum. **ACS Sensors,** v. 6, n. 3, p. 1270-1278, 2021/03/26 2021. Disponível em: < https://doi.org/10.1021/acssensors.0c02561 >.

[52] NASCIMENTO, E. D. et al. COVID-19 diagnosis by SARS-CoV-2 Spike protein detection in saliva using an ultrasensitive magneto-assay based on disposable electrochemical sensor. **Sensors and Actuators B: Chemical,** v. 353, p. 131128, 2022/02/15/ 2022. ISSN 0925-4005. Disponível em: < https://www.sciencedirect.com/science/article/pii/S0925400521016968 >.

[53] NGUYEN, N. H. L. et al. COVID-19 Spike Protein Induced Phononic Modification in Antibody-Coupled Graphene for Viral Detection Application. **ACS Nano,** v. 15, n. 7, p. 11743-11752, 2021/07/27 2021. ISSN 1936-0851. Disponível em: < https://doi.org/10.1021/acsnano.1c02549 >.

[54] RAZIQ, A. et al. Development of a portable MIP-based electrochemical sensor for detection of SARS-CoV-2 antigen. **Biosensors and Bioelectronics,** v. 178, p. 113029, 2021/04/15/ 2021. ISSN 0956-5663. Disponível em: < https://www.sciencedirect.com/science/article/pii/S0956566321000658 >.

[55] SEO, G. et al. Rapid Detection of COVID-19 Causative Virus (SARS-CoV-2) in Human Nasopharyngeal Swab Specimens Using Field-Effect Transistor-Based Biosensor. **ACS Nano,** v. 14, n. 4, p. 5135-5142, 2020/04/28 2020. ISSN 1936-0851. Disponível em: < https://doi.org/10.1021/acsnano.0c02823 >.

[56] YOUSEFI, H. et al. Detection of SARS-CoV-2 Viral Particles Using Direct, Reagent-Free Electrochemical Sensing. **Journal of the American Chemical Society,** v. 143, n. 4, p. 1722-1727, 2021/02/03 2021. ISSN 0002-7863. Disponível em: < https://doi.org/10.1021/jacs.0c10810 >.

[57] WANG, L. et al. Rapid and ultrasensitive electromechanical detection of ions, biomolecules and SARS-CoV-2 RNA in unamplified samples. **Nature Biomedical Engineering**, 2022/02/07 2022. ISSN 2157-846X. Disponível em: < https://doi.org/10.1038/s41551-021-00833-7 >.

[58] LASSERRE, P. et al. SARS-CoV-2 Aptasensors Based on Electrochemical Impedance Spectroscopy and Low-Cost Gold Electrode Substrates. **Analytical Chemistry,** v. 94, n. 4, p. 2126-2133, 2022/02/01 2022. ISSN 0003-2700. Disponível em: < https://doi.org/10.1021/acs.analchem.1c04456 >.

[59] PAHO, P. A. H. O. Reported cases of Dengue fever in the Americas. **PLISA health information platform for the Americas**, Disponível em: < https://www3.paho.org/data/index.php/en/mnu-topics/indicadores-dengue-en/dengue-nacional-en/252-dengue-pais-ano-en.html >. Acesso em: 07/03/2022.

[60] SILVA, J. V. J. et al. Current status, challenges and perspectives in the development of vaccines against yellow fever, dengue, Zika and chikungunya viruses. **Acta Tropica,** v. 182, p. 257-263, 2018. Disponível em: < https://linkinghub.elsevier.com/retrieve/pii/S0001706X17314444 >.

[61] EDUCATION, N. Dengue viruses. Scitable by Nature education, 2014. Disponível em: < https://www.nature.com/scitable/topicpage/dengue-viruses-22400925/ >. Acesso em: 07/03/2022.

[62] GANJI, L. V.; KANYALKAR, M. A. Non-structural Proteases as a Target of Dengue Virus. **Journal of Antivirals & Antiretrovirals,** v. 11, n. 4, 2019.

[63] WHO, W. H. O. Dengue and severe dengue. 2022. Disponível em: < https://www.who.int/news-room/fact-sheets/detail/dengue-and-severe-dengue >. Acesso em: 07/03/2022.

[64] ANUSHA, J. R. et al. Electrochemical biosensing of mosquito-borne viral disease, dengue: A review. **Biosensors and Bioelectronics,** v. 142, p. 111511, 2019/10/01/ 2019. ISSN 0956-5663. Disponível em: < http://www.sciencedirect.com/science/article/pii/S0956566319305901 >.

[65] NICOLINI, A. M.; MCCRACKEN, K. E.; YOON, J.-Y. Future developments in biosensors for field-ready Zika virus diagnostics. **Journal of Biological Engineering,** v. 11, n. 1, p. 7, 2017/01/23 2017. ISSN 1754-1611. Disponível em: < https://doi.org/10.1186/s13036-016-0046-z >.

[66] CECCHETTO, J. et al. Serological point-of-care and label-free capacitive diagnosis of dengue virus infection. **Biosensors and Bioelectronics,** v. 151, p. 111972, 2020/03/01/ 2020. ISSN 0956-5663. Disponível em: < http://www.sciencedirect.com/science/article/pii/S0956566319310498 >.

[67] CECCHETTO, J. et al. An impedimetric biosensor to test neat serum for dengue diagnosis. **Sensors and Actuators, B: Chemical,** v. 213, p. 150-154, 2015. Disponível em: < http://dx.doi.org/10.1016/j.snb.2015.02.068 >.

[68] CECCHETTO, J. et al. The capacitive sensing of NS1 Flavivirus biomarker. **Biosensors and Bioelectronics,** v. 87, n. June 2016, p. 949-956, 2017. ISSN 1873-4235 0956-5663. Disponível em: < http://dx.doi.org/10.1016/j.bios.2016.08.097 >.

[69] SILVA, M. M. S. et al. Electrochemical detection of dengue virus NS1 protein with a poly(allylamine)/carbon nanotube layered immunoelectrode. **Journal of Chemical Technology & Biotechnology,** v. 90, n. 1, p. 194-200, 2015/01/01 2015. ISSN 0268-2575. Disponível em: < https://doi.org/10.1002/jctb.4305 >. Acesso em: 2020/04/24.

[70] SINGHAL, C.; PUNDIR, C. S.; NARANG, J. A genosensor for detection of consensus DNA sequence of Dengue virus using ZnO/Pt-Pd nanocomposites. **Biosensors and Bioelectronics,** v. 97, p. 75-82, 2017/11/15/ 2017. ISSN 0956-5663. Disponível em: < http://www.sciencedirect.com/science/article/pii/S0956566317303640 >.

[71] PALOMAR, Q. et al. Impedimetric quantification of anti-dengue antibodies using functional carbon nanotube deposits validated with blood plasma assays. **Electrochimica Acta,** v. 274, p. 84-90, 2018/06/01/ 2018. ISSN 0013-4686. Disponível em: < http://www.sciencedirect.com/science/article/pii/S0013468618308557 >.

[72] OLIVEIRA, N. et al. A Sensitive and Selective Label-Free Electrochemical DNA Biosensor for the Detection of Specific Dengue Virus Serotype 3 Sequences. **Sensors,** v. 15, n. 7, 2015. ISSN 1424-8220.

[73] SANTOS, A.; BUENO, P. R.; DAVIS, J. J. A dual marker label free electrochemical assay for Flavivirus dengue diagnosis. **Biosensors and Bioelectronics,** v. 100, n. September 2017, p. 519-525, 2018. Disponível em: < http://dx.doi.org/10.1016/j.bios.2017.09.014 >.

[74] WHO, W. H. O. Dementia. 2019. Disponível em: < https://www.who.int/en/news-room/fact-sheets/detail/dementia >. Acesso em: 16/01/2020.

[75] MOLINUEVO, J. L. et al. **Current state of Alzheimer's fluid biomarkers**. Springer Berlin Heidelberg, 2018. 821-853 ISBN 0040101819. Disponível em: < https://doi.org/10.1007/s00401-018-1932-x >.

[76] ABCAM. Neuroinflammation and Alzheimer's disease poster. 2017. Disponível em: < https://www.abcam.com/neuroscience/neuroinflammation-and-alzheimers-disease-poster >. Acesso em: 09/03/2022.

[77] SCHELTENS, P. et al. Alzheimer's disease introduction. **The Lancet,** v. 6736, n. 15, p. 1-13, 2016. Disponível em: < http://dx.doi.org/10.1016/S0140-6736(15)01124-1 >.

[78] GROSSBERG, G. T. Cholinesterase inhibitors for the treatment of Alzheimer's disease: Getting on and staying on. **Current Therapeutic Research - Clinical and Experimental,** v. 64, n. 4, p. 216-235, 2003. ISSN 0011-393X.

[79] SHI, M. et al. Impact of Anti-amyloid-β Monoclonal Antibodies on the Pathology and Clinical Profile of Alzheimer's Disease: A Focus on Aducanumab and Lecanemab. **Front Aging Neurosci,** v. 14, p. 870517, 2022. ISSN 1663-4365 (Print).

[80] HUYNH, R. A.; MOHAN, C. Alzheimer's Disease: Biomarkers in the Genome, Blood, and Cerebrospinal Fluid. v. 8, n. March, 2017.

[81] TATEBE, H. et al. Quantification of plasma phosphorylated tau to use as a biomarker for brain Alzheimer pathology: pilot case-control studies including patients with Alzheimer's disease and down syndrome. **Molecular Neurodegeneration,** v. 12, n. 1, p. 63, 2017/09/04 2017. ISSN 1750-1326. Disponível em: < https://doi.org/10.1186/s13024-017-0206-8 >.

[82] COLCIAGHI, F. et al. α-Secretase ADAM10 as Well as αAPPs Is Reduced in Platelets and CSF of Alzheimer Disease Patients. **Molecular Medicine,** v. 8, n. 2, p. 67-74, 2002/02/01 2002. ISSN 1528-3658. Disponível em: < https://doi.org/10.1007/BF03402076 >.

[83] MANZINE, P. R. et al. ADAM10 in Alzheimer's disease: Pharmacological modulation by natural compounds and its role as a peripheral marker. **Biomedicine & Pharmacotherapy,** v. 113, p. 108661, 2019/05/01/ 2019. ISSN 0753-3322. Disponível em: < http://www.sciencedirect.com/science/article/pii/S075333221837032X >.

[84] COLCIAGHI, F. et al. Platelet APP, ADAM 10 and BACE alterations in the early stages of Alzheimer disease. **Neurology,** v. 62, n. 3, p. 498, 2004. Disponível em: < http://n.neurology.org/content/62/3/498.abstract >.

[85] PEREIRA VATANABE, I. et al. ADAM10 Plasma and CSF Levels Are Increased in Mild Alzheimer's Disease. **International Journal of Molecular Sciences,** v. 22, n. 5, 2021. ISSN 1422-0067.

[86] DE OLIVEIRA, T. R. et al. Early Diagnosis of Alzheimer's Disease in Blood Using a Disposable Electrochemical Microfluidic Platform. **ACS Sensors,** v. 5, n. 4, p. 1010-1019, 2020/04/24 2020. Disponível em: < https://doi.org/10.1021/acssensors.9b02463 >.

[87] KARIKARI, T. K. et al. Blood phosphorylated tau 181 as a biomarker for Alzheimer's disease: a diagnostic performance and prediction modelling study using data from four prospective cohorts. **The Lancet Neurology,** v. 19, n. 5, p. 422-433, 2020/05/01/ 2020. ISSN 1474-4422. Disponível em: < http://www.sciencedirect.com/science/article/pii/S1474442220300715 >.

[88] WANG, J. et al. Shape-dependent electrocatalytic activity of monodispersed gold nanocrystals toward glucose oxidation. **Chemical Communications,** v. 47, n. 24, p. 6894-6894, 2011. ISSN 1359-7345. Disponível em: < http://xlink.rsc.org/?DOI=c1cc11784j >.

[89] TRASATTI, S.; PETRII, O. A. Real surface area measurements in electrochemistry. **Pure and Applied Chemistry,** v. 63, n. 5, p. 711-734, 1991.

[90] HERMANSON, G. T. Bioconjugate Reagents. **Bioconjugate Techniques**, p. 214-233, 2008. ISSN 9780123705013.

[91] NOVOSELOV, K. S. et al. A roadmap for graphene. **Nature,** v. 490, n. 7419, p. 192-200, 2012/10/01 2012. ISSN 1476-4687. Disponível em: < https://doi.org/10.1038/nature11458 >.

[92] HARVEY, W. T. et al. SARS-CoV-2 variants, spike mutations and immune escape. **Nature Reviews Microbiology,** v. 19, n. 7, p. 409-424, 2021. ISSN 1740-1534. Disponível em: < https://doi.org/10.1038/s41579-021-00573-0 >.

[93] JEGERLEHNER, S. et al. Diagnostic accuracy of a SARS-CoV-2 rapid antigen test in real-life clinical settings. n. 1878-3511 (Electronic),

[94] WÖLFL-DUCHEK, M. et al. Sensitivity and Specificity of SARS-CoV-2 Rapid Antigen Detection Tests Using Oral, Anterior Nasal, and Nasopharyngeal Swabs: a Diagnostic Accuracy Study. n. 2165-0497 (Electronic),

[95] DENG, L.; KITOVA, E. N.; KLASSEN, J. S. Dissociation Kinetics of the Streptavidin–Biotin Interaction Measured Using Direct Electrospray Ionization Mass Spectrometry Analysis. **Journal of The American Society for Mass Spectrometry,** v. 24, n. 1, p. 49-56, 2013/01/01 2013. ISSN 1879-1123. Disponível em: < https://doi.org/10.1007/s13361-012-0533-5 >.

[96] GARROTE, B. L. et al. Field effect in molecule-gated switches and the role of target-to-receptor size ratio in biosensor sensitivity. **Biosensors and Bioelectronics,** v. 127, 2019.

[97] FARZIN, M. A.; ABDOOS, H. A critical review on quantum dots: From synthesis toward applications in electrochemical biosensors for determination of disease-related biomolecules. **Talanta,** v. 224, p. 121828, 2021/03/01/ 2021. ISSN 0039-9140. Disponível em: < https://www.sciencedirect.com/science/article/pii/S003991402031119X >.

[98] MUKHERJEE, A.; SHIM, Y.; MYONG SONG, J. Quantum dot as probe for disease diagnosis and monitoring. **Biotechnology Journal,** v. 11, n. 1, p. 31-42, 2016. ISSN 1860-6768. Disponível em: < https://onlinelibrary.wiley.com/doi/abs/10.1002/biot.201500219 >.

[99] FERNANDES, F. C. B. et al. Label free redox capacitive biosensing. **Biosensors and Bioelectronics,** v. 50, p. 437-440, 2013. Disponível em: < http://dx.doi.org/10.1016/j.bios.2013.06.043 >.

[100] FERNANDES, F. C. B. Comparing label free electrochemical impedimetric and capacitive biosensing architectures. **Biosensors and Bioelectronics,** v. 57, p. 96-102, 2014. Disponível em: < http://dx.doi.org/10.1016/j.bios.2014.01.044 >.

[101] MARQUES, S. M. et al. Sensitive label-free electron chemical capacitive signal transduction for D-dimer electroanalysis. **Electrochimica Acta,** v. 182, p. 946-952, 2015/11/10/ 2015. ISSN 0013-4686. Disponível em: < https://www.sciencedirect.com/science/article/pii/S0013468615305806 >.

[102] PICCOLI, J. et al. Redox capacitive assaying of C-reactive protein at a peptide supported aptamer interface. **Analytical Chemistry,** v. 90, n. 5, p. 3005-3008, 2018. Disponível em: < http://dx.doi.org/10.1021/acs.analchem.7b05374 >.

[103] BARADOKE, A. et al. Reagentless Redox Capacitive Assaying of C-Reactive Protein at a Polyaniline Interface. **Analytical Chemistry,** v. 92, p. 3508-3511, 2020/02/12 2020. ISSN 0003-2700. Disponível em: < https://doi.org/10.1021/acs.analchem.9b05633 >.

[104] BARADOKE, A. Introducing polymer conductance in diagnostically relevant transduction. **Biosensors and Bioelectronics,** v. 172, p. 112705, 2021/01/15/ 2021. ISSN 0956-5663. Disponível em: < https://www.sciencedirect.com/science/article/pii/S0956566320306941 >.